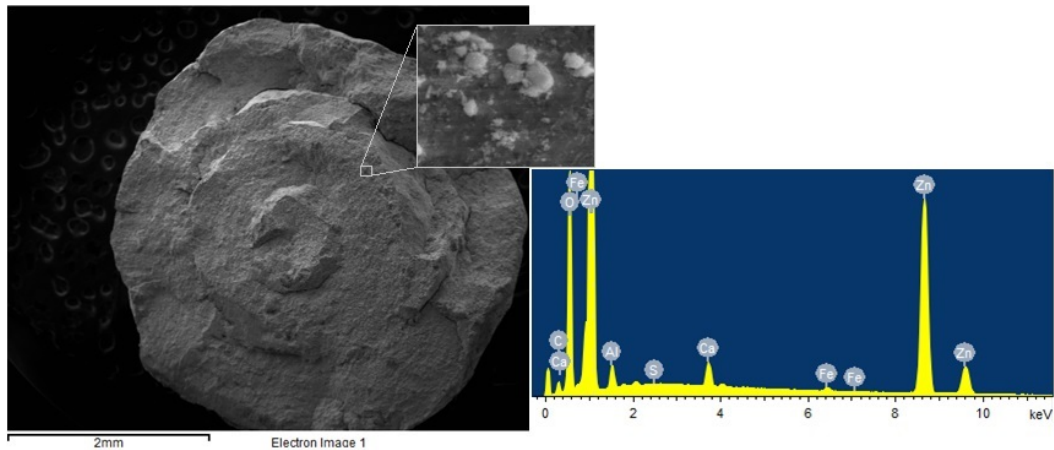


# CHALMERS



## Development of Desulphurisation Unit for Fuel Cell System

*Master's Thesis within the Innovative and Sustainable Chemical Engineering programme*

CARL-ROBERT FLORÉN

Department of Chemistry and Chemical Engineering  
Division of Applied Chemistry  
CHALMERS UNIVERSITY OF TECHNOLOGY  
Göteborg, Sweden 2015  
Master's Thesis 2015



MASTER'S THESIS

**Development of Desulphurisation Unit for Fuel Cell  
System**

Master's Thesis within the Innovative and Sustainable Chemical  
Engineering programme

CARL-ROBERT FLORÉN

SUPERVISORS

Ida Toftefors

Per Ekdunge

EXAMINER

Magnus Skoglundh

Department of Chemistry and Chemical Engineering

Division of Applied Chemistry

CHALMERS UNIVERSITY OF TECHNOLOGY

Göteborg, Sweden 2015

Master's Thesis 2015

Development of Desulphurisation Unit for Fuel Cell System  
CARL-ROBERT FLORÉN

© CARL-ROBERT FLORÉN, 2015

Department of Chemistry and Chemical Engineering  
Division of Applied Chemistry  
Chalmers University of Technology  
SE-412 96 Göteborg Sweden  
Telephone +46 (0)31-772 1000

Cover: SEM image and EDS spectrum of ZnO pellet

Göteborg, Sweden 2015

## Abstract

To make diesel usage more efficient within the transportation and telecom industry PowerCell Sweden AB (publ) is developing a fuel cell system with higher electrical efficiency compared to combustion engines and diesel generators. The system is called PowerPac and relies on reforming technology to convert liquid diesel into a gas mixture rich of hydrogen. PowerPac is planned to be used on board heavy duty trucks to supply electricity to the driver's cabin during idling hours and at remote areas where power supply is limited to supply telecom towers with electricity.

To make PowerPac durable it is necessary to remove sulphur components from the gas produced during diesel reforming which otherwise severely damages the fuel cell's different components. The desulphurisation unit holds spherical pellets of zinc oxide to remove H<sub>2</sub>S through reactive adsorption which chemically binds sulphur onto its surface. Hence importance lies in designing a desulphurisation unit that can maintain low levels of H<sub>2</sub>S for long periods of time to not damage the fuel cell system, which is the objective of the project.

The adsorbent was characterised and showed a BET surface area of 72 m<sup>2</sup>/g, pore volume of 0.17 cm<sup>3</sup>/g and a pore structure consisting primarily of pores of 25-120 Å in diameter. Prior to the project a long-term desulphurisation test using ZnO adsorbent was performed at and by PowerCell. One of the objectives was to evaluate its performance by analysing the adsorbent material properties at different positions in the bed after contamination. Chromium was discovered on the external surfaces of the pellets which is assumed to have affected the overall efficiency. Two mathematical models were developed from a global mass balance over the unit and adsorption is modelled through the shrinking core or linear driving force model. During experiments a large amount of slip around the pellets was observed why GHSV was lowered to counter the issue. The lowering resulted in a very long time needed for each experiment, over 105 h, which could not be given during the project and only one experiment could be performed. The experiment did not reach full saturation and the models could not be validated.

Even though the models could not be validated the shrinking core model was compared to similar literature data as a reality check but due to a large difference in particle sizes the model underestimates mass transfer resistances. Through the experiment performed the adsorption capacity of ZnO for sulphur could be estimated to 137 mg S/g adsorbent and 38 % of the adsorption sites in the pellet were covered by sulphur. Future work is recommended to target new experiments and giving the necessary time needed in order to validate the model.

**Keywords:** Desulphurisation, ZnO, adsorption, BET surface area, shrinking core, linear driving force, PEM fuel cells

## Sammanfattning

För att effektivisera användningen av diesel inom transport- och telekommärknaden utvecklar PowerCell Sweden AB (publ) ett bränslecellsystem med högre elektrisk verkningsgrad gentemot förbränningsmotorer och dieselaggregat. Systemet heter PowerPac och bygger på reformeringsteknik som omvandlar flytande diesel till en väterik gasblandning. Tanken är att PowerPac ska användas ombord på tunga lastbilar för att driva bekvämlighetsutrustning i hytten under tomgångskörning och på avlägsna platser där tillgången till kraftnätverket är begränsat för att driva telekommaster.

För att säkerställa att PowerPac kan hållas i drift utan att bränslecellsystemet tar skada av svavelgaser som bildats under reformeringen av diesel behövs en avsvavningsenhet för att säkert avlägsna svavelgaserna. Avsvavningsenheten består av sfäriska pellets av zinkoxid och bygger på den kemiska processen adsorption där  $H_2S$  binder kemiskt till ytan av adsorptionsmaterialet. Därför är det av betydande vikt att dimensionera en avsvavningsenhet som klarar av att hålla PowerPac i drift under långa perioder utan att skadas, vilket är målet för detta projekt.

Adsorptionsmaterialet karaktäriserades och har en ytarea av  $72 \text{ m}^2/\text{g}$ , porvolym av  $0.17 \text{ cm}^3/\text{g}$  and majoriteten av porstrukturen består av porer med 25-120 Å i diameter. Före projektet har adsorptionsmaterialet genomgått ett experimentellt långtidstest hos PowerCell. Ett av målen var att analysera materialets egenskaper efter den blivit kontaminerad av  $H_2S$  vid olika positioner i enheten för att utvärdera dess effektivitet. Via SEM-analys återfanns krom på pelletens yta vilket antas ha påverkat effektiviteten under testet. Två matematiska modeller har tagits fram vilka är baserade på en global massbalans över enheten där reaktionstermen modelleras via dem så kallade 'shrinking core'- eller 'linear driving force'-modellerna. Under experimenten upptäcktes en hög andel svavelväte som direkt passerade materialet utan att reagera. För att motverka trenden minskades GHSV men resulterade istället i att varje experiment tog över 105 timmar vilket inte var möjligt inom detta projekt, varför endast ett experiment kunde genomföras. Experimentet nådde inte full mättnad och modellerna kunde inte valideras.

Även om modellerna inte kunde verifieras jämfördes shrinking core-modellen med litterär data vid liknande betingelser för att undersöka dess trovärdighet. Resultatet verkar rimligt men underskattar transportmotståndet genom pelleten eftersom dess storlek skiljde sig mycket från den ur litteraturen. Utifrån det genomförda experimentet kunde en adsorptionskapaciteten för ZnO uppskattas till  $137 \text{ mg S/g adsorbent}$  där 38 % av adsorptionssätena i pelleten var täckta av svavel. För framtida undersökningar rekommenderas det att genomföra nya experimentella försök och ge dessa lång tid för att uppskatta nödvändiga parametrar och verifiera modellen.

**Nyckelord:** Avsvavning, ZnO, adsorption, BET ytarea, shrinking core, linear driving force, bränsleceller

## Acknowledgements

I would first like to express gratitudes to my supervisors, Ida Toftfors and Per Ekdunge at PowerCell Sweden AB (publ) for letting me take on this project and to all people at Chalmers that has helped me immensely during my experimental part of the project. Special thanks goes to my examiner Magnus Skoglundh who has always seemed to find some time to answer my questions and discuss the matter. Extra special thanks goes my supervisor Sheedeh Fouladvand who has helped me more than I could imagine during emerging issues during the my experiments. I would probably not have gotten through the first week without your help in the lab. I also want to thank all the people and friends I have met during my studies at Chalmers and not least my family who have always supported me through the years. Without you I would not have made it through at all.

Carl-Robert Florén, Göteborg April 6, 15

## Abbreviations

Autothermal reformer	ATR
Brunauer–Emmett–Teller	BET
Energy dispersive spectroscopy	EDS
Gas hourly space velocity	GHSV
Mass spectrometer	MS
Partial oxidation	PO
Proton exchange membrane	PEM
Preferential oxidation	ProX
Scanning electron microscope	SEM
Steam reforming	SR
Water-gas shift	WGS

## Symbols

$a$	surface area of pellet per unit volume [ $\text{m}^2/\text{m}^3$ ]
$C$	concentration [ $\text{mole}/\text{m}^3$ ]
$C^*$	equilibrium adsorbate concentration [ $\text{mole}/\text{m}^3$ ]
$C/C_{in}$	relative concentration
$D_e$	effective diffusion through product layer [ $\text{m}^2/\text{s}$ ]
$G$	Gibbs energy [ $\text{J}/\text{mole}$ ]
$H$	enthalpy [ $\text{J}/\text{mole}$ ]
$K_{eq}$	equilibrium constant
$k_B$	Boltzmann's constant [ $\text{J}/\text{K}$ ]
$k_f$	effective mass transfer [ $\text{m}/\text{s}$ ]
$k_g$	gas boundary layer diffusion [ $\text{m}/\text{s}$ ]
$k_s$	adsorption reaction rate at unreacted core surface [ $\text{m}/\text{s}$ ]
$L$	total bed length [ $\text{m}$ ]
$m/z$	mass-to-charge ratio [ $\text{C}/\text{kg}$ ]
$N_A$	Avogadro constant [ $\text{mole}^{-1}$ ]
$P$	pressure [ $\text{kPa}$ ]

$P_{vapour}$	Vapour pressure [kPa]
$q$	adsorbed $H_2S$ per pellet [mole/pellet]
$R_{drop}$	radius of droplet [m]
$R_p$	initial pellet radius [m]
$r_c$	radius of unreacted core surface [m]
$S$	entropy [J/mole K]
$S_g$	specific surface area [ $m^2/g$ ]
$T$	temperature [K]
$t$	time [h]
$t_{ideal}$	ideal breakthrough time [h]
$V_{bed}$	bed volume [ $m^3$ ]
$V_{drop}$	volume of droplet [ $m^3$ ]
$V_{pellet}$	pellet volume [ $m^3$ ]
$\dot{V}$	volumetric flow rate [ $m^3/h$ ]
$u$	bed void velocity [m/s]
$v$	volume adsorbed at STP [ $m^3$ ]
$v_m$	volume of a monolayer
$z/L$	relative bed length
$\alpha$	surface area per adsorbed molecule [ $m^2$ ]
$\gamma_{drop}$	surface tension [N/m]
$\epsilon$	void fraction [ $m^3/m^3$ ]
$\theta$	coverage
$\lambda$	air-to-fuel ratio

# Contents

<b>1</b>	<b>Introduction</b>	<b>1</b>
1.1	Background . . . . .	1
1.2	Objective . . . . .	2
1.3	Problem formulation . . . . .	2
1.4	Limitations . . . . .	3
<b>2</b>	<b>Theoretical background</b>	<b>4</b>
2.1	Fuel processing . . . . .	4
2.1.1	Diesel reforming . . . . .	4
2.1.2	Clean-up technologies . . . . .	6
2.2	Adsorption . . . . .	7
2.2.1	Fundamentals of adsorption . . . . .	7
2.2.2	Important factors . . . . .	8
2.2.3	Reactive sulphur adsorption . . . . .	8
2.2.4	Adsorption isotherms . . . . .	9
2.2.5	Adsorbent lifetime & modelling . . . . .	11
2.2.6	Adsorbent material . . . . .	14
2.3	Methods of analysis . . . . .	19
2.3.1	Surface area & Pore size distribution . . . . .	19
2.3.2	Scanning electron microscopy & Energy dispersive spectroscopy . .	19
2.3.3	Mass Spectrometry . . . . .	21
<b>3</b>	<b>Methodology</b>	<b>22</b>
3.1	ZnO characterisation . . . . .	22
3.1.1	BET surface area & Pore size distribution . . . . .	23
3.1.2	SEM & EDS analysis . . . . .	23
3.2	Experiments . . . . .	23
3.2.1	Parameters & calibration . . . . .	24
3.2.2	Experimental setup . . . . .	27
3.3	Breakthrough modelling . . . . .	27

---

<b>4</b>	<b>Results</b>	<b>29</b>
4.1	ZnO characterisation . . . . .	29
4.1.1	SEM & EDS . . . . .	29
4.1.2	BET surface area & pore volume . . . . .	31
4.1.3	Pore size distribution . . . . .	32
4.2	H <sub>2</sub> S Adsorption experiments . . . . .	33
4.3	Alternative adsorbent material . . . . .	35
<b>5</b>	<b>Discussion</b>	<b>36</b>
5.1	Design proposal . . . . .	36
5.2	Performance of the long-term test . . . . .	36
5.3	Adsorption model . . . . .	38
5.4	Evaluation of experiments . . . . .	40
5.5	Suggestions of improvement . . . . .	42
<b>6</b>	<b>Conclusion</b>	<b>43</b>
	<b>Bibliography</b>	<b>45</b>
<b>A</b>	<b>Appendix</b>	<b>51</b>
A.1	Equilibrium calculations . . . . .	51
A.2	Experiments . . . . .	55
A.3	ZnO sulphur content . . . . .	57

# 1

## Introduction

### 1.1 Background

One of the main contributors for greenhouse gas emissions today is the transportation sector. Transportation by road represents about 20 % of the total CO<sub>2</sub> emissions in the EU. Further, heavy-duty trucks transporting goods constitutes for 5 % of the total CO<sub>2</sub> emissions and 25 % of the road transportation CO<sub>2</sub> emissions in EU [1]. Along with increasing population and consumption patterns, the heavy-duty truck traffic has increased in EU between 1990 and 2010 which in turn has increased the CO<sub>2</sub> emissions by 36 % [1]. The same trend can be seen in the U.S where the emissions from heavy-duty trucks increased with 57 % from 1990 to 2003 [2].

Statistics have shown that the numbers of heavy-duty trucks powered by diesel is still increasing [3]. Even though they are among the most fuel efficient vehicles they are also the most fuel consuming vehicles and belong to the vehicle class with the largest milage per year. Thereby every improvement in fuel economy can make a significant difference [3][4][5].

During long distance transportation the drivers usually spend around 8 hours per day of rest in the cabin and running the engine in idle mode to provide electricity for heating, ventilation and other electrical appliances. It has been reported that heavy-duty trucks idle for about 40 % of the engine run-time which typically is 1830 hours per truck and year, combusting about 5300 liters of diesel. [6][7].

Diesel generators are also often used for decentralized and stationary energy generation as for the telecom market in remote areas with no access to an electricity grid [8]. These generators requires maintenance and regular checks which increases their running costs [8][9]. For example in India over 50 % of the telecom towers did not have any access to a power grid or had access to an unreliable grid with frequent power cuts in 2011. About 90 % of the latter ones were supplied with backup diesel generators [10].

To counter the increasing trend of inefficient diesel combustion for electricity gener-

ation, PowerCell Sweden AB (publ) is developing a proton exchange membrane (PEM) fuel cell system called PowerPac to be used as an auxiliary power unit. It is aimed to supply electricity to heavy-duty truck cabins during idling hours and remote telecom stations with no grid access [8]. Using fuel cells for these applications has been extensively discussed and has been given a lot of interest [11][12][13].

PowerPac consists of a fuel cell stack and a diesel reformer which enables the system to utilize conventional diesel instead of pure hydrogen gas. The advantage of using diesel is that it is commercially available worldwide compared to hydrogen gas which is yet very limited for transportation purposes [13][14]. The diesel reformat enters the fuel cell where  $H_2$  is converted to  $H_2O$  and electricity [8]. This solution benefits of low operating costs during idling, improving driver environment and reduced environmental impact. PowerPac also benefits from a significantly higher electrical efficiency compared to idling main engine [8].

Diesel reforming produces impurities as  $H_2S$  which strongly affects the downstream fuel cell and reduces its performance. Even at very small concentrations of  $H_2S$  parts as membranes and electrodes are severely damaged [15][16]. Therefore desulphurisation of the reformat gas before entering the fuel cell is needed in order to make PowerPac durable. Desulphurisation and sulphur adsorption is a well-know process at industrial scale but due to special conditions in the reformer system knowledge is limited for PEM fuel cell system applications.

## 1.2 Objective

The objective of this study is to analyse a desulphurisation unit which has been through a long-term test at PowerCell Sweden AB (publ), here after referred to as PowerCell, to evaluate its performance and adsorbent material properties. Sulphur adsorption and the unit is later modelled to propose a design suitable for the PowerPac fuel cell system developed at PowerCell. A secondary objective is to investigate if there are other more promising materials that can be used for desulphurisation applications in PEM fuel cell systems.

## 1.3 Problem formulation

The desulphurisation unit to be analysed contains solid spherical pellets of zinc oxide which is known to have adsorptive properties towards sulphur to clean the incoming gas mixture. The  $ZnO$  pellets have been exposed to  $H_2S$  containing reformat through a long-term test at PowerCell and will be analysed at different locations in the bed to evaluate its performance in  $H_2S$  adsorption. Interest lies in analysing pellets extracted from the unit in axial direction but also individual pellets in radial direction by their sulphur content, surface area and pore volumes. Through there measurements the performance can be discussed.

To propose a design of the desulphurisation unit an experimental investigation of the adsorption process is performed at Chalmers University of Technology. The experiments

should provide values for developing and validating a mathematical model at the specific conditions found in the reformer system. To get results that are comparable and possible to up scale the gas flow rate is measured in gas hourly space velocity (GHSV) which is defined as

$$GHSV = \frac{\dot{V}}{V_{bed}} \quad (1.1)$$

where  $\dot{V}$  is the volumetric flow rate in  $\text{m}^3/\text{h}$  and  $V_{bed}$  is the pellet bed volume in  $\text{m}^3$ .

## 1.4 Limitations

Even though  $\text{H}_2\text{S}$  adsorption is well known in industrial applications, the conditions adopted in PowerPac has not been extensively examined which makes it hard to pinpoint the most important factors. Model limitations is therefore proposed and should at maximum only include varying concentrations in  $\text{H}_2\text{S}$ ,  $\text{H}_2\text{O}$ ,  $\text{CO}$ ,  $\text{CO}_2$  and  $\text{H}_2$ , residence time and temperature. The temperature range of interest is decided as 80-350 °C. Lower temperatures can not be achieved due to absence of a heat sink while higher temperatures are thermodynamically unfavourable in adsorption processes. Sulphur in the reformat is assumed to be present as  $\text{H}_2\text{S}$  only.

# 2

## Theoretical background

To understand the desulphurisation process and to develop a mathematical model it is necessary to deepen the knowledge in adsorption separation principles. Because the reformat gas that enters the desulphurisation unit is produced in a fuel reformer basic knowledge is also necessary in diesel reforming.

### 2.1 Fuel processing

To produce hydrogen gas from liquid fuel a fuel processor is required in which the liquid feed is converted into a gas mixture rich of hydrogen [17]. The liquid fuel enters a reforming stage to produce the gas mixture, called reformat gas, which is led through clean-up stages to increase overall hydrogen conversion and reduce damaging components that reduces the upstream fuel cell system performance [18].

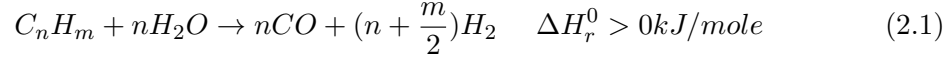
#### 2.1.1 Diesel reforming

Comparing different liquid fuels, diesel has promising properties to act as a source for hydrogen production but also due to its worldwide availability. Its volumetric energy density [ $\text{MJ}/\text{m}^3$ ] compared to other fuels capable for hydrogen production is high and because it is kept in liquid form there is no need for pressure vessels which makes handling easier [19].

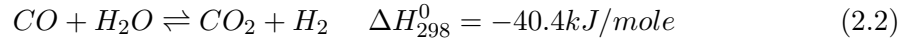
The diesel is passed through a fuel reformer and converted to reformat containing hydrogen and carbon oxides [20][21]. The reformat composition and quality varies with several possible by-products depending on the diesel characteristics and reforming conditions. To reform diesel and liquid fuels, three different methods are utilised and very briefly described here.

### Steam reforming

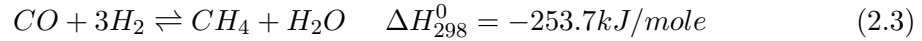
Steam reforming (SR) uses steam as an oxidant for oxidation of the hydrocarbon fuel to produce  $H_2$  and  $CO$ . The reactions during steam reforming are shown below in 2.1-2.3. In total SR is endothermic and has to be supplied with energy [20][22].



Along with hydrogen and carbon monoxide, water reacts with produced  $CO$  according to water-gas shift reaction (WGS) as



According to methanation reaction, methane is also produced to a smaller extent but suppressed at higher reforming temperatures and in presence of steam according to [20]



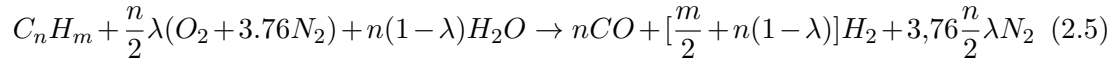
### Partial oxidation

Instead of steam as an oxidant, partial oxidation (PO) uses air to oxidise the fuel and the reaction is highly exothermic and shown in reaction 2.4 [22]. The PO reaction is significantly faster than SR and produces more carbon monoxide compared to SR. This implies that after partial oxidation the need for downstream clean-up is increased in  $CO$  sensitive fuel cells. Coke formation can also be an important issue in PO where hydrogen reacts with carbon monoxide which reduces the accessibility of the catalyst through blocking of pore volumes. The thermodynamic equilibrium of coke formation is however suppressed by presence of steam [20].



### Autothermal reforming

A third reforming method is autothermal reforming (ATR) which is a combination of SR and PO as shown in reaction 2.5 [20][22]. They occur simultaneously along the reactor but with the reaction rate of PO being faster than for SR, partial oxidation dominates the first part of the reactor and decreases as the oxygen supply is reduced. The effect is that PO is dominating in the first part of the reformer and SR in the later. With PO being exothermic and SR endothermic, the generated heat from the first part can be used to fuel the later part of the reformer. It is therefore possible to adjust the heat generation from 2.5 to balance the steam reforming implying that a thermodynamic maximum efficiency can be obtained in terms of air to fuel ratio,  $\lambda$ . This optimum is however only theoretical and does not account for heat losses and the practical maximum is also dependent on the choice of fuel [20].



As reaction 2.5 proceeds the water-gas shift and methanation reactions occur simultaneously to produce a gas composed of  $H_2$ ,  $H_2O$ ,  $CO_2$ ,  $CO$ ,  $CH_4$  and a varying amount of contaminants as  $H_2S$  depending on diesel quality [20][22][23]. Other contaminants include species as  $SO_X$  but there are not examined further and are assumed to not affect the desulphurisation process.

### 2.1.2 Clean-up technologies

Due to deactivation of PEM fuel cells by carbon monoxide it should be removed to acceptable levels to ensure durable operation. This reduction is achieved using the water-gas shift reaction and preferential oxidation (PrOx) to convert CO to  $CO_2$  [20][24].

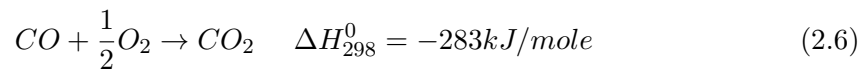
Apart from the produced carbon monoxide, U.S ultra low sulphur diesel contains at maximum 15 ppm of sulphur which during reforming inevitably produces a small but significant amount of  $H_2S$  in a reduced atmosphere. The sulphur contaminants strongly affect the fuel cell systems performance and severely damages vital parts of the fuel cell system and must be removed from the reformat to ensure durability [15][25]. The sulphur removal is discussed in a separate section due to its importance for the thesis.

#### Water-gas shift

The water-gas shift reaction is an exothermic reaction and is often used to clean gases from CO and at the same time increase the concentration of hydrogen, see reaction 2.2. WGS is typically performed at high temperatures due to faster reaction rates but at the cost of decreased thermodynamic equilibrium concentration of hydrogen. To enhance total conversion the reaction is therefore often divided into a high- and low-temperature water gas shift reaction at a temperature interval of 310 - 450 °C and 180 - 250 °C respectively [24].

#### Preferential oxidation

Another used clean-up reaction of CO is the preferential oxidation reaction. PrOx uses air to oxidise CO into  $CO_2$  according to reaction 2.6 and can reduce CO concentration down to 10 ppm. The reaction is carried out in excess of air of  $\lambda \approx 1.5 - 2$  and is followed by an unavoidable loss of hydrogen by combustion and reverse water-gas shift reaction [18][20].



## 2.2 Adsorption

In the adsorption process molecules from a gas phase or solution bind directly to a solid or liquid surface to form a condensed layer. Molecules binding to the surface are called adsorbate and the surface molecules are called adsorbent. The reverse reaction where the adsorbate is released from the surface is called desorption [26].

### 2.2.1 Fundamentals of adsorption

Heterogeneous gas-solid adsorption involves direct bondings to the surface but also condensation in the pores of a porous material. The latter is controlled by surface tension forces according to the Kelvin equation 2.7

$$k_b T \ln\left(\frac{P_{drop}}{P_{vapour}}\right) = \frac{2\gamma_{drop}V_{drop}}{R_{drop}} \quad (2.7)$$

where  $P_{vapour}$  is the vapour pressure of bulk fluid,  $\gamma_{drop}$  is the surface tension of the drop,  $R_{drop}$  is its radius,  $V_{drop}$  is the molar volume of the drop,  $k$  is the Boltzmann's constant and  $T$  is the temperature. As a result of the Kelvin equation, adsorbate can condense when entering the pores due to a lowering of liquid vapour pressure [26].

Gases adsorb in general first directly onto the adsorbent surface by physical or chemical bondings to form a monolayer that in an ideal case covers the whole available surface area. The monolayer is then covered by a secondary adsorbate layer on top of the first and so on, referred to as multilayers. The covering layers interact strongly with the previous layer and weakly with adsorbent surface, hence adsorbate-adsorbate interactions are important instead of adsorbate-adsorbent interactions in multilayer adsorption. Multilayer adsorption is a condensation process where the layers interact and form a condensate film on top of the first layer and pore surface [26].

### Chemisorption & Physisorption

Depending on the nature of forces acting between adsorbate and adsorbent, the adsorption is categorised as physisorption or chemisorption. When a molecule is chemically bonded directly onto a surface it is chemisorbed. A chemisorbed molecule shares electrons with the adsorbent in a covalent bond and thereby changing the electronic structure of the adsorbent. Hence chemisorption is selective and the adsorbate is adsorbed on specific materials and active sites. Due to the strong covalent bondings and coulombic forces, chemisorption is more difficult to reverse [27][28]. Typical energies for chemisorption are 15-100 kcal/mole for simple molecules [26].

In physisorption polarisation forces as van der Waals bonds dominate the interactions and no direct bond is present between adsorbate and adsorbent. This type is often associated with weak solid-gas interactions and due to their nature they are non-specific and the electronic structure is not significantly affected. The relatively weak van der Waals bonds are easily reversed and the adsorbate can diffuse along the surface [27].

Typical energies for physisorption is 2-10 kcal/mole [26]. Further the electronic structure is not affected in physisorption.

### 2.2.2 Important factors

As adsorption is a dynamic equilibrium process it is necessary to optimise operating conditions to maximise the capacity. It is also important to know how and to what extent the equilibrium is affected when operational conditions are changed.

#### Surface area & Pore size distribution

An important factor for adsorption potential is the adsorbent surface area which can be controlled through the manufacturing process and morphology of the adsorbent. An adsorbent with a microporous structure can result in a surface area as large as 1200 m<sup>2</sup>/g [29]. It is important to differentiate between the total surface area and the surface area available for adsorption. The latter meaning the pore area that is accessible by the species targeted for adsorption as pores can be too small to allow molecules to enter.

Pore sizes are defined by IUPAC (International Union of Pure and Applied Chemistry) as; micropores are <20 Å, mesopores are 20-500 Å and macropores are >500 Å [30]. The pore size distribution is a measurement of how the pore volumes and areas are distributed over a range of pore diameters. Analysing a fresh and a contaminated adsorbent by its surface area and pore size distribution it is possible to determine how the pore structure has been affected by adsorption and if any pores have been subjected to blocking or clogging.

#### Temperature

Adsorption is always exothermic and involves heat generation which can be shown by starting with equation 2.8.

$$\Delta G = \Delta H - T\Delta S \quad (2.8)$$

where G is the Gibbs energy [J/mole], H is the enthalpy [J/mole], T is the temperature in Kelvin and S is the entropy [J/mol×K] [31]. For a spontaneous process as adsorption  $\Delta G < 0$  and due to the ordering of molecules onto the surface also  $\Delta S < 0$ . Insertion into equation 2.8 shows that  $\Delta H < 0$ .

Due to the exothermic nature of adsorption and according with Le Chatelier's principle, the equilibrium adsorption capacity is inversely proportional to temperature.

### 2.2.3 Reactive sulphur adsorption

Many articles discussing gas phase sulphur removal have used metal oxides as their adsorbent and most frequently ZnO or zinc-based mixtures [32][33][34][35]. At lower temperatures, zinc-based adsorbents show promising properties and can be promoted by

several other transition metals in order to achieve a satisfactory sulphur capacity [35]. The adsorption process of  $H_2S$  over  $ZnO$  is a hydrolysis reaction, inherently exothermic and shown in reaction 2.9 [36].



The observed reaction rate can be controlled by either; mass transfer through gas boundary layer surrounding the adsorbent, pore diffusion or intrinsic reaction rate [37]. It is important to state that pore diffusion resistance changes as sulphur is adsorbed onto surfaces by affecting pore sizes and volumes as the hydrolysis reaction continues. The adsorbed sulphur product is also larger in radius which can lead to blocking of pore openings and thus reducing the available active area and porosity [38][39]. Several articles have discussed the importance of each of the possible rate limiting steps by fitting experimental values to mathematical models as the grain-, pore and shrinking core model [39][40][41]. The experiments differ though in used metal oxides, adsorbent and gas compositions, reaction conditions and cannot be directly compared to each other. Most commonly the mathematical models do account for all three diffusional regimes and conclude that the internal and intrinsic reaction rate to be most influencing and external mass transfer being negligible [36][37][40][42].

An interesting addition to this assumption was concluded by using the work of Yoshida et al. for a syngas mixture and evaluating the relative importance of the rate determining steps; it showed that for a fresh adsorbent particle, the external mass transfer resistance was significant and increased with temperature whether the internal diffusion was relatively negligible [38]. As soon as a sulphur product layer started to form over the particle the internal transport resistance took over to be rate limiting. The result indicates that physical properties and morphology of the adsorbent are important factors for optimising the adsorbent material and enhancing overall reaction. It is also interesting to note that the intrinsic reaction rate would only become limiting at lower temperatures ( $\approx 50^\circ C$ ) whether at higher temperatures diffusional resistances should be the limiting factors [38].

#### 2.2.4 Adsorption isotherms

Gas-solid adsorption is often expressed in terms of relative pressure of adsorbate ( $P_{adsorbate}/P_0$ ) in gas phase and loading which is the amount adsorbed species onto the adsorbent. The latter is usually expressed in mass per unit mass of adsorbent. By keeping temperature constant and plotting the loading as a function of relative pressure an adsorption isotherm is constructed. These are also referred to as equilibrium isotherms because their derivation assumes equilibrium conditions [29].

There are five different types of isotherms associated with adsorption and they describe different adsorption behaviours, see figure 2.1 [28][29].

Type I isotherm is most simple assuming monolayer adsorption and a maximum adsorption capacity. The isotherm is often used for gases above their critical temperature where condensation is not possible. The type II isotherm is more complex and accounts

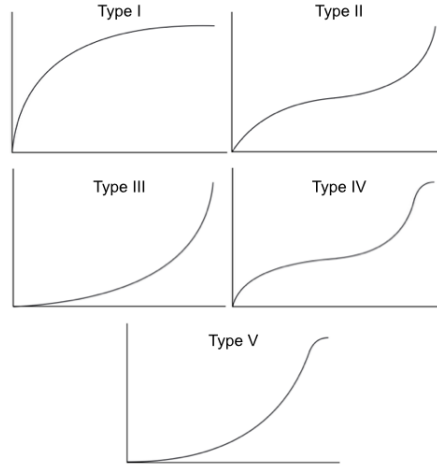


**Figure 2.1:** Adsorption isotherms

for multilayer adsorption according to the so called BET theory, which will be briefly explained later. For a type II isotherm the heat of adsorption reduces as more and more layers form, meaning that less and less heat is required to form the multilayers. The isotherm can be seen for gases below their critical temperature and pressures approaching vapour pressure. These two isotherms are favourable for their tendency to adsorb at low relative pressures [29].

For an unfavourable adsorption, a type III isotherm can be observed. This process is multilayered and according to BET theory, the heat of adsorption increases as more layers form. The major downsides of type II and type III isotherms is the prediction that adsorption goes to infinity as the relative pressure approaches one. As a material can not adsorb an infinite amount of adsorbate, the BET isotherm limits the amount by saying that the number of layers is restricted by the pore size and capillary condensation is assumed to be present at a lower vapour pressure according to equation 2.7. The result allows for predicting adsorption isotherms of type IV and V, which are versions of type II and III respectively but includes capillary condensation [29].

There are several models to mathematically describe isotherm types. Three common ones are Langmuir, Freundlich and BET isotherm. Langmuir is the most simplest one, able to describe type I isotherms as

$$\theta = \frac{K_{eq}P_A}{K_{eq}P_A + 1} \quad (2.10)$$

where  $K_{eq}$  is the adsorption equilibrium constant,  $P_A$  is partial pressure of adsorbate and  $\theta$  is coverage of adsorbate into adsorbent [29].

Freundlich adds two fitting parameters,  $K$  and  $n$  which are dependent on adsorbent and operating conditions, making it more flexible for type I isotherms [29]. This isotherm describes coverage as

$$\theta = KP_A^{\frac{1}{n}} \quad (2.11)$$

The more complex BET isotherm was derived by Brunauer, Emmett and Teller (BET) for multilayer adsorption, able to describe IV and V type isotherms [28][29]. The model assumes ideal gas behaviour and that multiple molecules can be adsorbed on each site, an adsorbed molecule can act as a site for the next layer, the sites are equivalent, no interactions between adsorbate species, once a molecule has been adsorbed it is immobile, molecules in the second and higher layers act as liquids [43]. The BET isotherm is shown in 2.12

$$\frac{P}{v(P_0 - P)} = \frac{1}{v_m} + \frac{(c - 1)}{v_m c} \left(\frac{P}{P_0}\right) \quad (2.12)$$

where  $v$  is the volume adsorbed at STP,  $P$  is the total pressure,  $P_0$  is the vapour pressure of  $N_2$  at operating temperature,  $v_m$  is the volume of one monolayer at STP and  $c$  is a constant related to the heat of adsorption [29].

### 2.2.5 Adsorbent lifetime & modelling

As adsorption is an equilibrium process it is necessary to monitor the degree of saturation of the bed. Consider an ideal adsorption process with plug flow, no external and internal mass transfer resistance associated with the adsorbent, no axial dispersion and an isotherm that starts at the origin. When adsorbate in a bulk gas phase is fed to the fresh bed its concentration will immediately drop down to equilibrium level when coming into contact with adsorbent material. Due to plug flow and no resistances a sharp stoichiometric front in the form of a step function will move through the bed at velocity  $u$ , separating it into two sections. The section downstream and upstream of the front is saturated adsorbent and unused adsorbent, respectively. As the front reaches the outlet of the bed, or  $z/L=1$ , at the ideal breakthrough time,  $t_{ideal}$ , the bed is spent and must be changed or regenerated [29]. This is illustrated in figure 2.2.

As the adsorbent is subjected to mass transfer resistances and axial dispersion the concentration front will instead become S-shaped. The same reasoning can be applied as for the ideal case but includes a mass transfer zone as shown in figure 2.3. At the mass transfer zone equilibrium is not yet reached with the surrounding bulk fluid because of non-ideal behaviour. Due to the S-shape there will be no sharp breakthrough time as the front reaches the outlet and some adsorbate will exit the bed before it as a whole has reached equilibrium. By monitoring the outlet concentration of adsorbate and defining a maximum allowed concentration called breakthrough concentration, often

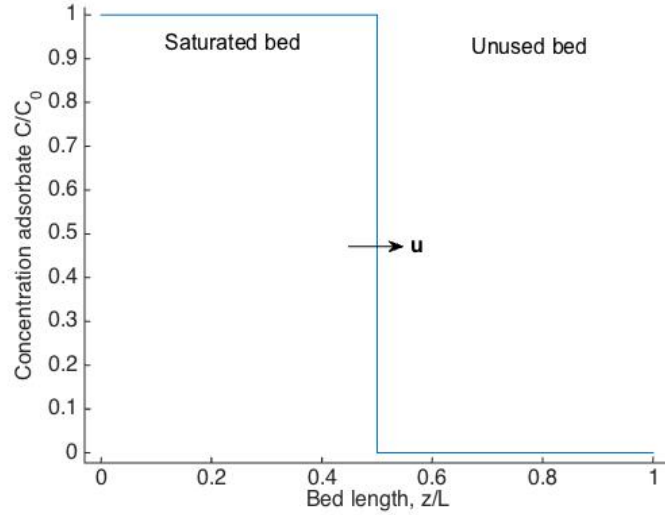


**Figure 2.2:** Concentration front for ideal adsorption

defined in sizes as  $0.05 \times C_0$ , it is possible to monitor the process. Plotting the outlet concentration to time gives a breakthrough profile and a corresponding breakthrough time at the predetermined breakthrough concentration. The shape of the breakthrough profile is important for designing adsorption beds and its integral is related to bed capacity. A wide mass transfer zone indicates a significant amount of mass transfer resistance and a longer bed is needed to maintain the same level of performance [29]. If a breakthrough profile has long breakthrough times it can be assumed that reaction rates are faster and more sulphur can be adsorbed [32]. As the breakthrough profile describes the characteristics of the process it is possible to derive and fit a mathematical model to the adsorption and verify its validity through experiments.

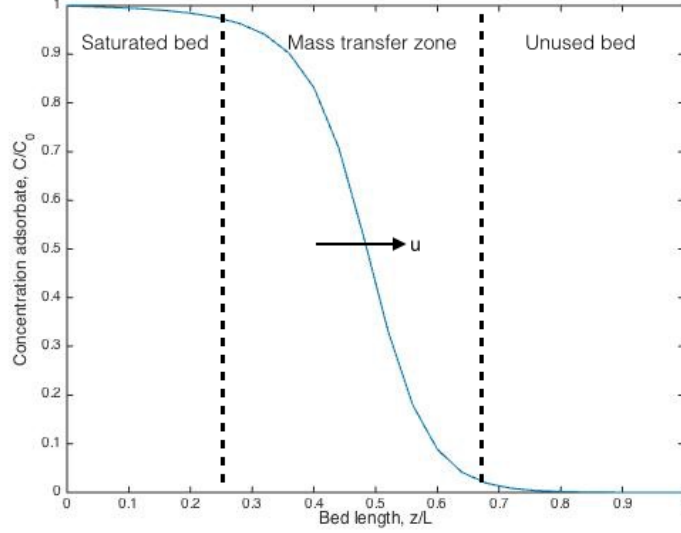


**Figure 2.3:** Mass transfer zone

Assuming isothermal and isobaric operation, no competitive adsorption and plug flow with constant velocity  $u$ , the mass balance for adsorbate over the bed is

$$u \frac{\partial C}{\partial z} + \frac{\partial C}{\partial t} + \frac{(1 - \epsilon_b)}{\epsilon_b V_{\text{pellet}}} \frac{\partial q}{\partial t} = D_L \frac{\partial^2 C}{\partial z^2} \quad (2.13)$$

where the first term accounts for axial flow, second term for accumulation, third term for reaction and takes into account the internal mass transfer resistances into the pellet with  $q$  being amount of adsorbate per volume of adsorbent, the fourth term accounts for axial dispersion [29]. The latter is only being significant at low space velocities and is hence ignored from now on.

The reaction term has to be modelled to take an adsorption process into account. One method is using the so called shrinking core model as illustrated in figure 2.4. The model regards the initial adsorbent pellet material as an unreacted sphere with an outer radius  $R$ . Adsorption takes place on the unreacted core surface at  $r_c$  which shrinks as reaction continues until the entire sphere has been converted. The contaminated part of the pellet is made up of a solid product layer which increases the diffusion length for the reactant to reach  $r_c$ , making adsorption more and more difficult as the process continues [44]. Assuming the apparent reaction rate to be controlled by diffusion in gas boundary layer, the product layer and reaction rate the third term is modelled by equation 2.14 [45].

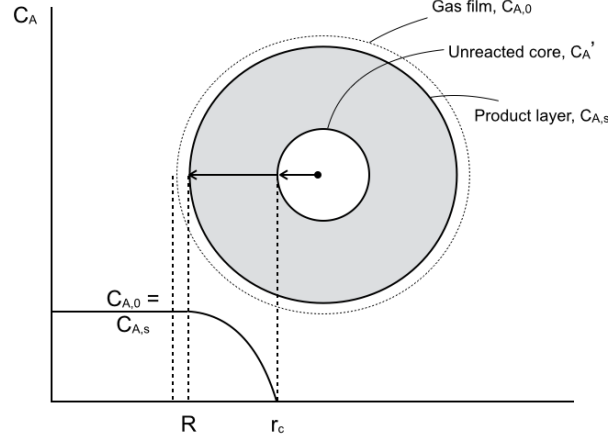


**Figure 2.4:** Illustration of shrinking core model

$$-\frac{\partial q}{\partial t} = \frac{4\pi r_c^2 C}{\frac{1}{k_s} + \frac{r_c(R_p - r_c)}{R_p D_e} + \frac{r_c^2}{k_g R_p^2}} \quad (2.14)$$

where  $k_s$  is the adsorption reaction rate at  $r_c$ ,  $R_p$  is the initial pellet radius,  $D_e$  is the effective diffusivity through forming product layer and  $k_g$  is the gas boundary layer diffusion. The latter is assumed to be negligible according to 2.2.3 but can easily be included at the cost of the extra fitting parameter,  $k_g$ .

An other widely used method for modelling the reaction term is called linear-driving-force (LDF) assumption which linearises the third term to equation 2.15.

$$\frac{(1 - \epsilon_b) \partial q}{\epsilon_b V_{\text{pellet}} \partial t} = -k_f a (C - C^*) \quad (2.15)$$

where  $k_f$  is the effective mass transfer coefficient,  $a$  is the pellet surface area per unit volume,  $C$  is the adsorbate bulk concentration and  $C^*$  is the equilibrium adsorbate bulk concentration that corresponds to the pellet loading [46]. By applying LDF species are only adsorbed at the outer surface of the material until  $C^*$  reaches saturation concentration and no internal diffusional resistances are accounted for.

### 2.2.6 Adsorbent material

Evaluating and finding an alternative material as adsorbent is a complex matter where both the material properties and manufacturing process must be taken into account. Because little research is available in the open literature on the specific application for PEM fuel cell systems it is necessary to look at other but similar conditions to try getting

a perception of the choice of material and its effect. This section is purely a literature review and no experiments evaluating different materials has been performed during the thesis.

Studies that use metal oxides for sulphur adsorbents most frequently use ZnO due of its favourable thermodynamic properties compared to other metal oxides [35][38][39][41]. Unfortunately ZnO is reported to possess a lower reaction rate for sulphur adsorption than other metal oxides [47]. The idea in this section is that the inherently low reaction rate can be compensated by using favourable morphology, pure or promoted with other metal oxides to enhance adsorption capacity and efficiency [35][41][48][49]. Thereby not treating other metal oxides.

A study where a pure ZnO adsorbent was prepared from commercial zinc oxide (from Aldrich) by using different methods, the glycerine- and combustion method, showed that the BET surface area varied significantly with preparation method [38]. These prepared samples were compared to a ZnO supplied by the same manufacturer (Aldrich). In the glycerine method  $\text{Zn}(\text{NO}_3)_2 \cdot 6\text{H}_2\text{O}$  was mixed with 40 w% glycerine (from Fluka) and 40 w% of water and slowly heated to 120 °C where  $\text{NO}_x$  started to produce. The mixture was poured into a stainless steel vessel and heated to 180 °C for 30 min. Large amounts of steam,  $\text{CO}_2$  and  $\text{NO}_x$  were formed and thus creating a solid and porous foam. The foam was finally grounded and calcined for 2h at 300, 400, 500 and 600 °C. In the combustion method, or urea method,  $\text{Zn}(\text{NO}_3)_2 \cdot 6\text{H}_2\text{O}$  and  $\text{CO}(\text{NH}_2)_2$  both supplied by Aldrich were dissolved and stirred in as little water as possible ( $\approx 5$  mL for 1 g of final ZnO). The solution was heated at a temperature of 500 or 700 °C. The solution first dehydrated until it started to swell and froth, then an explosive reaction occurred forming large amounts of gases and ZnO. The gas consisted mostly steam but also  $\text{N}_2$ ,  $\text{CO}_2$ . Product ZnO was ground to a fine powder and calcined at 600 °C for 1h [38].

The glycerine method showed a higher BET surface area than the commercial sample which increased with decreasing calcination temperature. At a calcination temperature of 300 and 600 °C the BET surface area was 50.3  $\text{m}^2/\text{g}$  and 10.1  $\text{m}^2/\text{g}$  respectively, compared to 7.8  $\text{m}^2/\text{g}$  of the commercial sample. A larger pore volume was also observed, a maximum of 0.30  $\text{cm}^3/\text{g}$  at a calcination temperature of 400 °C compared to 0.07  $\text{cm}^3/\text{g}$  [38]. The combustion method showed a lower BET surface area compared to commercial sample and maintained a relatively unchanged pore volume. They were experimentally evaluated by their breakthrough time and sulphur capacity using a feed of 100 ppm  $\text{H}_2\text{S}$  and He as balance at 250 °C and a GHSV of 100 000  $\text{h}^{-1}$ . The breakthrough time was determined to the time it took to measure 2 ppm of  $\text{H}_2\text{S}$  in the outlet gas [38]. Both the breakthrough time and sulphur capacity increased with surface area and pore volume, as would be expected due to a higher sulphur storage capacity and favourable morphology. The breakthrough times increased from 20 min for the commercial sample to 550 min prepared by the glycerine method with a calcination temperature of 300 °C and decreased rapidly with increased calcination temperature. More interesting is that a large jump in breakthrough time was observed between 400 and 500 °C, from 430 min to 20 min which might be due to different pore volume distributions obtained by different

calcination temperatures. Upon analysing the pore volumes before and after adsorption it showed that the majority of the smaller pores ( $<50 \text{ \AA}$ ) which had been dominating in the fresh sample were blocked [38]. Assumably by adsorbed sulphur.



**Figure 2.5:** ZnO pellets from PowerCell

When comparing sulphur capacity, the sulphur breakthrough capacity was  $31.4 \text{ mg S/g}$  adsorbent for the sample prepared by glycerine method at  $300 \text{ }^\circ\text{C}$ , instead of  $5 \text{ mg S/g}$  adsorbent as for the commercial ZnO. It was further concluded by a validated and experimentally fitted numerical model that the adsorption reaction is mainly controlled by internal transport of  $\text{H}_2\text{S}$  into the pellet core [38].

Similar results have been obtained when comparing the adsorption performance of a commercial ZnO 3mm extrudate samples (HTZ-5) supplied by Haldor-Topsoe and a modified ZnO powder with 42 w% Ca-bentonite prepared by Engelhard Corporation. The samples from Engelhard were prepared by mixing 12 g ZnO powder with 40 mL of saturated solution of water and  $(\text{NH}_4)_2\text{CO}_3$  and stirred for 2 h. 8 g of Ca-bentonite was calcined for 2 h in air at  $200 \text{ }^\circ\text{C}$ . The binder and ZnO solution was mixed and extruded followed by drying for 2 h at  $120 \text{ }^\circ\text{C}$  and calcination at  $300 \text{ }^\circ\text{C}$  for 2 h.

Using a feed with 8 ppm  $\text{H}_2\text{S}$ , 37 %  $\text{H}_2$ , 20 %  $\text{H}_2\text{O}$  ( $\text{N}_2$  as balance) at gas hourly space velocity (GHSV)  $8775 \text{ h}^{-1}$  and  $400 \text{ }^\circ\text{C}$ , showed that the Ca modified sample had a significantly longer breakthrough time of  $\approx 4 \text{ h}$  (at 0.1 ppm in outlet). Where the commercial extrudate sample exceeded breakthrough immediately. The sulphur capacity also increased from 12 to  $47 \text{ mg S/g}$  adsorbent [50]. The trend could be explained after examining the particles by scanning electron microscope (SEM) where a large difference in morphology was revealed, the Ca modified sample had a flake form whether the commercial sample was aggregated particles. If internal mass transfer diffusion is limiting and much due to the forming ZnS layer, the effectiveness of the flakes could be explained by its high external surface area and low internal mass transfer resistance [50]. Through these result one can again assume that morphology and structure through sample preparation methodology are two of the most important factors when using ZnO for adsorbent for sulphur species.

Evaluating the effect of introducing silica support to ZnO has been performed by preparing the Zn/SiO<sub>2</sub> samples using incipient impregnation of silica followed by drying

and calcination. ZnO was supplied by Sud-Chemie (G-72E) and BASF (SG-901) and samples were prepared with different amounts of ZnO. Analysing each showed that as the pure SiO<sub>2</sub> showed a large surface area of 330 m<sup>2</sup>/g and decreased rapidly as zinc content increased, possibly due to blocking of the smaller pores belonging to the SiO<sub>2</sub> structure. At the same time as the zinc content increased the sulphur capacity was enhanced until 21 wt% Zn where it levelled out. Through XRD analyses it was concluded that most zinc atoms were located within the pore system [35][48]. This indicates of a cooperation between the two species, a trade-off between accessible surface area and sulphur capacity. It should therefore theoretically be possible to find an optimum where the as many pores as possible are coated without being blocking the smaller ones by an excess amount of zinc.

Copper has been shown to be an effective dopant for ZnO/SiO<sub>2</sub> prepared by the incipient wetness method and sulphur capacity was reported to increase from  $\approx 53$  to  $\approx 77$  mg S/g adsorbent. Using iron promotion of ZnO/SiO<sub>2</sub> by the same procedure also enhanced the sulphur capacity to  $\approx 70$  mg S/g adsorbent [35].

Alumina support has also been examined due to its similar surface area of silica. The ZnO-Al<sub>2</sub>O<sub>3</sub> was prepared by heterogeneous precipitation. 0.3 M of zinc acetate dehydrate, Zn(CH<sub>3</sub>COO)<sub>2</sub> \* 2H<sub>2</sub>O (99.5 %), supplied by Merck was mixed with urea (Merck, 98 %) at a mole ratio 1:6. To the solution bayerite powder, Al(OH)<sub>3</sub> (98 %) supplied by Ardakan Industrial Ceramics Co. with a mean particle size of 4  $\mu$ m was added and placed in an oil bath followed by heating to 90 °C for 4 h. Precipitation started of zinc carbonate hydroxide, Zn<sub>5</sub>(CO<sub>3</sub>)<sub>2</sub>(OH)<sub>6</sub>, onto bayerite particles during the heating which was refluxed, filtered and washed with distilled water several times. The samples were then dried at 40 °C for 24 h and calcined at 400 °C for 3 h. The reference sample of pure ZnO was prepared by the same method but without the addition of bayerite powder [51].

It was reported that in a mixture of 20 wt% Al<sub>2</sub>O<sub>3</sub> and 80 wt% ZnO the surface area increased to 96 m<sup>2</sup>/g compared to pure ZnO of 16 m<sup>2</sup>/g [51]. In the same mixture the pore volume increased from 0.13 cm<sup>3</sup>/g to 0.29 cm<sup>3</sup>/g. With a feed of 1.02 % H<sub>2</sub>S (N<sub>2</sub> as balance) at 150 °C and 2000 h<sup>-1</sup> the breakthrough capacity (breakthrough at 5 ppm) increased from 0.028 g S/g sorbent of pure ZnO to 0.052 g S/g sorbent of ZnO-Al<sub>2</sub>O<sub>3</sub>. At the same time breakthrough time increased from 76 to 140 min respectively [51]. Once more result show that increasing the surface area and improving morphology are important factors for enhancing sulphur adsorption.

An interesting observation was reported on iron doped ZnO powder (from Umicore HP grade >99,99 %) prepared through the solid and liquid combustion method. After preparation by solid combustion the sample bulk density increased from 0.5 to 2.71 g/mL and its BET surface area decreased from 5 to 0.7 m<sup>2</sup>/g. After liquid preparation the opposite was observed with a decrease in bulk density to 0.12 g/mL and an increase in area to 39.6 m<sup>2</sup>/g. One could expect that the latter sample would have a longer breakthrough time due to its higher area. Testing these with 5000 ppm H<sub>2</sub>S in He at a temperature of 400 °C and GHSV of 12000 h<sup>-1</sup> showed that the sample prepared via solid combustion

was the better with longer breakthrough time followed by the commercial ZnO powder [33]. The answer seems to be in the differences in sulphur capacities, preparation through solid and liquid combustion method resulted in an adsorbent with high  $\text{H}_2\text{S}$  uptake/ $\text{m}^2$  and high  $\text{H}_2\text{S}$  uptake/g adsorbent, respectively. With solid combustion being better (with a high sulphur capacity per  $\text{m}^2$ ) even though liquid combustion gave a sample with high surface area, one can assume that through solid combustion the morphology and pore sizes is much more favourable. It should also be noted that the breakthrough profiles showed that preparing an adsorbent through both liquid or solid combustion reduced the overall transport resistance due to their sharper breakthrough behaviour. This might indicate that the transport resistance of both prepared adsorbents is more favourable compared to that of commercial zinc oxide but the pore sizes are better suited for  $\text{H}_2\text{S}$  adsorption when the adsorbent is prepared through the solid combustion method.

Using activated carbon with and without impregnation as a sulphur adsorbent has been studied due to its high surface area [52]. The activated carbon was supplied by Carbokarn Company Limited and impregnated by soaking it in KOH solution for 30 min followed by heating to  $100\text{ }^\circ\text{C}$  for dehydration; the finished sample contained 7 w% KOH. When impregnated the sample showed a considerable increase of sulphur capacity and breakthrough time. While the presence of  $\text{H}_2\text{O}$  promoted the sulphur capacity,  $\text{CO}_2$  decrease the overall adsorption performance due to competition of active sites [52]. The same effect of water was reported over activated carbons impregnated by other strongly basic compounds [53]. It has however been discussed and evaluated through mathematical models that formation of  $\text{SO}_2$  takes place over activated carbon in the presence of  $\text{O}_2$  and can be significant at higher temperatures ( $>300\text{ }^\circ\text{C}$ ). The reaction rate of  $\text{SO}_2$  was reported to be dependent on  $P_{\text{H}_2\text{S}}$ ,  $P_{\text{H}_2\text{O}}$ ,  $P_{\text{O}_2}$ , amount of adsorbed sulphur and the reactor temperature. It was however also concluded that  $\text{SO}_2$  formation is controlled by the partial pressure of sulphur and  $\text{O}_2$ . [54].

## 2.3 Methods of analysis

Analysis performed within this thesis are Brunauer-Emmett-Teller (BET) surface area, Barrett-Joyner-Halenda (BJH) pore size and volume analysis for pore structure evaluation and scanning electron microscopy (SEM) with energy-dispersive spectroscopy (EDS) is used to evaluate the contents of the adsorbent material. During experiments the product flow was continuously monitored by mass spectrometry (MS).

### 2.3.1 Surface area & Pore size distribution

The BET multilayer adsorption model makes it possible to evaluate surface areas in porous solids. The BET isotherm equation is shown in equation 2.12.

To analyse the surface area using the BET method, nitrogen is condensed and physisorbed onto the porous surface area at pressures varying from vacuum range of 5 mmHg up to saturation pressure,  $P_0$ . In order to be able to condense  $N_2$  inside the pores and determine its volume, the apparatus operates at  $-195.8$  °C, the boiling point of  $N_2$  [55]. To evaluate the pore volumes and their size distribution nitrogen is condensed inside the pores according to the Kelvin equation, equation 2.7. As relative pressure increases, nitrogen is first condensed inside small pores and fills up larger ones as pressure increases, the volume is measured continuously hence giving a volume distribution. Upon reaching saturation pressure the whole pore structure is filled with liquid. Using the obtained experimental values of  $v$  for a corresponding  $P$  the BET equation is used to determine  $v_m$  which in turn is used to calculate the surface area  $S_g$  through equation 2.16 [29].

$$S_g = \frac{\alpha v_m N_A}{V} \quad (2.16)$$

The same procedure is performed afterwards but with decreasing pressure hence desorbing the liquefied nitrogen inside the pores. The difference between the adsorption and desorption isotherm is called hysteresis and can be seen for porous solids. The hysteresis behaviour holds information about volume, size and area of the pores [56].

### 2.3.2 Scanning electron microscopy & Energy dispersive spectroscopy

Instead of using light as an ordinary optical microscope, higher resolution can be achieved by using electrons with a smaller wavelength. During SEM analysis an electron beam is generated by an electron gun which is focused and controlled by electromagnetic lenses and coils. The focused beam is directed to collide and interact with a sample resulting in a scattering of electrons when e.g interacting with a nucleus or other electron. There are different types of scattering but two common types are the primary and secondary backscattering electrons [57]. Secondary scattering are low energy electrons backscattered by coulombic interactions with the electrons in the sample and the emissions increases with increasing angle between the incident beam and the normal of the surface. The scattered electrons are collected by a detector to give a computer image. To analyse rough surfaces the angle can be varied to give a black and white image with great contrast where

the white parts correspond to high electron emissions and black parts to low electron emissions.

Primary backscattering are higher in energy where the incident electrons are backscattered by their inability to penetrate into the sample due to nuclei blocking its path, being at the surface or inside the sample. With increasing beam voltage the electrons can penetrate the sample further in before being backscattered, making the analysis deeper into the sample and hence over a larger volume. A higher atomic number (larger nucleus) increases the emissions of primary backscattering proportionally [57]. Analysing by primary backscattered electrons can therefore tell apart different atoms in a sample by their weight. [58]

To make a chemical analysis of a sample using EDS, the sample is bombarded with high-energy electrons that excite electrons belonging to the sample from their current orbital level to a higher energy orbital. The now vacant sites are reoccupied by electrons from orbitals further away from the nucleus, i.e having higher energy. The electron movements from high energy orbitals to a low energy orbitals are accompanied by releases of energy in the form of X-rays as shown in figure 2.6 [59][60]. These acts as identifiers for a specific atom and its orbitals why collecting and counting as many of the X-rays as possible is of interest to get a reliable result. If some are left aside their relative intensities are reduced compared to other atoms and thus the calculated compositions will not represent the sample [61].

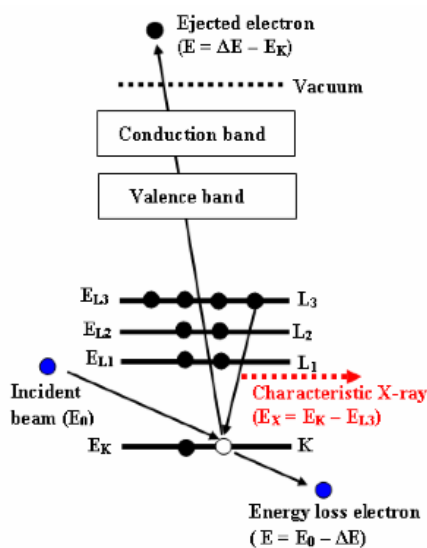


Figure 2.6: X-rays production in EDS [60]

### 2.3.3 Mass Spectrometry

Mass spectroscopy (MS) is a tool to analyse the molecular masses in a sample and the apparatus can be divided into three parts. First the sample enters the ioniser where species are ionised by one of several different ionisation methods. The pressure in the ionisation chamber is kept very low, usually at  $10^{-6}$ - $10^{-8}$  mbar, to minimise reaction tendencies between ions and molecules. Secondly the ions go through the analyser which functions as a separator and separates the different species by their mass-to-charge ratio ( $m/z$ ). Last in line is the detector which measures and amplifies the ion current and monitors it as a mass spectrum in a computer software program [62]. The most common detector is the electron multiplier which has a fast response and high sensitivity [63].

# 3

## Methodology

The work procedure towards a design proposal of the desulphurisation unit includes adsorbent characterisation, modelling and experimental investigations. Characterisation of fresh and sulphur contaminated pellets is performed to evaluate the amount of adsorbed sulphur and how the adsorbent has been affected by the process. Experiments are performed to validate the models using experimental conditions as similar as possible to the real fuel cell system.

### 3.1 ZnO characterisation

The adsorbent was prepared and bought by an external company hence exact properties are little known about. What could safely be stated in the beginning of the project is that the adsorbent consists of spherical pellets of zinc oxide with a diameter of 2-5 mm. By analysing the pellets before and after the long-term test sulphur adsorption its properties are evaluated in more detail. The test was a full scale, performed for 1535 h and connected to a diesel reformer with an average diesel sulphur content of 4.8 mg/kg. It was not run until reaching saturation of the ZnO pellets why saturation experiments in lab-scale at Chalmers are to be performed.

The tested adsorption unit at PowerCell was constructed in five cylindrical layers in axial direction separated by a metal web. To analyse pellet efficiency at different locations in the unit it was necessary to extract them in the same way from each layer why a metal cutter was constructed, its template is shown in figure 3.1. The layers were numbered one to five from inlet to outlet and the extracted samples were analysed from each compartment to determine how the properties changed throughout the bed. Samples were at first hand chosen from the center compartments of the adsorption bed and along its axial direction because they were believed to give most information and otherwise more samples could be analysed later on by the same procedure. A sample of fresh pellets was also analysed to determine its pure properties as comparison. The

samples will hereinafter be referred to as 1C, 2C, 3C, 4C, 5C and fresh sample, the number denotes which layer the sample was extracted from and the letter denotes the center compartment. The six different samples were also analysed for their sulphur content by an external company. This analysis was performed on 10 g of pellets from each sample to measure an average value, hence not giving any readings in radial directions. To be able to compare radial SEM measurement with the an average value, the SEM measurements were integrated to obtain a average value over the pellet volume.

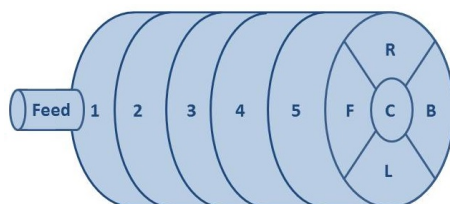


**Figure 3.1:** Template for pellet extraction

### 3.1.1 BET surface area & Pore size distribution

Samples 1-5C and a fresh sample were dried in nitrogen at 180 °C for 3 hours for degassing before mounted and analysed using a Micromeritics Tristar 3000 instrument. The apparatus uses liquid nitrogen adsorption to determine their surface area and pore distribution according to section 2.3.1. An equilibration interval of 5 seconds was used to allow equilibrium at each point of measurement and the operating temperature was -195.8 °C.

### 3.1.2 SEM & EDS analysis

Quantitative EDS measurements of the different samples were conducted using a Quanta 200 FEG-ESEM from FEI. The analysis was performed at settings of low vacuum, an accelerating voltage of 20 keV with a live time (sampling time) of 60 seconds. The samples were analysed for their sulphur content. Each pellet sample was cut into two half spheres, one was placed on the holder with its convex side upwards and the other with its cross section upwards and kept in place by carbon tape. This made it possible to measure the sulphur content both at the pellet surface and in radial direction. The radial measurements in each sample were made twice at three different radii, but at different directions from the center. One measurement was made on the surface of each pellet. The measurements were made over a small area at the locations instead of at a point to reduce local variations.

## 3.2 Experiments

To perform the experiments at Chalmers University of Technology an isolated reactor was packed with fresh ZnO pellets and the outlet gas composition was analysed continuously

using MS apparatus. The final experimental design included H<sub>2</sub>S, H<sub>2</sub>O, H<sub>2</sub> and inert Ar at temperatures between 100 and 300 °C.

### 3.2.1 Parameters & calibration

According to section 2.1, reformat contains a mixture of H<sub>2</sub>, H<sub>2</sub>O, CO, CO<sub>2</sub> and H<sub>2</sub>S which all can be varied during the experiments to analyse their dependencies. In addition also temperature and GHSV are important operating conditions and thus could be varied which in total leaves a large number of experiments.

To simplify and reduce the number of experiments, HSC Chemistry 7.0 (Outokumpu Research Oy, Pori, Finland) was used to evaluate which gas components could be neglected due to an insignificant effect on adsorption equilibrium. The commercial software calculates pure equilibrium conditions and does not take any reaction rates or mass transfer resistances into account. The calculations were performed for a gas composition as shown in table 3.1 and over a stoichiometric excess amount of ZnO compared to H<sub>2</sub>S.

**Table 3.1:** Composition used at equilibrium calculations

Species	Concentration
H <sub>2</sub> O	35 %
CO <sub>2</sub>	20 % (dry)
CO	5 % (dry)
H <sub>2</sub>	40 % (dry)
H <sub>2</sub> S	0.67 ppm (dry)
N <sub>2</sub>	Balance

Each concentration of the components as well as temperature were varied to evaluate their effect on the hydrolysis reaction and H<sub>2</sub>S equilibrium. Their dependencies at 300 °C are shown in appendix A.1. A significant effect on the equilibrium concentration was only observed for H<sub>2</sub>O and temperature, while the dependency shown for CO was explained by the water-gas shift reaction which consumes water thereby improves adsorption efficiency according to the hydrolysis reaction. The findings meant that CO, CO<sub>2</sub> and H<sub>2</sub> could be kept constant in the background mixture to reduce the number of experiments but still including their effect on molecular transport. Note that the constant value for H<sub>2</sub>S does not imply that H<sub>2</sub>S has no effect on adsorption, as more H<sub>2</sub>S is available more ZnS will be produced according to hydrolysis reaction and hence keeping H<sub>2</sub>S at its equilibrium concentration. The steep increase at low concentrations of H<sub>2</sub>S was explained by the hydrolysis reaction equilibrium constant which was very large at 300 °C compared to the amount of H<sub>2</sub>S making the latter limiting. This was not observed for lower temperatures where equilibrium concentration of H<sub>2</sub>S was constant for the entire concentration interval.

By keeping three parameters constant a fractional factorial design of  $2^{7-3}$  with 2

center points was chosen for the experiments and shown in appendix A.2, where '0' denotes conditions at the center point, '+' is an increase and '-' is a decrease relative to the center point. The eighteen experiments should give a good understanding in the adsorption and its dependencies but due to problems with the mass flow controllers CO and CO<sub>2</sub> could not be included in the gas mixture. Conditions for the experimental plan are shown in table 3.2. The reason for not including the same amount of water as found in the reformat, see table 3.1, was because condensation could become a problem if exceeding 10 %. The background gas mixture was not allowed to contain more than 4 % H<sub>2</sub> due to safety precautions.

**Table 3.2:** Experimental point conditions, X denotes value that must be determined

	-	0	+
H <sub>2</sub> S [ppm]	100	150	200
H <sub>2</sub> O [%]	6	8	10
Temperature [°C]	100	200	300
GHSV [h <sup>-1</sup> ]	X	X	X

Because of the small amount of information known about the ZnO pellets and because no articles could be found that discuss the same experimental conditions and sizes of spherical ZnO pellets (diameter: 4 mm), a suitable value for GHSV could not be predetermined for the experiments at this time. It was therefore important to find a value that would result in reaching adsorption equilibrium in a reasonable amount of time in order to be able to perform all experiments. The plan was to find a GHSV that corresponded to a experimental time of 30-60 min. This was done in a "trial-and-error" fashion by varying the bed length of the fresh ZnO pellets through its weight, starting at a qualified initial guess. The initial guess was calculated by assuming a specific capacity of H<sub>2</sub>S for the ZnO based on similar research experiments and then determining a stoichiometric time at which the assumed amount of H<sub>2</sub>S had passed the reactor. This assumes that all sulphur atoms entering the systems are adsorbed. Feed flow rate was set to 3449 ml/min, close to the highest recommended for the equipment, to keep a high inflow of H<sub>2</sub>S and therefore experimental times low.

By the described procedure it was found out that the pellets were affected by a large slip. This was observed because breakthrough was immediately registered on the MS and the GHSV had to be decreased, by increasing bed weight. The bed weight was increased several times before no immediate breakthrough was observed and experiments could start. After determining a maximum GHSV that can be used for the experiments, a calibration curve had to be produced as the MS apparatus does not directly measure concentrations but mass-to-charge ratios. The calibrations were experimentally produced by analysing the MS signal of H<sub>2</sub>S at different temperatures and feed compositions to an empty reactor. Each point was held for one hour in order to get a converged signal and hence obtaining a corresponding signal strength to concentration of H<sub>2</sub>S. After a drifting signal for argon in the MS apparatus was found the analysed signal of H<sub>2</sub>S was

weighted with a factor as

$$H_2S \text{ signal}_{at \text{ time } t} \times \frac{Ar \text{ signal}_{at \text{ time } t}}{Ar \text{ signal}_{at \text{ } t=0}}$$

By the multiplication a drift in the MS was compensated for by assuming that all gas components were equally effected by the drift. The argon drift during an experiment can be seen in appendix A.2

It was later however discovered that the measured time between injecting H<sub>2</sub>S and registering it on the MS was due to a significant sticking onto surrounding surfaces, as glass tube and pipes, why experiments had to be aborted and GHSV to be reduced even further. By the time the bed was long enough to trap incoming H<sub>2</sub>S, the value for GHSV was 43900 h<sup>-1</sup>. The whole procedure of finding a suitable GHSV took longer time than expected due to issues with the equipment which delayed the experimental section of the project. The delay resulted in that after finding the GHSV, the experimental design in appendix A.2 had to be simplified down to only varying the H<sub>2</sub>O concentration and the temperature as shown in table 3.3.

**Table 3.3:** Simplified and final experimental design

H <sub>2</sub> O	Temperature
+	+
-	+
+	-
-	-
0	0
0	0

As experiments were resumed with a lower GHSV, experiments were started with center point conditions now as shown in table 3.4.

**Table 3.4:** Center point gas composition

Parameter	Value
H <sub>2</sub> O	9.6 %
Temperature	200 °C
H <sub>2</sub> S	102 ppm
H <sub>2</sub>	413 ppm
Ar	Balance
GHSV	43900 h <sup>-1</sup>

### 3.2.2 Experimental setup

Experiments were performed using a quartz tube reactor surrounded by insulation to reduce heat losses. A schematic view of the setup is shown in figure 3.2. The quartz reactor tube had a inner diameter of 22 mm and to reduce wall effects the inside of the tube was coated with quartz wool which resulted in an effective inner diameter of  $\approx 10$  mm to be filled with fresh ZnO pellets. Experiments were performed with 6,1 g ZnO pellets which resulted in a bed length of  $\approx 6$  cm and a GHSV of  $43900 \text{ h}^{-1}$ .

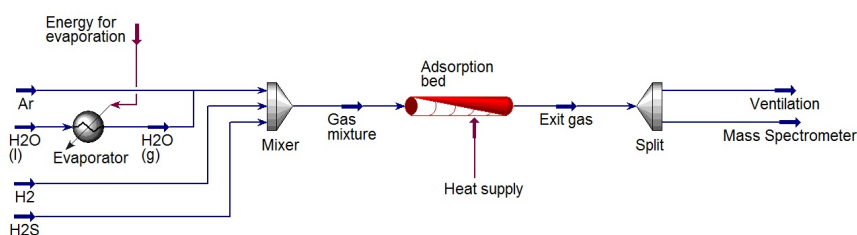


**Figure 3.2:** Flow scheme of experimental setup

### Mass Spectrometry

A Hiden HPR-20/QIC transient mass spectrometer with a quadrupole mass analyser was used to measure  $\text{H}_2\text{S}$  in the exiting gas and to determine the breakthrough profile. The detector used during experiments was the secondary electron multiplier detector for its higher sensitivity with an amplification set to 835 V. The measured masses are shown in table 3.5.

**Table 3.5:** Measures values in mass spectrometer

Species	Measured value [m/z]
$\text{H}_2$	2
$\text{H}_2\text{O}$	18
Ar	20
$\text{O}_2$	32
$\text{H}_2\text{S}$	34

## 3.3 Breakthrough modelling

To model the breakthrough profile a set of partial differential equations in axial length and time were derived from a global material balance over the adsorption bed as seen in equation 3.1. The mass balance assumes an uncontaminated adsorbent bed at time

$t=0$  with no axial dispersion. The void fraction is estimated to 0.26 by assuming the pellets to be perfectly packed in a hexagonal close-packed structure. The adsorption term was modelled through the reaction term using the shrinking core model and the linear driving force model explained in section 2.2.5.

Substituting the reaction term in 3.1 with equation 3.2 the shrinking core model is obtained, the linear driving force model is obtained if instead substituted with equation 3.3.

Global mass balance:

$$u \frac{\partial C}{\partial z} + \frac{\partial C}{\partial t} + \frac{(1 - \epsilon_b)}{\epsilon_b V_{\text{pellet}}} \frac{\partial q}{\partial t} = D_L \frac{\partial^2 C}{\partial z^2} \quad (3.1)$$

where  $u$  is bulk flow velocity,  $C$  is bulk concentration of  $\text{H}_2\text{S}$ ,  $\epsilon_b$  is bed void fraction and  $q$  is  $\text{H}_2\text{S}$  loading on pellet.

Shrinking core model:

$$-\frac{\partial q}{\partial t} = \frac{4\pi r_c^2 C}{\frac{1}{k_s} + \frac{r_c(R_p - r_c)}{R_p D_e}} \quad (3.2)$$

where  $R_p$  is the initial pellet radius,  $r_c$  is radius of the unreacted core surface and  $k_s$  is rate of adsorption at  $r_c$  and  $D_e$  is the effective product layer diffusion rate. Note that the gas boundary layer diffusion term in equation 2.14 is assumed negligible.

Linear driving force:

$$\frac{(1 - \epsilon_b)}{\epsilon_b V_{\text{pellet}}} \frac{\partial q}{\partial t} = -k_f a (C - C^*) \quad (3.3)$$

where  $k_f$  is the effective mass transfer coefficient,  $a$  is the pellet surface area per unit volume,  $C$  is the adsorbate bulk concentration and  $C^*$  is the equilibrium adsorbate bulk concentration that corresponds to the pellet loading.  $C^*$  is calculated at each time step through one of the adsorption isotherms; Langmuir, Freundlich or BET isotherm by knowing coverage ( $\theta$ ). Coverage can be calculated as the ratio of adsorbed sulphur to adsorbent capacity. This makes capacity an important parameter to estimate for the ZnO pellet and is obtained by calculating the integral above the breakthrough profile of a saturated sample.

# 4

## Results

The results from the analyses are reported for the fresh and used ZnO pellets in terms of sulphur content, BET surface area and pore size distributions. The experimental procedure after adopting a low GHSV due to a large slip resulted in very time consuming experiments and the result is shown.

### 4.1 ZnO characterisation

Pellets from the desulphurisation unit having undergone the long-term test were evaluated by their sulphur content, BET surface and pore size distribution. The analyses was performed for samples 1-5C and for a fresh sample for reference. Due to suspicions of an uneven flow distribution, the rest of the compartments of the first layer was examined for their sulphur content at pellet surfaces.

#### 4.1.1 SEM & EDS

The evaluated sulphur content of the long-term test pellets from PowerCell are shown in figure 4.1. The pellet is analysed in radial direction at its center,  $\frac{R}{3}$ ,  $\frac{2R}{3}$  and surface where R is the pellet radius relative its center. It is seen that the surface of sample 1C has not trapped as much sulphur as the three downstream layers (2-4C). This raises questions because the concentration should be higher in the first part of the bed and have trapped more sulphur according to section 2.2.5. Otherwise the results seems reasonable and a clear gradient is seen in radial direction of the pellet with less sulphur at its center for all samples. The radial gradient for sample 2C is shown in figure 4.2. Complete EDS tabular values and radial plots for all of the samples can be seen in appendix A.3.

Because of the anomaly in sample 1C, all of the compartments in the the first layer were examined to evaluate if the flow had been unevenly distributed in the first layer through the test due to the radial inlet, as was shown in figure 3.1. The sulphur content of the

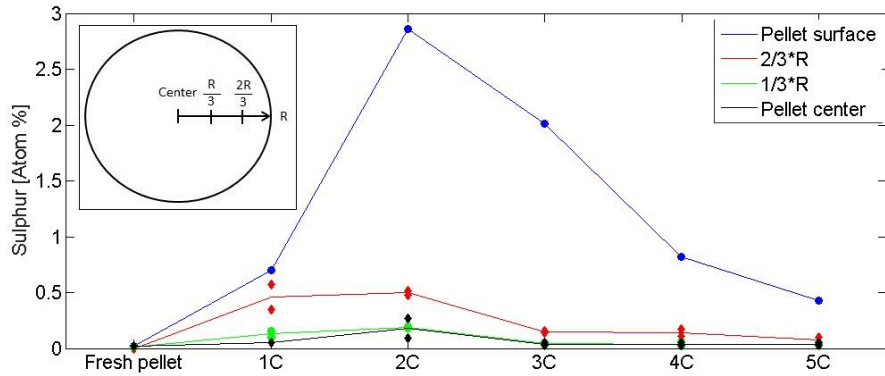


**Figure 4.1:** Sulphur content in center compartments

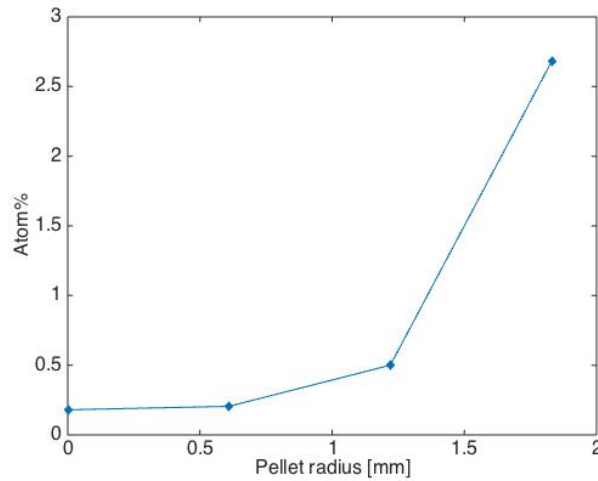


**Figure 4.2:** Radial sulphur content in 2C

pellets for the first layer is shown in figure 4.3. The small variance indicates that the flow indeed have been dispersed in the first layer. Note that the content at sample 1C showed a small increase compared to previous analysis but not enough to suspect that the anomaly could be caused by a bad reading.

The anomaly in sample 1C was also compared to the analysis performed by an external company. It is important to mention that the external analysis was made over 10 g of pellets from each sample unlike from the SEM-EDS measurements. SEM-EDS analyses were made on one pellet from each of the samples 1-5C and local variations may affect its reliability. The comparison is shown in figure 4.4 and it is seen that the trends contradicts each other where the external analysis shows a more reasonable concentration front inside the desulphurisation unit. Tabular values can be seen in appendix A.3.

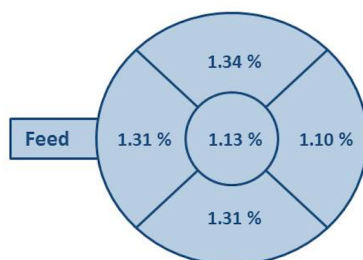


**Figure 4.3:** Sulphur content in first layer

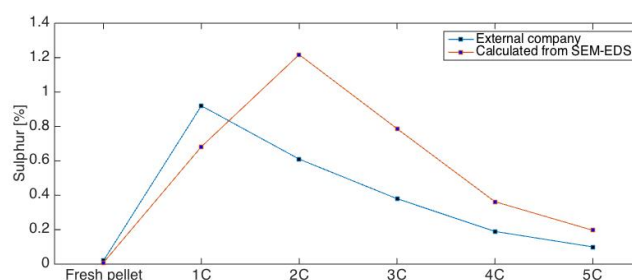


**Figure 4.4:** Comparison of sulphur content

During the SEM-EDS analysis an additional observation that chromium is present on the pellet surfaces was made. As chromium was not observed on fresh pellets it had entered the system during the long-term test. Presumably it comes from upstream stainless steel pipes, which can and is assumed to have affected the sulphur removal performance during the long-term test. The chromium content at pellet surfaces in samples 1-5C is shown in figure 4.5. The complete EDS tabular values for each of the samples can be seen in appendix A.3. Note that chromium was only observed at the surfaces and had not entered the pellet porous structure as the case for sulphur.

#### 4.1.2 BET surface area & pore volume

Surface areas and pore volumes are reported in table 4.1 for samples 1-5C and fresh sample. It is clearly shown that after adsorption the specific area is significantly reduced, presumably as trapped sulphur or chromium blocks some pores and making them inaccessible. However, the the measured BET area is specific, i.e. divided by the weight of the sample, a weight increase of the sample due to e.g sulphur adsorption would result in a lower specific surface area whether or not pore are blocked by any adsorbent. Note that the area for sample 1C is again not following the expected trend. As layer one is in the first part of the bed a larger amount of adsorbed sulphur is assumed with more blocked pores which reduces the accessible surface area and volume.

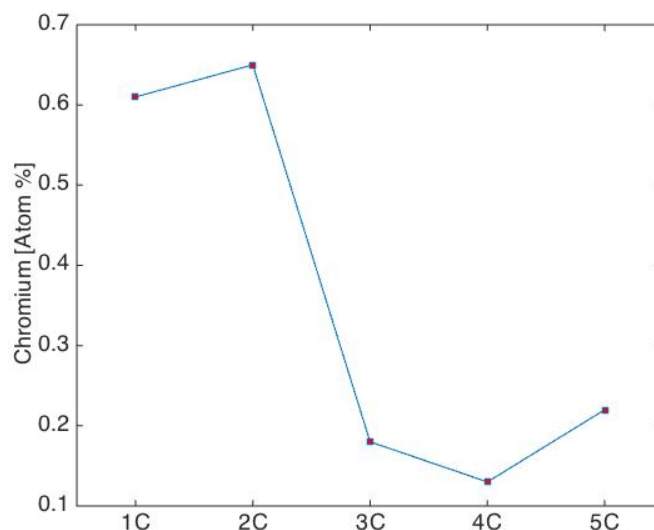


**Figure 4.5:** Content of chromium at pellet surfaces for each sample

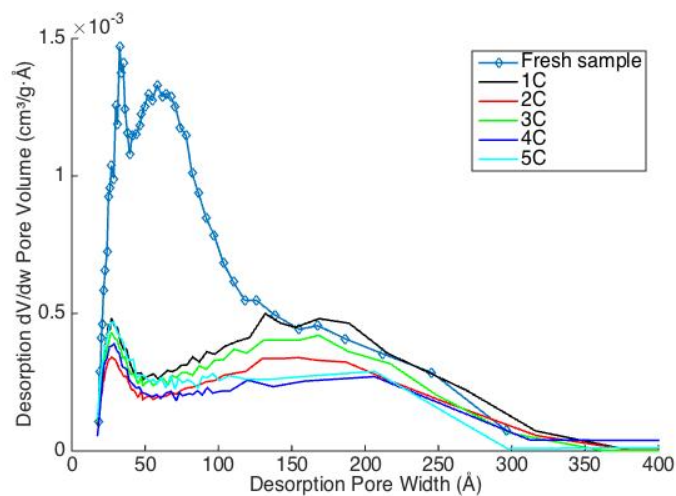
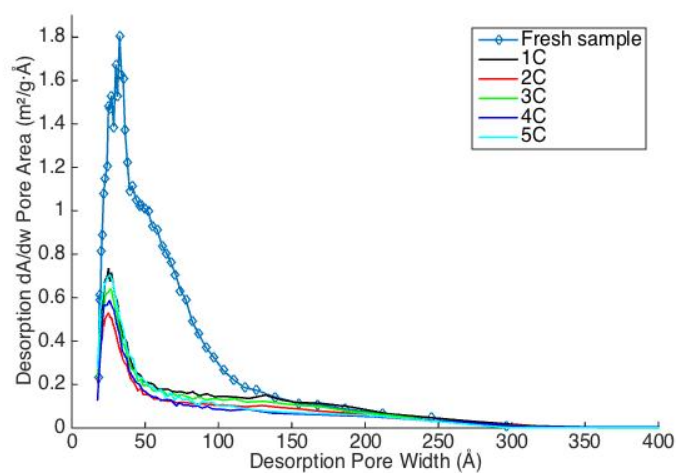
**Table 4.1:** BET Surface area

Sample	Fresh	1C	2C	3C	4C	5C
<b>BET Surface area <math>\text{m}^2/\text{g}</math></b>	72.5	37.1	27.6	32.2	32.0	32.9
<b>Pore volume <math>\text{cm}^3/\text{g}</math></b>	0.17	0.11	0.08	0.09	0.12	0.09

### 4.1.3 Pore size distribution

Measured pore volume and pore area distributions for samples 1-5C and the fresh sample are shown in figure 4.6-4.7. The graphs are a representation of the distribution of desorption pore volumes,  $V$ , and areas,  $A$ , versus pore width,  $w$ , according to section 2.3.1. In figure 4.6 it is seen that a large fraction of the pore volume is made up by pores of size 30-150 Å. It is also noticed that the pore volume is reduced after adsorption for all pore widths but especially for small mesopores (25-120 Å). The result indicates that trapping sulphur within the pore system significantly reduces the availability of volume present in the pellet which is assumed to reduce the overall efficiency of the material. It is here not possible to evaluate the individual contribution of the trapped sulphur and chromium on the pore volume change.

The same reasoning can be applied to figure 4.7 which reveals that the majority of the available area is made up of pores of size 25-110 Å and decreases with increasing pore size. After adsorption, pores of sizes 20-120 Å are significantly reduced in their available surface area. As adsorption is a surface process the significantly lower area is assumed to slow down the the overall reaction rate. Again, it is not here possible to evaluate individual effects of sulphur and chromium.

**Figure 4.6:** Pore volume distribution**Figure 4.7:** Pore area distribution

## 4.2 H<sub>2</sub>S Adsorption experiments

H<sub>2</sub>S adsorption experiments started out as initially planned according to section 3.2 with a considerably lower GHSV than initially expected. After performing an experiment and fitting calibration data a H<sub>2</sub>S breakthrough profile is obtained by plotting outlet concentration versus time. The breakthrough profile for an experiment using a feed of 102 ppm H<sub>2</sub>S, 9.6 % H<sub>2</sub>O, 413 ppm H<sub>2</sub> at 200 °C and a GHSV of 43900 h<sup>-1</sup> is shown in figure 4.8.

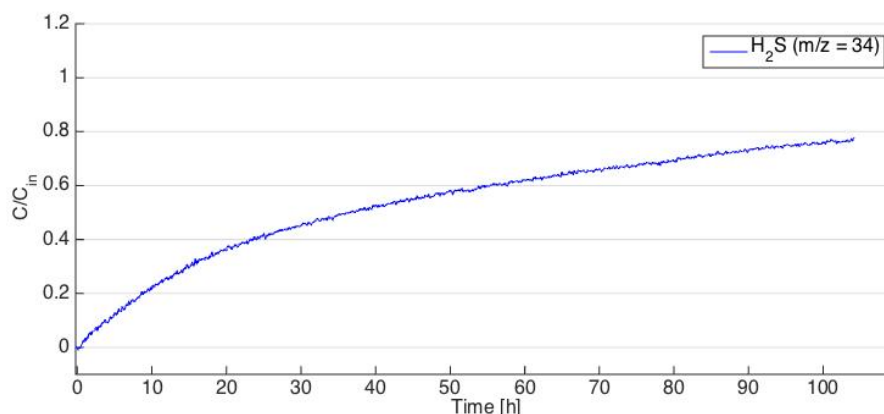


**Figure 4.8:** Adsorption experiment for 102 ppm H<sub>2</sub>S, 9.6 % H<sub>2</sub>O, 413 ppm H<sub>2</sub> at 200 °C and GHSV=43900 h<sup>-1</sup>

From figure 4.8 it is seen that the outlet concentration did not reach the inlet ( $C/C_{in}=1$ ) and hence the ZnO adsorbent never reached saturation which affects the upcoming estimation on sulphur capacity. More important is the fact that it took over 105 hours to reach a value of  $C/C_{in}=0.77$  with  $GHSV=43900$  h<sup>-1</sup>. This issue was not expected and the experiment had to be cancelled after 105 h because the reserved experimental time had run out. The stretched out look of the H<sub>2</sub>S breakthrough profile reveals that the system deviates much from ideal adsorption behaviour and is affected to a large extent by mass transfer resistances, as discussed in section 2.2.5. The amount of time needed to reach saturation of the pellets could not be given each experiment with the experimental plan developed in section 3.2, why only one experiment could be performed due to the time delay from finding an appropriate GHSV.

The experiment can however be used to estimate the sulphur capacity of the pellets by assuming that the material is saturated or close to saturation. The integral above the H<sub>2</sub>S breakthrough profile and up to  $C/C_{in}=1$  is proportional to amount of trapped sulphur and after applying calibrational data this amount can be calculated. The sulphur capacity of the pellets was estimated in this way while the amount of H<sub>2</sub>S being adsorbed onto surrounding equipment surfaces was neglected. Adsorption on equipment was evaluated by comparison with a H<sub>2</sub>S breakthrough profile in an empty reactor, shown in appendix A.2. The profile shows the first injection of H<sub>2</sub>S during calibration and corresponds to a feed of 51 ppm of H<sub>2</sub>S, 9.7 % H<sub>2</sub>O, 417 ppm H<sub>2</sub> at 200 °C and a GHSV of 43900 h<sup>-1</sup>. It took 7 min for the MS to register H<sub>2</sub>S in the outlet gas which indicated that there are tendencies for H<sub>2</sub>S to adsorb onto the surrounding walls of the reactor and tubes. The 7 minutes would be a significant factor indeed if short breakthrough experiment were performed but as the H<sub>2</sub>S adsorption experiment continued for 105 h the sticking is neglected.

Calculating the integral and assuming that the zinc content is 92 % (according to manufacturer) showed that 0.026 mole sulphur has been trapped by the adsorbent. With

a bed weight of 6.1 g pellets the value corresponds to a molar sulphur-to-zinc ratio of 0.379 in the pellets, hence 37.9% of the ZnO has been converted according to the hydrolysis reaction 2.9. By assuming that the pellet is saturated its capacity is 137.4 mg S/g pellet.

### 4.3 Alternative adsorbent material

The literature review in section 2.2.6 treated some different material compositions and manufacturing processes and their influence on sulphur adsorption efficiency was discussed. When comparing them individually it is difficult to say which adsorbent would be best suited for PEM fuel cell systems. Constraints do however not allow doping of metals as copper or iron due to contamination of downstream catalysts and adsorbent efficiency should be optimised for low temperatures, low sulphur and high steam inlet concentrations. The review states that compact ZnO pellets is not the best option due to a low BET surface area, pore volume and sulphur capacity. These properties should be enhanced e.g. by introducing a pore system of appropriate dimensions in the solid adsorbent and importance lies in achieving favourable pore sizes that reduce the internal mass transfer resistance. From the results given in section 4.1.3 it was seen that 25-120 Å pores were effected to a large extent during the long-term test. Although it is difficult to determine the best material, it is recommended to use a mixture of ZnO and either SiO<sub>2</sub> or Al<sub>2</sub>O<sub>3</sub> and interest lies in testing ZnO/SiO<sub>2</sub> with 21 wt% of ZnO to optimise surface area and pore volumes and thereby sulphur capacity.

Another interesting possibility that was found during the literature review is to use activated carbons which has large surface areas and after impregnation with KOH shows good capabilities to act as a sulphur trap. Particular interest of using activated carbons in PEM fuel cells comes from the fact that steam promoted the sulphur capacity, which is high in the system at PowerCell and today reduces the overall desulphurisation effectiveness according to hydrolysis reaction 2.9. The issue of SO<sub>2</sub> production would also be counteracted by the reducing atmosphere in the reformat gas.

# 5

## Discussion

### 5.1 Design proposal

Due to the long experimental time of the lab-scale H<sub>2</sub>S adsorption experiment it was not possible to perform all the planned experiments and the objective of proposing a design of a full-scale desulphurisation unit was not met. In order to safely propose a design the adsorption model developed needs to be validated through reliable experiments. Effort were made to search literature for values for diffusivity and reaction rates needed for validation but no reliable values were to be found. The experiments had either been performed with a dissimilar gas composition or ZnO composition and morphology.

### 5.2 Performance of the long-term test

The long-term test at PowerCell was analysed in axial direction of the adsorbent bed to evaluate the amount of adsorbed sulphur. As the long-term test had not saturated the pellets a concentration gradient of trapped sulphur was to be expected as discussed in 2.2.5. The question of why the first layer shows a lower sulphur content is not answered. One cause was thought to be an uneven flow distribution due to a radial inlet direction or a misleading analysis on the pellet surface. Answers were believed to be given by analysing the whole first layer and sample 1C again on a different pellet. If there had been an uneven flow it would be seen as a significant difference in the amount of trapped sulphur between the compartments and if there was a misreading on sample 1C the first time it would be seen as a significantly higher sulphur content in the new analysis. Suspicions of an uneven flow were ruled out due to no significant variance in the first layers and the extra analysis on sample 1C only gave a slightly higher but otherwise similar result which makes a misreading more unlikely. If flow indeed was evenly dispersed in the first layer it seems unlikely that it would be uneven in the upcoming ones. An uneven flow would in that case probably be due to creation of canals inside the bed but keeping in

mind that the average pellet diameter is relatively large with  $\approx 4$  mm together with a low flow rate the latter cause also seems unlikely.

To further investigate the issue, the radial sulphur readings from SEM-EDS were integrated to get a content over the whole pellet and compared to an external company's analysis where average sulphur contents in sample 1-5C were evaluated. It is important to mention that the external analysis was performed over a larger amount of pellets from each compartment while SEM-EDS analyses were performed over only one pellet which can deviate from the average but the same trend would be expected from both. A tabular comparison can be seen in appendix A.3.

The external analysis contradicts the SEM-EDS readings showing an expected decrease in sulphur content from the inlet to the outlet of the adsorbent bed but also shows a lower amount of sulphur for all layers except for the first, see figure 4.4. This trend is more likely but with both SEM-EDS and BET area analyses following the same trend it would be of interest to continue analysing the layers to clarify the different results. One possibility is local variations when making point analysis with SEM-EDS and there is a chance that the analyses on the surface on samples 2C and 3C was performed at a local high values and hence also giving a higher integrated amount of sulphur. Apart from the anomaly at the surface of sample 1C the SEM-EDS readings are reasonable with a decreasing sulphur content for downstream layers with a clear sulphur gradient inside the pellet indicating a significant mass transfer resistance. The mass diffusion resistance was also observed during experiments as a large slip around the pellets and it took time for sulphur to diffuse into the porous structure of the pellet.

Another possibility for the anomaly measured by SEM-EDS is that chromium is affecting the adsorption performance and blocking some of the pore structure. In figure 4.5 below it is seen that the first two layers from the inlet showed much larger content of chromium which might have affected the sulphur removal. It is not possible to say from the measurements alone when or how long into the long-term test chromium started to coat the pellets surfaces. If chromium had entered the system in an early stage it is possible that its coating complicated the sulphur adsorption in the first layer and hence letting  $\text{H}_2\text{S}$  slip through into the second layer, which would explain the high sulphur content in sample 2C. As chromium has covered the pellets in the first layer it continues into the second and the bed is subjected by two concentration fronts, one of sulphur and one of chromium. By looking at the chromium front in figure 4.5, it shows a more ideal behaviour than the for sulphur and it does not experience a lot of mass transfer resistances in the bed which agrees with the observation that chromium is only trapped on the surfaces where mass transfer resistances are low. This assumes that chromium can not enter the ZnO pores. The whole reasoning does however not explain the differences between the external analysis and SEM measurements.

The results from BET analysis showed that the pore structure in terms of volume and area is made up by small meso pores of widths ranging from 30-150 Å and 25-110 Å

respectively. After the long-term test at PowerCell the pore structure was affected to a large extent in both volume and area distribution. The adsorption process reduced the area distribution for all pore widths but to a lesser extent pores with sizes around 25 Å which were able to maintain about half of their specific area. The pore structure's volume was reduced for pores between 25-125 Å after adsorption but relatively unchanged for larger pores. These results indicates that the adsorbent material's pore structure is being blocked during the desulphurisation process and it is likely that active sites of ZnO are made unavailable hence reducing total capacity and effectiveness. Whether the blockings are by chromium or sulphur is not possible to evaluate exactly here but is assumed to be a combination where chromium is blocking the surfaces and sulphur is blocking both surfaces and internal structure.

It can be assumed that a larger pore will maintain unblocked for a longer time but it can not safely be said that an adsorbent having larger pores are intrinsically better because the bondings of zinc and sulphur is not evaluated here. Larger pores also reduces the total surface area as a pellet can hold fewer large pores than small pores. Exactly how the pore structure affects the adsorption is yet unknown but it is more likely that sulphur atoms bind at the surface where they are more likely to collide with an site of ZnO which is also assumed in both shrinking core and linear driving force model.

### 5.3 Adsorption model

The objective for this thesis was to propose a design for a desulphurisation unit but without complete experimental results the model validation and design proposal remains to be done and left for future work. Its development is however finished by applying a global mass balance over the desulphurisation unit and modelling the reaction term by either the linear driving force or shrinking core model.

The developed model can however be tested to make sure it models a somewhat similar H<sub>2</sub>S breakthrough profile as the one obtained during the lab-scale experiment at Chalmers. This was done by using literature values for diffusional and reaction rates where a shrinking core model was validated on pure ZnO granulates of 0.34 mm using a gas composition of 100 ppm H<sub>2</sub>S in He at 250 °C. The reported values are  $D_{eff}=5\times 10^{-8}$  m<sup>2</sup>/s and  $K_r=1107\times \exp(\frac{-3257.17}{T})$ . The procedure does not validate or dismiss the model in any way but only used as a reality check and the values are validated for only similar but not equal conditions. The biggest difference is the small granulate size which is a factor ten smaller than the ZnO at PowerCell and the experiment does not include H<sub>2</sub>. Using literature values in the unvalidated shrinking core model and putting conditions and bed dimensions as the one used during the lab-scale experiment at Chalmers the following result is obtained, see figure 5.1-5.2.

The model seems to overestimate the outlet concentration of H<sub>2</sub>S compared to the experiment over the whole time range of 105 h. By defining a breakthrough concentration as  $C/C_{in}=0.05$  the experiment with its calibration gave a breakthrough time of 93 min while the model predicted 43 min. The difference is significant but much likely to be

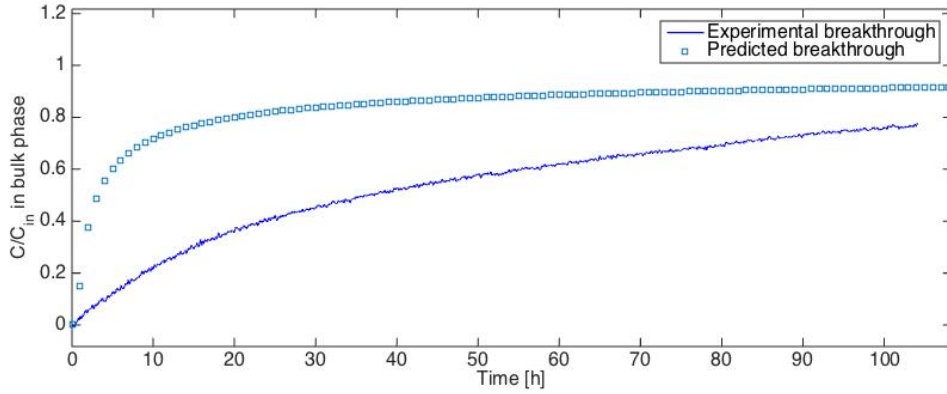


**Figure 5.1:** Predicted  $\text{H}_2\text{S}$  breakthrough profile for the experiment by shrinking core model for 102 ppm  $\text{H}_2\text{S}$  at 200 °C and  $\text{GHSV}=43900 \text{ h}^{-1}$

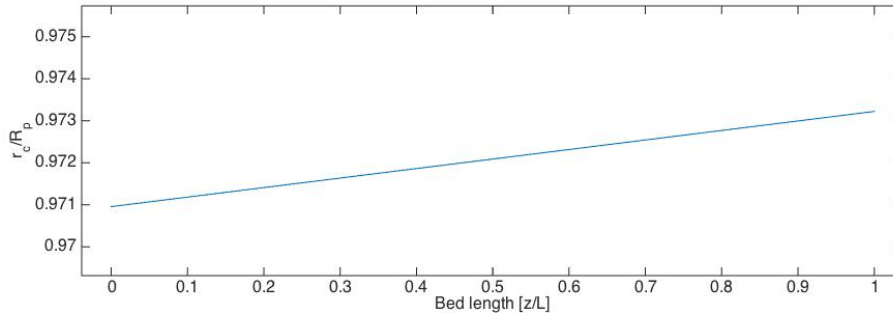


**Figure 5.2:** Predicted ratio between unreacted and initial pellet radius through the bed after 110 h for 102 ppm  $\text{H}_2\text{S}$  at 200 °C and  $\text{GHSV}=43900 \text{ h}^{-1}$

due to incorrect diffusivities and reaction rates as the samples differ in sizes by a factor of 10. What is most important is that the model is showing the same trend as the the experiment but with considerably less mass transfer resistances, hence the sharper breakthrough behaviour. As the adopted literature values were validated for small particles a lower mass transfer resistance comes as no surprise. A figure showing the predicted and experimental  $\text{H}_2\text{S}$  breakthrough profile together for times up to 120 min can be seen in appendix A.2.

An interesting note is that the model predicts that only a small part of the pellet radius is converted into  $\text{ZnS}$ . Similar results have been obtained by others as mentioned in section 2.2.3 where only diffusion through the sulphide product layer and reaction rate were reported as limiting. Keeping in mind that it was previously estimated that 37.9 % of a pellet radius had been converted the model in this case seems to underestimate the depth of adsorbed sulphur in the pellet. The comparison acts as no validation but as a reliability check and the model needs experimental values to be confirmed.

When comparing the shrinking core model with the linear driving force model, SCM is a more physical way of describing the process as it does account for internal and external transport resistances. Its major downside is that the model requires smaller time steps when solving the PDE and hence easily diverging. In contrast the LDF model is less detailed and only account for an effective reaction rate at the pellet surface and making a relatively fast model. As the LDF model only accounts for a surface reaction where the amount of adsorbed sulphur is averaged over the whole pellet, it can be discussed whether LDF is a reasonable model. The plan for including LDF was to evaluate if the desulphurisation could in fact be modelled in a good way by this model and in that case save a lot of time. Unfortunately due to lack of experimental values this could not be determined.

## 5.4 Evaluation of experiments

It was previously mentioned in section 3.2 that a drift in the MS signal for argon was seen and why the measured  $\text{H}_2\text{S}$  signal at  $m/z=34$  was weighted with the relative signal increase for argon. The drift can be an effect of several reasons as fouling and thermal expansions of capillary surface into the MS which affects the gas flow.

One may ask why the experiments had to be performed over such a long time period when it was planned to determine the bed weight and length so saturation could be reached in a reasonable amount of time as 30 to 60 min. During calibration stage as mentioned in section 3.2 the calculated bed weight was tested in the trial-and-error way explained but a large slip of  $\text{H}_2\text{S}$  was observed at the corresponding GHSV and breakthrough was immediately measured on the MS. The immediate breakthrough indicated that GHSV was far to large for the pellet material and must be reduced. Reducing GHSV can either be done by reducing flow rate or increasing bed length and decision was made to increase the bed length until an immediate breakthrough could no longer be measured. The result was a bed of 6.1 g of ZnO adsorbent with a corresponding GHSV of  $43900 \text{ h}^{-1}$  and a very long saturation time. The same effect would have been observed if it was decided to reduce flow rate but a longer bed was chosen to avoid having the bed short as the length of just a few pellets which was though not to be a good representation of the system.

Why no articles were found to have been discussing similar conditions as the one adopted here might in fact be due to the necessity of a low GHSV for ZnO pellets with a diameter of  $\approx 4 \text{ mm}$ . If long experimental times is not an issue it is recommended to continue performing the experimental plan developed here or pellets can be crushed into smaller particles or a powder. By crushing the pellets the time needed for each experiment is greatly reduced at the cost of information about internal resistances as the external surface area becomes more significant as the particles get smaller. Applying the model to a powder would not result in the same diffusivity constants and reaction rates and not truly explain the ZnO pellets but a ZnO powder. In the case of PowerCell were the ZnO is used to clean an incoming reformat, powder is not recommended as it would result in an adsorbent loss which can be caught by the gas phase and dragged

along downstream. In that case it would probably be better to coat a monolith with the powder and use a monolithic bed instead. That would of course need new types of experiments.

It was also noticed during the experimental part that  $\text{H}_2\text{S}$  is a gas with tendencies to adsorb onto surrounding surfaces as pipes and quartz wool. It is therefore recommended to make the experiment twice but one in an empty reactor tube to act as a calibration for the specific conditions. In that way it is possible to more exactly determine the amount of  $\text{H}_2\text{S}$  sticking to surrounding area and subtract it from the adsorbed amount. An issue related to the sticking is that the equipment has to be cleaned after each experiment to be sure of a clean surface. In case the surrounding surfaces is contaminated from the start  $\text{H}_2\text{S}$  can be released when increasing temperature and starting the injection of water, as adsorption equilibrium is affected by these factors. If  $\text{H}_2\text{S}$  is released from a point downstream of the fresh sample it will adsorb the passing gas hence contaminating the sample before any controlled injection of  $\text{H}_2\text{S}$  has occurred. This issue was encountered during the experiments and solved by a desorption procedure between each experiment where  $\text{H}_2\text{S}$  had been injected into the system. The system was regarded as clean after raising temperature to 500 °C and injecting 9.6 %  $\text{H}_2\text{O}$  with a balance over a time period of 10 h.

#### Comparison to similar experiment

The article that in section 2.2.6 described the preparation and examination of a ZnO adsorbent prepared by the glycerine and combustion method also fitted a shrinking core model which showed a similar appearance as the breakthrough in this project. During their experiment a feed composition of 100 ppm  $\text{H}_2\text{S}$  (He as balance) was used and breakthrough was defined at  $C/C_{in}=0.02$  which resulted in a breakthrough time of between 5-550 min depending on preparation method. As a comparison, the experiment performed at Chalmers and by defining breakthrough equally it had a breakthrough time of 330 min. The closest of the observed values in the article is 430 min but the adsorbent had a lower BET surface area and a larger pore volume as 43.3  $\text{m}^2/\text{g}$  and 0.30  $\text{cm}^3/\text{g}$  respectively compared to the one at PowerCell. The difference in breakthrough time is probably explained by the different morphology of the ZnO adsorbents.

It was previously determined that by assuming the pellet from the experiment at Chalmers to be saturated its capacity was 137.4 mg S/g pellet. The value seems probable compared to literature values and remembering that adsorption is an equilibrium process where 100 % conversion is not achievable. The capacity of 137.4 mg S/g pellet can be compared to the value of 48 mg S/g adsorbent for the similar ZnO experiments with a breakthrough time of 430 min as mentioned above, keeping in mind that the adsorbents are of different sizes. Further the true capacity of the analysed ZnO pellet is believed to be even higher as the experiment only reached  $C/C_{in}=0.77$ .

## 5.5 Suggestions of improvement

The remarkable amount of slip observed proved to be a lot more significant than initially thought. According to methodology it was desired to use high GHSV in order to have a large input of  $\text{H}_2\text{S}$  and to keep experiments short but the pellets proved to not be optimised for the high flow rate. The issue put constraints on the experimental part which complicated model validation because no diffusivity or reaction constants could be obtained. The constraints meant that a large amount of time is needed for each experiment to reach saturation which could not be given here. Recommendations for future experimental evaluations for the pellets are thereby adopting a GHSV lower than  $43900 \text{ h}^{-1}$  at the expense of a long experimental time. Preferably by using a longer bed together with a reduced flow rate, because it otherwise is limited by pellet size and could result in a bed length of only one pellet long and not give a good representation of the problem. Further the initial experimental plan was to use a reformat gas composition as table 3.1 during the experiments which is highly recommended to get all dependencies on molecular transport into account when determining diffusional and reaction coefficients.

# 6

## Conclusion

Adsorbent material of ZnO pellets for desulphurisation of reformat gas used at PowerCell Sweden AB (publ) was characterised and found to have a BET surface area of 72.5 m<sup>2</sup>/g and pore volume of 0.17 cm<sup>3</sup>/g. The majority of the pores consisted of pores of width 25-120 Å and pores of sizes 25-150 Å were most affected by the H<sub>2</sub>S adsorption process with a reduction in both their area and volume during the long-term test performed at PowerCell. Chromium was found on pellet surfaces which is assumed to have affected the desulphurisation negatively and might have caused a low reading of sulphur content in the first part of the adsorption bed.

Two models for predicting breakthrough profile behaviour of ZnO pellets of sizes 2-5 mm were developed. One was derived through the shrinking core model and one through the linear driving force model. Both were planned to be validated and fitted to lab-scale experiments performed at Chalmers University of Technology but due to an unexpectedly large slip of H<sub>2</sub>S around the pellets a reduction in GHSV was required. The lower GHSV resulted in a very long time to reach saturation and as a result only one experiment could be performed but lacked the necessity of complete saturation to validate any models. Thus validating the models remains to be done in order to obtain correct diffusivity coefficient and reaction rates. The experiment was performed at Chalmers with 102 ppm H<sub>2</sub>S, 9.6 % H<sub>2</sub>O, 413 ppm H<sub>2</sub> with a balance of argon at 200 °C and a GHSV of 43900 h<sup>-1</sup>.

The shrinking core model was reality checked by adopting literature values from a similar experiment and showed an overall similar H<sub>2</sub>S breakthrough profile behaviour, keeping in mind that the values are not completely true for the ZnO pellets at PowerCell.

Through the performed experiment at Chalmers University of Technology it was possible to make an estimate of the sulphur capacity of the adsorbent to a value of 137.4 mg S/g pellet which corresponds to a 37.9 % conversion of the total amount of ZnO into ZnS according to the hydrolysis reaction.

ZnO is one of the most commonly used metal oxides used for the application and even though there are other interesting materials such as KOH impregnated active carbon it can safely be used to remove the sulphur gas before being fed to the fuel cell system at a low enough GHSV. Interest could lie in experimentally evaluating an active carbon in parallel to ZnO because of the reported advantage of H<sub>2</sub>O enhancing adsorption equilibrium which otherwise counteracts the adsorption of sulphur over metal oxides. The latter is an issue today because reformat can include large amounts of steam and reduced the overall potential of the adsorbent material.

Future work should target a new set of experiments which have to be allowed to proceed undisturbed for several days at a time. The long experimental time comes from a large slip around the pellets and a maximum GHSV of 43900 h<sup>-1</sup> was found for the ZnO pellets. Due to equipment problems the experimental plan had to be simplified and it highly is recommended to use a gas comprising of H<sub>2</sub>S, H<sub>2</sub>O, H<sub>2</sub>, CO<sub>2</sub>, CO and inert during future experiments to obtain diffusivities and reaction rates as close to the real value as possible.

# Bibliography

- [1] Reducing CO<sub>2</sub> emissions from Heavy-Duty Vehicles. European Commission. [Internet]  
Available: [ec.europa.eu/clima/policies/transport/vehicles/index\\_en.htm](http://ec.europa.eu/clima/policies/transport/vehicles/index_en.htm)  
(visited 2014-09-5).
- [2] Greenhouse Gas Emission from the U.S Transportation Sector: 1990-2003. U.S. Environmental Protection Agency and Office of Transportation and Air Quality, March 2006. [Internet]  
Available: [www.epa.gov/otaq/climate/420r06003.pdf](http://www.epa.gov/otaq/climate/420r06003.pdf).
- [3] U.S Department of Energy. [Internet]  
Available: [www.afdc.energy.gov/data](http://www.afdc.energy.gov/data) (visited 2014-09-03).
- [4] Oak Ridge National Laboratory. 2013 Vehicle Technologies Market Report. Technical report, Vehicle Technologies Office, March 2013.
- [5] European Vehicle Market Statistics 2013. International Council on Clean Transportation, 2013. [Internet]  
Available: [www.theicct.org/sites/default/files/publications/EU\\_vehiclemarket\\_pocketbook\\_2013\\_Web.pdf](http://www.theicct.org/sites/default/files/publications/EU_vehiclemarket_pocketbook_2013_Web.pdf).
- [6] DieselNet. Idling Emissions. [Internet]  
Available: [www.dieselnet.com/tech/emissions\\_idle.php](http://www.dieselnet.com/tech/emissions_idle.php) (visited 2014-09-04).
- [7] Idling Pushes Profits out the Tailpipe. U.S Department of Energy, March 2012.
- [8] PowerCell. [Internet] [www.powercell.se](http://www.powercell.se) (visited 2014-09-04).
- [9] Backup Power for Telecommunication Applications: Comparing Fuel Cells to Diesel Generators. Relion, 2011. [Internet]  
Available: [www.relion-inc.com/pdf/ReliOn\\_BackupPowerComparison\\_0611.pdf](http://www.relion-inc.com/pdf/ReliOn_BackupPowerComparison_0611.pdf).

- [10] Energy for the Telecom Towers: India Market Sizing and Forecasting. GSMA, 2010. [Internet]  
Available: [www.gsma.com/mobilefordevelopment/energy-for-the-telecom-towers-india-market-sizing-and-forecasting](http://www.gsma.com/mobilefordevelopment/energy-for-the-telecom-towers-india-market-sizing-and-forecasting).
- [11] The Department of Energy Hydrogen and Fuel Cells Program Plan. U.S. Department of Energy, September 2011.
- [12] EPA and NHTSA Adopt First-Ever Program to Reduce Greenhouse Gas Emissions and Improve Fuel Efficiency of Medium-and Heavy-Duty Vehicles, August 2011.
- [13] U.S Department of Energy. [Internet]  
Available: [www.energy.gov](http://www.energy.gov) (visited 2014-09-06).
- [14] Jonathan Wing. Analyst View: The Propagation of Hydrogen Stations. Fuel Cell Today, April 2013. [Internet]  
Available: [www.fuelcelltoday.com/media/1861054/13-04-10\\_the\\_propagation\\_of\\_hydrogen\\_stations.pdf](http://www.fuelcelltoday.com/media/1861054/13-04-10_the_propagation_of_hydrogen_stations.pdf).
- [15] Hui Li, Shanna Knights, Zheng Shi, John W. Van Zee, and Jiujun Zhang, editors. *Proton Exchange Membrane Fuel Cells: Contamination and Mitigation Strategies*. Green chemistry and chemistry engineering. CRC Press, 2010.
- [16] Vijay Sethuraman and John Weidner. Analysis of sulfur poisoning on a PEM fuel cell electrode. *Electrochimica Acta*, 55(20):5683–5694, August 2010.
- [17] Fuel Cell Technologies Program. U.S Department of Energy, November 2010. [Internet]  
Available: [www1.eere.energy.gov/hydrogenandfuelcells/pdfs/fct\\_h2\\_production.pdf](http://www1.eere.energy.gov/hydrogenandfuelcells/pdfs/fct_h2_production.pdf).
- [18] Xanthias Karatzas. *Rhodium diesel-reforming catalysts for fuel cell applications*. PhD thesis, KTH - Royal Institute of Technology, 2011.
- [19] E. Tzimas, C. Filiou, and S.D. Peteves. Hydrogen storage: State-of-the-art and future perspective. Technical Report ISBN: 92-894-6950-1, European Commission, Joint Research Center, 2003.
- [20] Gunther Kolb. *Fuel Processing for Fuel Cells*. Wiley-VCH, 2008. ISBN: 978-3-527-31581-9.
- [21] C. Pereira, R. Wilkenhoener, S. Ahmed, and M. Krumpelt. Liquid Fuel Reformer Development. Technical report, Argonne National Laboratory, 1999.
- [22] B. Lindström, J.A.J. Karlsson, and P. Ekdunge. Diesel fuel reformer for automotive fuel cell applications. *International Journal of Hydrogen Energy*, 34(8):3367–3381, May 2009.

- [23] J. Pasel, J. Meißner, Z. Porš, C. Palm, P. Cremer, R. Peters, and D. Stolten. Hydrogen Production via Autothermal Reforming of Diesel Fuel. *Fuel Cells*, 4(3):225–230, 2004.
- [24] C.M. Kalamaras and A.M. Efstathiou. Hydrogen Production Technologies: Current State and Future Developments. *Conference Papers in Energy*, 2013(Article ID 690627):9 pages, 2013.
- [25] Heavy-Duty Engine and Vehicle Standards and Highway Diesel Fuel Sulfur Control Requirements. U.S Environmental Protection Agency, December 2000.
- [26] Richard I. Masel. *Principles of Adsorption and Reaction on Solid Surfaces*, chapter 3, pages 108–234. John Wiley & Sons, 1996. ISBN: 0-471-30392-5.
- [27] Paul A. Webb. Introduction to Chemical Adsorption Analytical Techniques and their Applications to Catalysis. Technical report, Micromeritics Instrument Corp., 2003.
- [28] S. J. Gregg and K. S. W. Sing. *Adsorption, surface area and porosity*. Academic Press Inc. (London), 2 edition, 1982.
- [29] J. D. Seader and Ernest J. Henley. *Separation Process Principles*, chapter 15, pages 548–620. John Wiley & Sons, 2 edition, 2006.
- [30] IUPAC. *Compendium of Chemical Terminology (the "Gold Book")*. Blackwell Scientific Publications, Oxford, 2 edition, 1997. XML on-line corrected version: <http://goldbook.iupac.org> (2006-) created by M. Nic, J. Jirat, B. Kosata; updates compiled by A. Jenkins. ISBN 0-9678550-9-8. doi:10.1351/goldbook.
- [31] J. Elliott and C. Lira. *Introductory Chemical Engineering Thermodynamics*. Pearson, 2 edition, 2011.
- [32] Hongyun Yang, Ryan Sothen, Donald R. Cahela, and Bruce J. Tatarchuk. Break-through Characteristics of Reformate Desulfurization Using ZnO Sorbents for Logistic Fuel Cell Power Systems. *Industrial & Engineering Chemistry Research*, 47(24):10064–10070, 2008.
- [33] J-C. Hogue, George P. Karagiannakis, Julia A. Valla, Christos C. Agrafiotis, and Athanasios G. Konstandopoulos. Gas and liquid phase fuels desulphurization for hydrogen production via reforming processes. *International Journal of Hydrogen Energy*, 34(11):4953 – 4962, 2009. 2nd International Workshop on Hydrogen 2nd International Workshop on Hydrogen.
- [34] Liyu Li and David L. King. H<sub>2</sub>S removal with ZnO during fuel processing for PEM fuel cell applications. *Catalysis Today*, 116(4):537 – 541, 2006. Sulfur Removal to Produce Ultra Clean Fuel.

- [35] Priyanka P. Dhage. *Promoted Zinc Oxide Sorbents for Wide Temperature Range Hydrogen Sulfide/Carbonyl Sulfide Removal for Applications in Fuel Cells*. PhD thesis, Auburn University, 2011.
- [36] Richard Turton, David A. Berry, Todd H. Gardner, and Angela Miltz. Evaluation of Zinc Oxide Sorbents in a Pilot-Scale Transport Reactor: Sulfidation Kinetics and Reactor Modeling. *Industrial & Engineering Chemistry Research*, 43(5):1235–1243, 2004.
- [37] Miguel Pineda, José M. Palacios, Enrique García, Cristina Cilleruelo, and José V. Ibarra. Modelling of performance of zinc ferrites as high-temperature desulfurizing sorbents in a fixed-bed reactor. *Fuel*, 76(7):567–573, May 1997.
- [38] Ilaria Rosso, Camilla Galletti, Massimo Bizzi, Guido Saracco, and Vito Specchia. Zinc Oxide Sorbents for the Removal of Hydrogen Sulfide from Syngas. *Industrial & Engineering Chemistry Research*, 42(8):1688–1697, 2003.
- [39] Evangelos A. Efthimiadis and Stratis V. Sotirchos. Reactivity evolution during sulfidation of porous zinc oxide. *Chemical Engineering Science*, 48(5):829 – 843, 1993.
- [40] Susan Lew, Adel F. Sarofim, and Maria Flytzani-Stephanopoulos. Modeling of the sulfidation of zinc-titanium oxide sorbents with hydrogen sulfide. *AIChE Journal*, 38(8):1161–1169, 1992.
- [41] Yanxu Li, Hanxian Guo, Chunhu Li, and Shuanbing Zhang. A Study on the Apparent Kinetics of H<sub>2</sub>S Removal Using a ZnO-MnO Desulfurizer. *Industrial & Engineering Chemistry Research*, 36(9):3982–3987, 1997.
- [42] Evangelos A. Efthimiadis and Stratis V. Sotirchos. A partially overlapping grain model for gas-solid reactions. *Chemical Engineering Science*, 48(7):1201–1212, 1993.
- [43] Derivation of the BET and Langmuir Isotherms. University of Colorado, 5 October 2011. [Internet]  
Available: [chem.colorado.edu/chem4581\\_91/images/stories/IsothermDerv.pdf](http://chem.colorado.edu/chem4581_91/images/stories/IsothermDerv.pdf).
- [44] R. Bellman, E. Stanley Lee, and K.M. Wang. Invariant imbedding and solid-fluid reactions I: The unreacted core model. *Chemical Engineering Science*, 32(9):1051 – 1054, 1977.
- [45] S. Ramanathan. HetCat-ShrinkingCoreModel. Department of Chemical Engineering, Indian Institute of Technology Madras, 2013. [Internet]  
Available: [www.che.iitm.ac.in/~srinivar/course/CH5010/HetCat-ShrinkingCoreModel.pdf](http://www.che.iitm.ac.in/~srinivar/course/CH5010/HetCat-ShrinkingCoreModel.pdf).

- [46] T.S.Y. Choong and D.M. Scott. The linear driving force model for cyclic adsorption and desorption: the effect of external fluid-film mass transfer. *Chemical Engineering Science*, 53(4):847–851, 1998.
- [47] Phillip R. Westmoreland, James B. Gibson, and Douglas P. Harrison. Comparative kinetics of high-temperature reaction between hydrogen sulfide and selected metal oxides. *Environmental Science & Technology*, 11(5):488–491, 1977.
- [48] Priyanka Dhage, Alexander Samokhvalov, Michael L. McKee, Evert C. Duin, and Bruce J. Tatarchuk. Reactive adsorption of hydrogen sulfide by promoted sorbents Cu-ZnO/SiO<sub>2</sub>: active sites by experiment and simulation. *Surface and Interface Analysis*, 45(5):865–872, 2013.
- [49] Sibel Ozdemir and Tefvik Bardakci. Hydrogen sulfide removal from coal gas by zinc titanate sorbent. *Separation and Purification Technology*, 16(3):225–234, 1999.
- [50] Ivan I. Novochinskii, Chunshan Song, Xiaoliang Ma, Xinsheng Liu, Lawrence Shore, Jordan Lampert, and Robert J. Farrauto. Low-Temperature H<sub>2</sub>S Removal from Steam-Containing Gas Mixtures with ZnO for Fuel Cell Application. 1. ZnO Particles and Extrudates. *Energy & Fuels*, 18(2):576–583, 2004.
- [51] Hamid Tajizadegan, Mehdi Rashidzadeh, Majid Jafari, and Reza Ebrahimi-Kahrizangi. Novel ZnO-Al<sub>2</sub>O<sub>3</sub> composite particles as sorbent for low temperature H<sub>2</sub>S removal. *Chinese Chemical Letters*, 24(2):167–169, 2013.
- [52] Russamee Sitthikhankaew, David Chadwick, Suttichai Assabumrungrat, and Navadol Laosiripojana. Effects of humidity, O<sub>2</sub>, and CO<sub>2</sub> on H<sub>2</sub>S adsorption onto upgraded and KOH impregnated activated carbons. *Fuel Processing Technology*, 124:249 – 257, 2014.
- [53] Yehya Elsayed, Mykola Seredych, Andrew Dallas, and Teresa J. Bandosz. Desulfurization of air at high and low H<sub>2</sub>S concentrations. *Chemical Engineering Journal*, 155(3):594–602, 2009.
- [54] Ajay K. Dalai and Eric L. Tollefson. Kinetics and reaction mechanism of catalytic oxidation of low concentrations of hydrogen sulfide in natural gas over activated carbon. *The Canadian Journal of Chemical Engineering*, 76(5):902–914, 1998.
- [55] R.L. Brown and S.E. Stein. *NIST Chemistry WebBook, NIST Standard Reference Database Number 69*, chapter Boiling Point Data. National Institute of Standards and Technology, Gaithersburg MD, 20899. (retrieved November 20, 2014).
- [56] Gas Adsorption Theory. Micromeritics Instrument Corporation. [Internet] Available: [www.micromeritics.com/repository/files/gas\\_adsorption\\_theory\\_poster.pdf](http://www.micromeritics.com/repository/files/gas_adsorption_theory_poster.pdf).

- [57] William T. Becker and Roch J. Shipley. *ASM Handbook*, volume Volume 11 - Failure Analysis and Prevention, chapter 31. Scanning Electron Microscopy, pages 516–526. ASM International, 1986; 2002.
- [58] Background Theory and Terminology for Electron Microscopy. The University of Queensland. [Internet]  
Available: [www.uq.edu.au/nanoworld/documents/Background%20theory%20CLASS%20RESOURCE.ppt](http://www.uq.edu.au/nanoworld/documents/Background%20theory%20CLASS%20RESOURCE.ppt).
- [59] Introduction to Energy Dispersive X-ray Spectroscopy (EDX) of bulk specimens. University of California, Riverside. [Internet]  
Available: <http://cfamm.ucr.edu/documents/aem-intro.pdf>.
- [60] Bob Hafner. Energy Dispersive Spectroscopy on the SEM: A Primer. Characterization Facility, University of Minnesota. [Internet]  
Available: [http://www.charfac.umn.edu/instruments/eds\\_on\\_sem\\_primer.pdf](http://www.charfac.umn.edu/instruments/eds_on_sem_primer.pdf).
- [61] William T. Becker and Roch J. Shipley. *ASM Handbook*, volume Volume 11 - Failure Analysis and Prevention, chapter 26. Chemical Analysis of Metals in Failure Analysis, pages 429–436. ASM International, 1986; 2002.
- [62] Alison E. Ashcroft. An Introduction to Mass Spectrometry. Astbury Centre for Structural Molecular Biology, The University of Leeds. [Internet] Available: [www.astbury.leeds.ac.uk/facil/MStut/mstutorial.htm](http://www.astbury.leeds.ac.uk/facil/MStut/mstutorial.htm).
- [63] Augustine Ofori Agyeman. Mass Spectrometry I - Principles and Applications. Department of Natural Sciences, Clayton State University. [Internet]  
Available: [faculty.clayton.edu/Portals/95/Imported/a-s.clayton.edu/aagyeman/CHEM4811/Chapter%209-Mass-Spec-1.ppt](http://faculty.clayton.edu/Portals/95/Imported/a-s.clayton.edu/aagyeman/CHEM4811/Chapter%209-Mass-Spec-1.ppt).

# A

## Appendix

### A.1 Equilibrium calculations

The following equilibrium dependencies were determined for gas condition as shown in table A.1.

**Table A.1:** Composition used at equilibrium calculations

Species	Value
H <sub>2</sub> O	35 %
CO <sub>2</sub>	20 % (dry)
CO	5 % (dry)
H <sub>2</sub>	40 % (dry)
H <sub>2</sub> S	0.67 ppm (dry)
N <sub>2</sub>	Balance
Temperature	300 °C

The equilibrium dependencies shows the equilibrium concentration of H<sub>2</sub>S in gas bulk phase for varying background mixture. When varying the concentration of a species or temperature it is varied around its standard value as shown in table A.1, while the other species is kept constant.

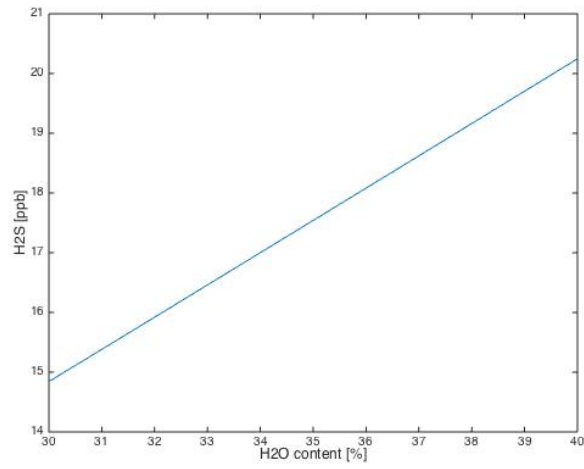


**Figure A.1:** H<sub>2</sub>S gas bulk phase equilibrium concentration for a varying concentration of H<sub>2</sub>O at conditions as shown in table A.1

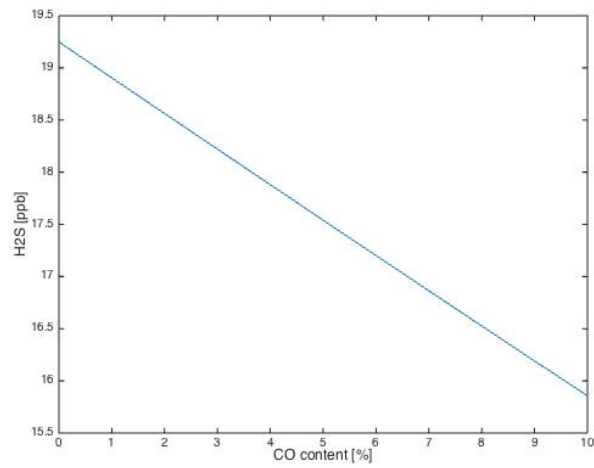


**Figure A.2:** H<sub>2</sub>S gas bulk phase equilibrium concentration for a varying concentration of CO at conditions as shown in table A.1

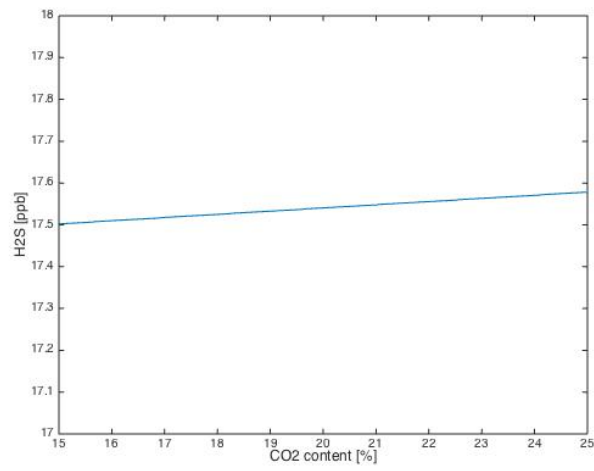


**Figure A.3:** H<sub>2</sub>S gas bulk phase equilibrium concentration for a varying concentration of CO<sub>2</sub> at conditions as shown in table A.1

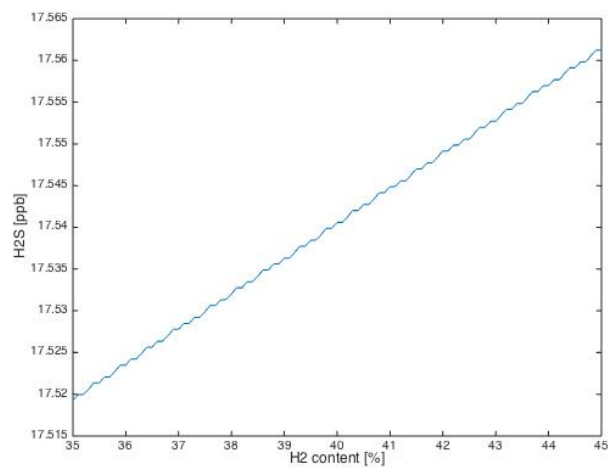


**Figure A.4:** H<sub>2</sub>S gas bulk phase equilibrium concentration for a varying concentration of H<sub>2</sub> at conditions as shown in table A.1

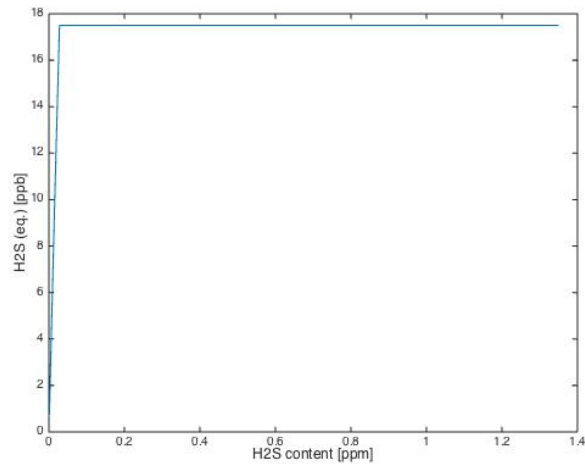


**Figure A.5:** H<sub>2</sub>S gas bulk phase equilibrium concentration for a varying concentration of H<sub>2</sub>S at conditions as shown in table A.1

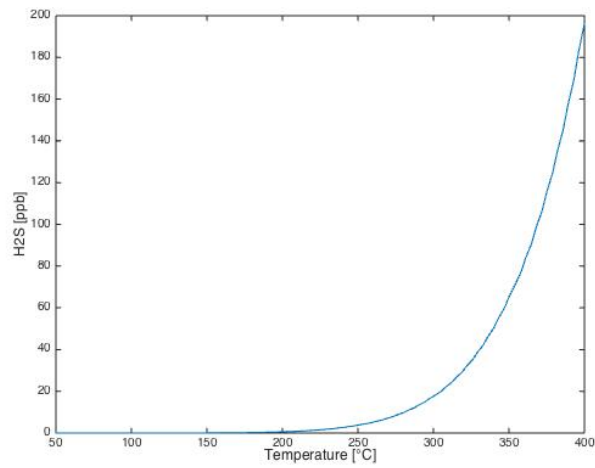


**Figure A.6:** H<sub>2</sub>S gas bulk phase equilibrium concentration for a varying temperature at conditions as shown in table A.1

## A.2 Experiments

**Table A.2:** Complete experimental plan

Experimental run	H2S	H2O	Temperature	GHSV
1	0	0	0	0
2	0	0	0	0
3	+	+	+	+
4	+	+	+	-
5	+	+	-	+
6	+	+	-	-
7	+	-	+	+
8	+	-	+	-
9	+	-	-	+
10	+	-	-	-
11	-	+	+	+
12	-	+	+	-
13	-	+	-	+
14	-	+	-	-
15	-	-	+	+
16	-	-	+	-
17	-	-	-	+
18	-	-	-	-

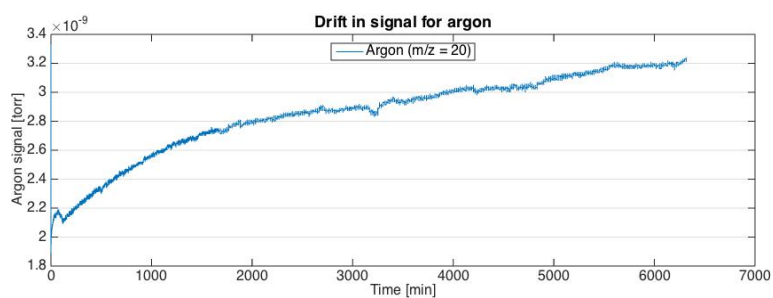


**Figure A.7:** Drifting signal for argon which increased significantly during the experiment

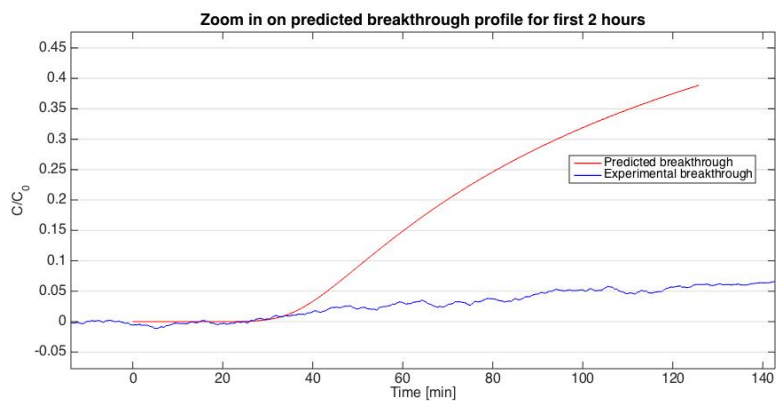


**Figure A.8:** Comparison of modelled and experimental breakthrough over the first 2 hours

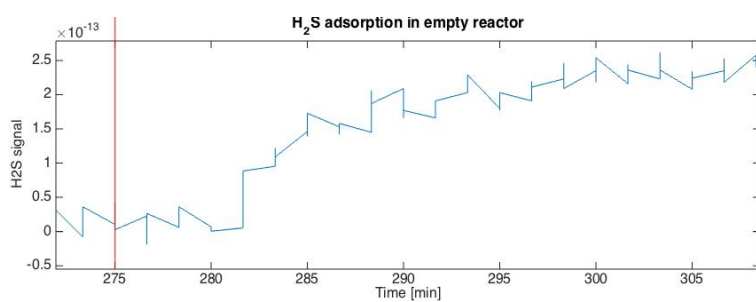


**Figure A.9:** Time between injecting and registering 51 ppm of H<sub>2</sub>S at 200 °C and GHSV=43900 h<sup>-1</sup> in an empty reactor

### A.3 ZnO sulphur content

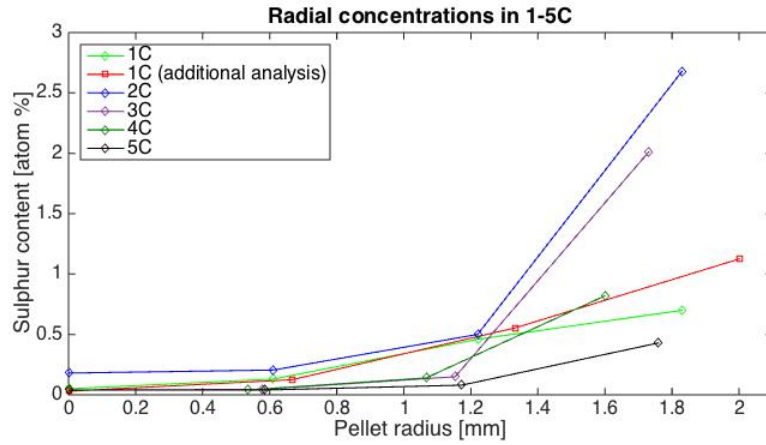


Figure A.10: Radial sulphur concentration gradients for 1-5C

Table A.3: Pellet sulphur concentration compared to external analysis

Layer	1C	2C	3C	4C	5C
Calculated through SEM [%]	0.9233	1.6183	0.9133	0.4517	0.2567
External company [%]	0.9200	0.6100	0.3800	0.1900	0.1000

## Clean pellet

2014-11-18 08:04:56

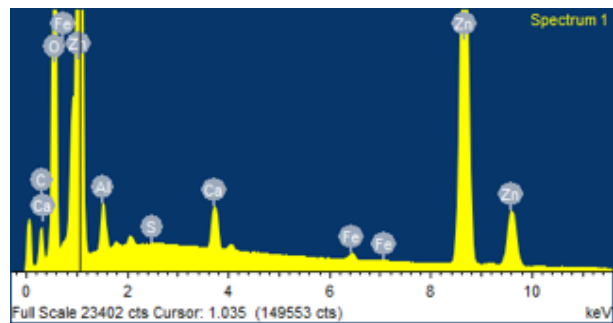
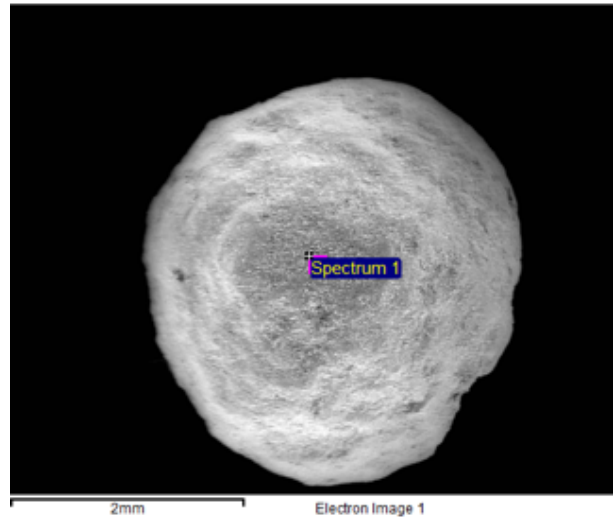
Spectrum processing :

Peaks possibly omitted : 10.594, 17.262, 18.220 keV

Processing option : All elements analyzed (Normalised)

Number of iterations = 5

Element	Weight%	Atomic%
C K	6.52	16.61
O K	26.60	50.90
Al K	1.22	1.38
S K	0.02	0.02
Ca K	1.04	0.80
Fe K	0.39	0.21
Zn L	64.20	30.07
Totals	100.00	



INCA

Comment: Clean, pellet surface

## Clean pellet

2014-11-18 08:05:22

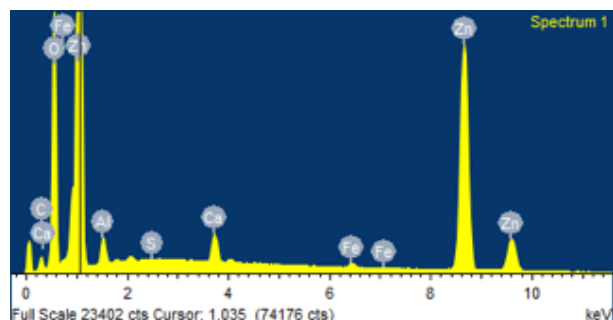
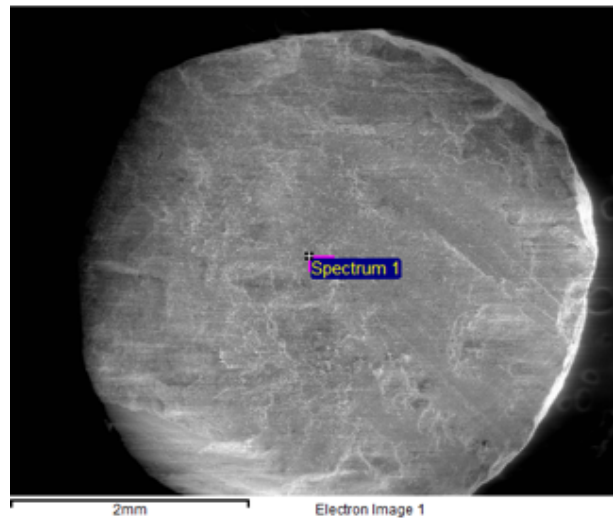
Spectrum processing :

Peaks possibly omitted : 4.520, 10.585, 17.265, 18.192 keV

Processing option : All elements analyzed (Normalised)

Number of iterations = 5

Element	Weight%	Atomic%
C K	4.91	12.94
O K	26.45	52.33
Al K	1.49	1.75
S K	0.02	0.02
Ca K	1.32	1.04
Fe K	0.50	0.28
Zn L	65.31	31.63
Totals	100.00	



INCA

Comment: Clean, pellet center

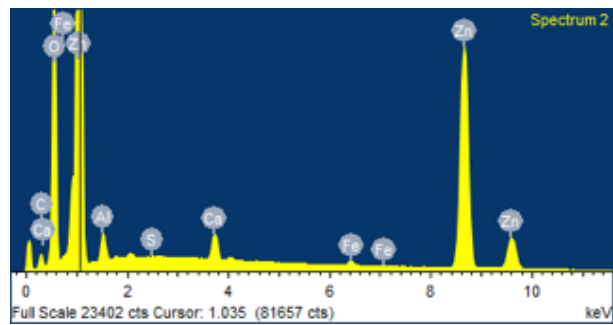
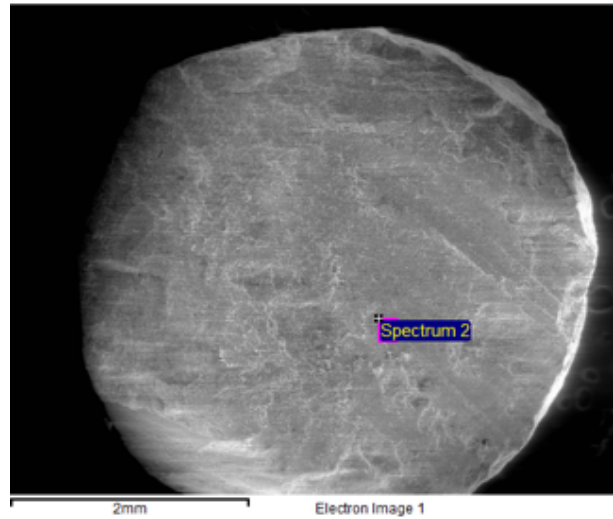
Spectrum processing :

Peaks possibly omitted : 10.568, 17.274, 18.230 keV

Processing option : All elements analyzed (Normalised)

Number of iterations = 5

Element	Weight%	Atomic%
C K	4.93	13.07
O K	26.10	51.96
Al K	1.40	1.65
S K	0.01	0.01
Ca K	1.14	0.91
Fe K	0.47	0.27
Zn L	65.95	32.13
Totals	100.00	



Comment: Clean, R/3

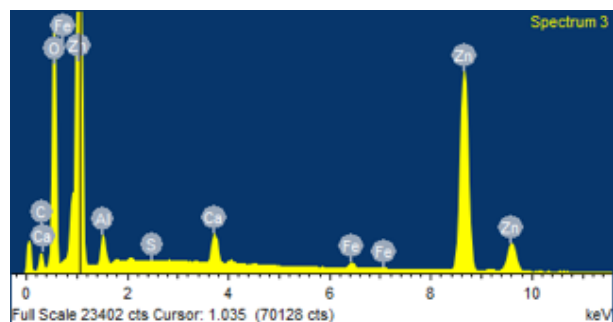
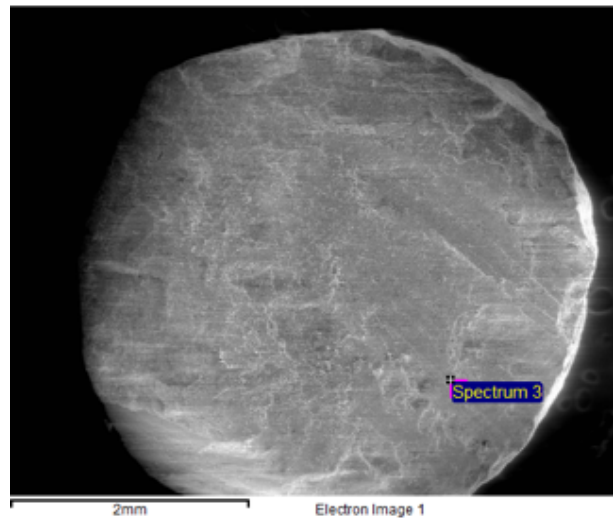
Spectrum processing :

Peaks possibly omitted : 4.505, 10.599, 17.256, 18.195 keV

Processing option : All elements analyzed (Normalised)

Number of iterations = 5

Element	Weight%	Atomic%
C K	6.64	16.92
O K	26.19	50.11
Al K	1.57	1.78
S K	0.00	0.00
Ca K	1.42	1.09
Fe K	0.64	0.35
Zn L	63.53	29.75
Totals	100.00	



Comment: Clean, 2R/3

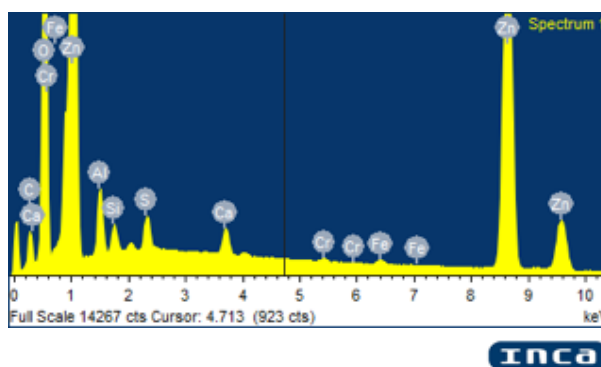
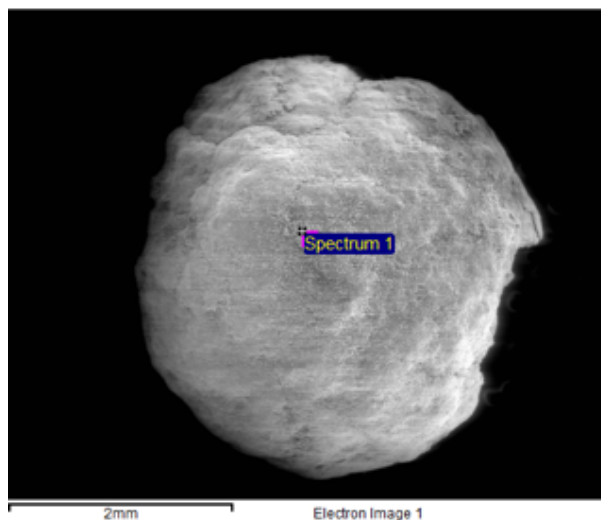
Spectrum processing :

Peaks possibly omitted : 10.566, 17.242, 18.223 keV

Processing option : All elements analyzed (Normalised)

Number of iterations = 6

Element	Weight%	Atomic%
C K	7.05	17.44
O K	27.19	50.53
Al K	1.76	1.94
Si K	0.68	0.72
S K	0.75	0.70
Ca K	0.63	0.47
Cr K	0.16	0.09
Fe K	0.29	0.16
Zn L	61.49	27.96
Totals	100.00	



Comment: 1C, pellet surface

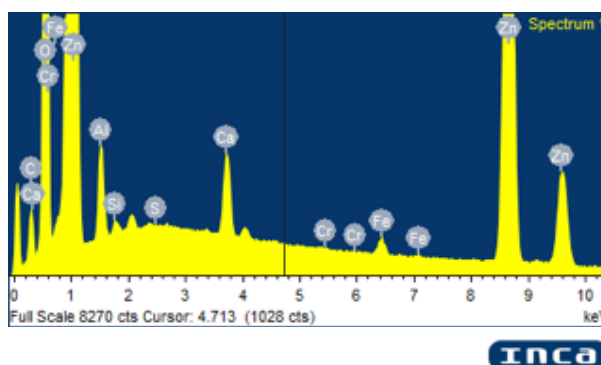
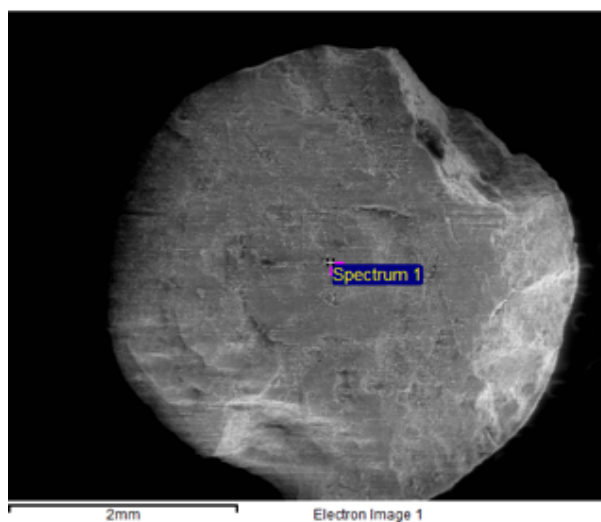
Spectrum processing :

Peaks possibly omitted : 10.524, 17.271, 18.201 keV

Processing option : All elements analyzed (Normalised)

Number of iterations = 5

Element	Weight%	Atomic%
C K	5.93	15.53
O K	25.35	49.82
Al K	1.52	1.78
Si K	0.19	0.21
S K	0.05	0.05
Ca K	1.18	0.93
Cr K	0.01	0.01
Fe K	0.59	0.33
Zn L	65.18	31.35
Totals	100.00	



Comment: 1C, pellet center

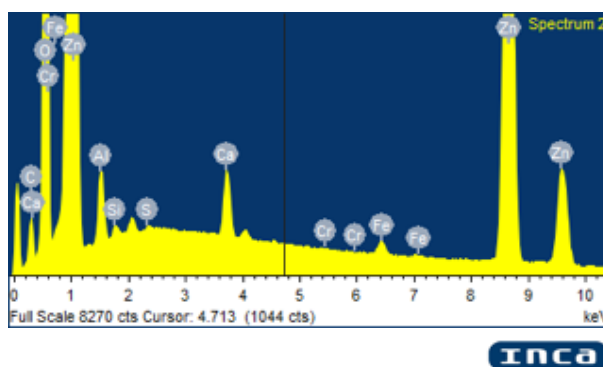
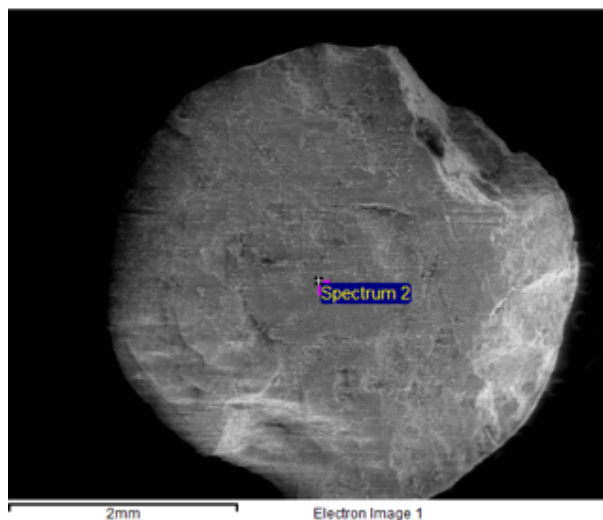
Spectrum processing :

Peaks possibly omitted : 4.515, 10.577, 17.257, 18.213 keV

Processing option : All elements analyzed (Normalised)

Number of iterations = 5

Element	Weight%	Atomic%
C K	5.55	14.78
O K	24.89	49.79
Al K	1.25	1.48
Si K	0.19	0.22
S K	0.05	0.05
Ca K	1.02	0.81
Cr K	0.03	0.02
Fe K	0.49	0.28
Zn L	66.53	32.57
Totals	100.00	



Comment: 1C, pellet center

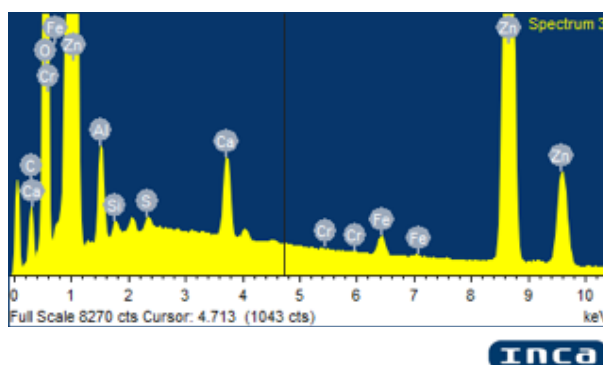
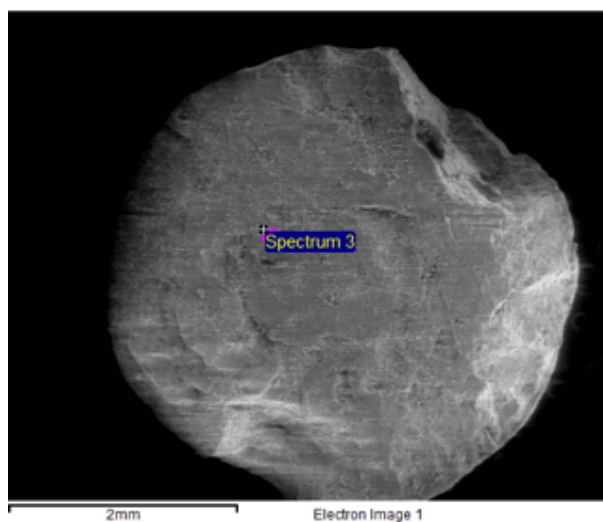
Spectrum processing :

Peaks possibly omitted : 4.505, 10.573, 17.255, 18.200 keV

Processing option : All elements analyzed (Normalised)

Number of iterations = 5

Element	Weight%	Atomic%
C K	6.53	16.78
O K	25.62	49.44
Al K	1.59	1.82
Si K	0.24	0.26
S K	0.17	0.16
Ca K	1.19	0.92
Cr K	0.04	0.02
Fe K	0.70	0.39
Zn L	63.94	30.21
Totals	100.00	



Comment: 1C, R/3

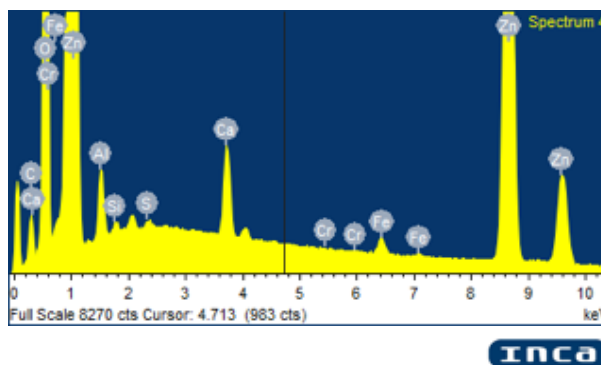
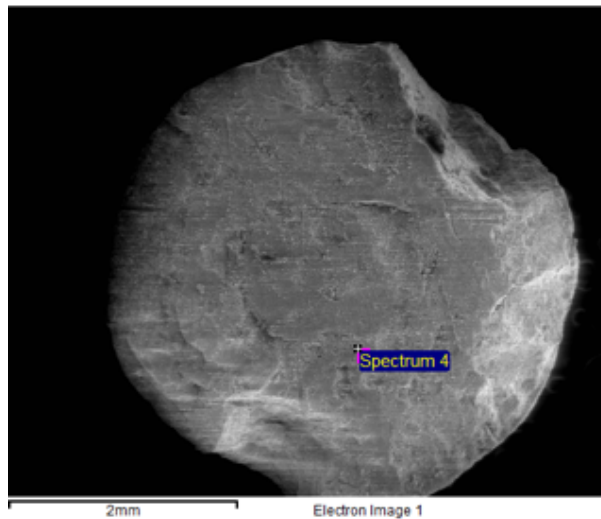
Spectrum processing :

Peaks possibly omitted : 4.515, 10.585, 17.264, 18.155 keV

Processing option : All elements analyzed (Normalised)

Number of iterations = 5

Element	Weight%	Atomic%
C K	5.58	14.77
O K	25.21	50.14
Al K	1.15	1.35
Si K	0.17	0.19
S K	0.10	0.10
Ca K	1.34	1.06
Cr K	0.01	0.00
Fe K	0.60	0.34
Zn L	65.86	32.05
Totals	100.00	



Comment: 1C, R/3

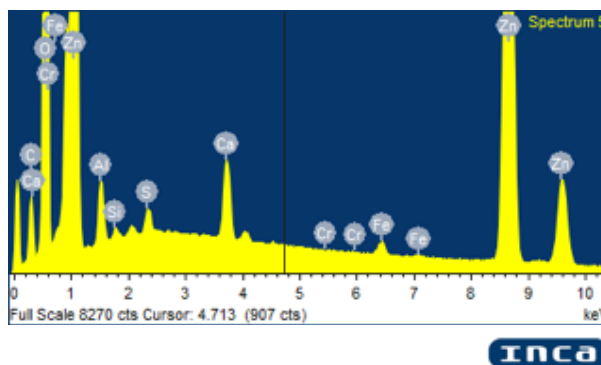
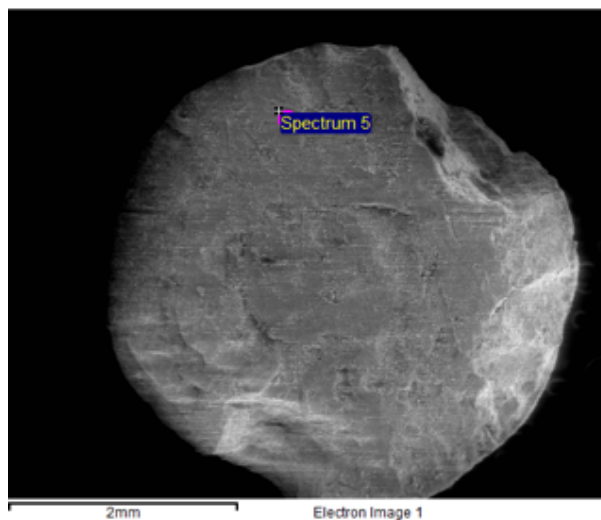
Spectrum processing :

Peaks possibly omitted : 17.265, 18.216 keV

Processing option : All elements analyzed (Normalised)

Number of iterations = 5

Element	Weight%	Atomic%
C K	8.64	21.48
O K	25.06	46.77
Al K	1.14	1.26
Si K	0.17	0.19
S K	0.38	0.35
Ca K	1.35	1.00
Cr K	-0.01	0.00
Fe K	0.56	0.30
Zn L	62.71	28.65
Totals	100.00	



Comment: 1C, 2R/3

Spectrum processing :

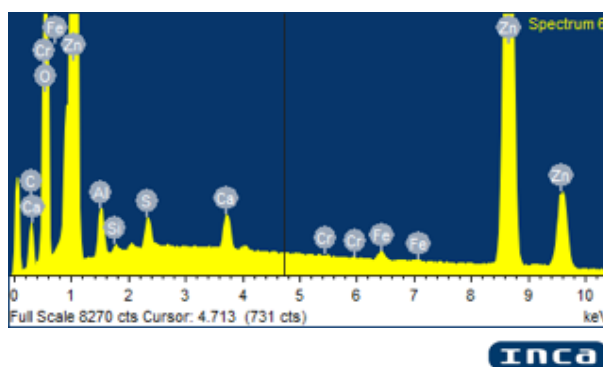
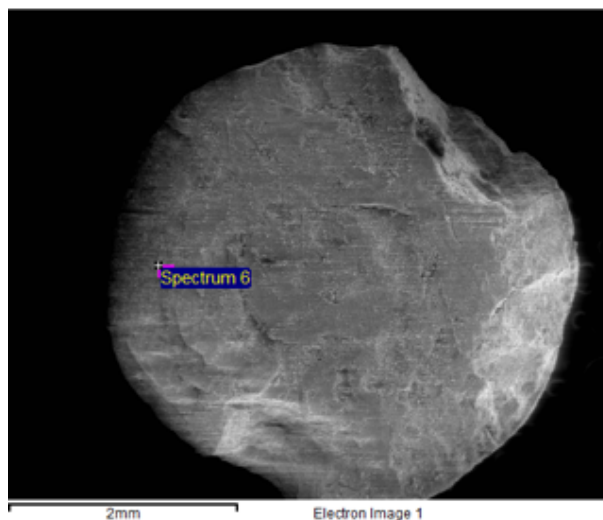
Peak possibly omitted : 17.262 keV

Processing option : All elements analyzed (Normalised)

Number of iterations = 5

Element	Weight%	Atomic%
C K	8.25	20.68
O K	25.00	47.06
Al K	1.27	1.42
Si K	0.17	0.18
S K	0.61	0.57
Ca K	0.83	0.63
Cr K	0.03	0.02
Fe K	0.48	0.26
Zn L	63.35	29.18
Totals	100.00	

Comment: 1C, 2R/3



Spectrum processing :

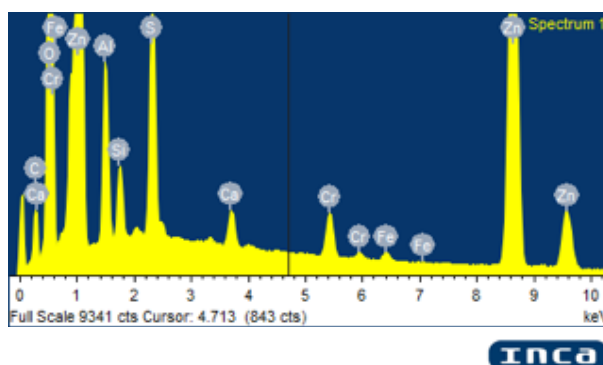
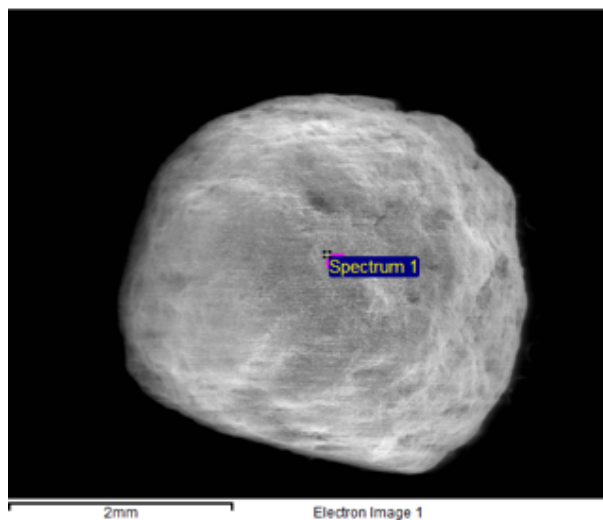
Peaks possibly omitted : 10.558, 17.262, 18.255 keV

Processing option : All elements analyzed (Normalised)

Number of iterations = 6

Element	Weight%	Atomic%
C K	6.57	15.00
O K	32.42	55.55
Al K	2.72	2.77
Si K	1.04	1.01
S K	3.14	2.68
Ca K	0.54	0.37
Cr K	1.23	0.65
Fe K	0.31	0.15
Zn L	52.03	21.82
Totals	100.00	

Comment: 2C, pellet surface



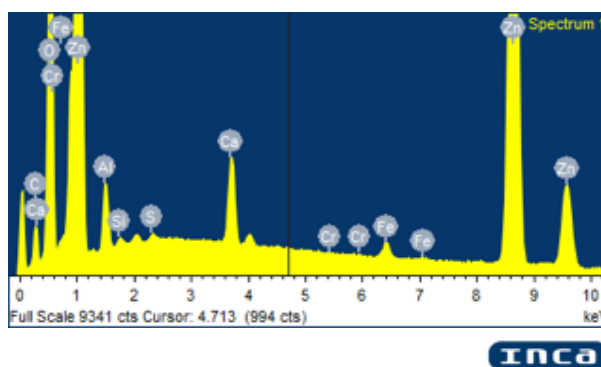
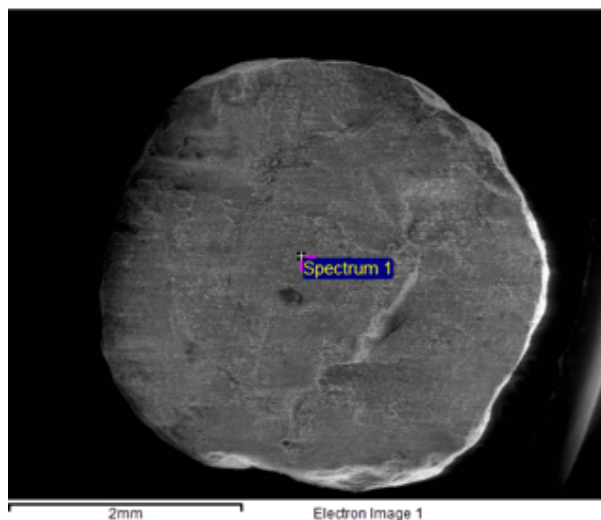
Spectrum processing :

Peaks possibly omitted : 4.495, 17.264, 18.179 keV

Processing option : All elements analyzed (Normalised)

Number of iterations = 5

Element	Weight%	Atomic%
C K	6.37	16.50
O K	25.27	49.17
Al K	1.53	1.76
Si K	0.18	0.20
S K	0.10	0.09
Ca K	1.75	1.36
Cr K	0.02	0.01
Fe K	0.75	0.42
Zn L	64.03	30.49
Totals	100.00	



Comment: 2C, pellet center

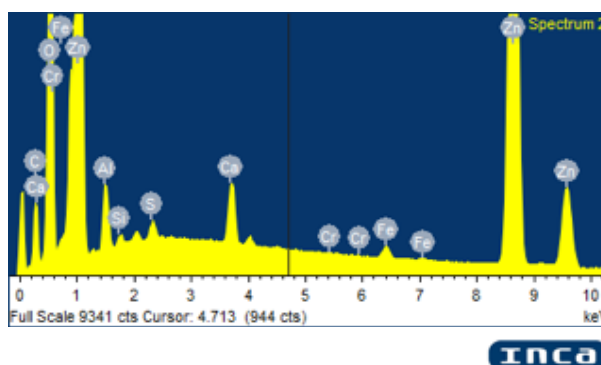
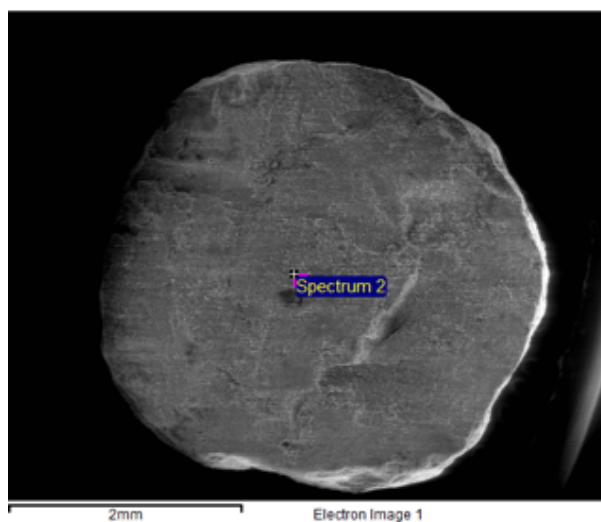
Spectrum processing :

Peaks possibly omitted : 4.519, 17.258, 18.187 keV

Processing option : All elements analyzed (Normalised)

Number of iterations = 6

Element	Weight%	Atomic%
C K	9.52	23.16
O K	25.25	46.13
Al K	1.40	1.52
Si K	0.20	0.21
S K	0.29	0.27
Ca K	1.19	0.87
Cr K	0.02	0.01
Fe K	0.58	0.30
Zn L	61.56	27.53
Totals	100.00	



Comment: 2C, pellet center

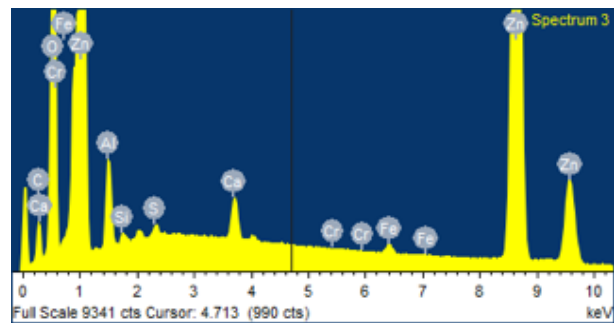
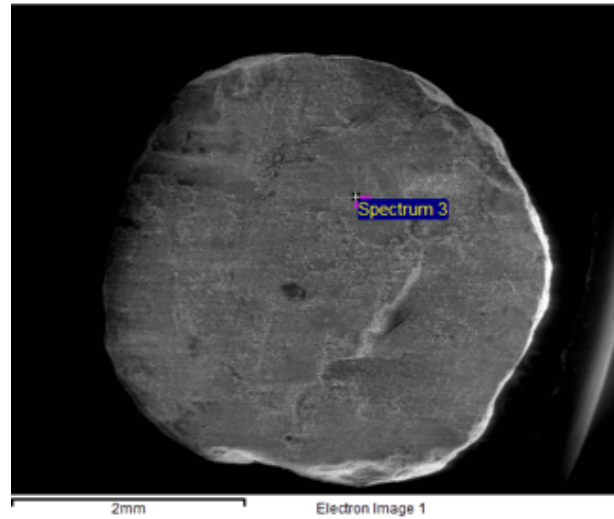
Spectrum processing :

Peaks possibly omitted : 10.575, 17.259, 18.234 keV

Processing option : All elements analyzed (Normalised)

Number of iterations = 5

Element	Weight%	Atomic%
C K	6.54	16.99
O K	24.74	48.27
Al K	2.09	2.41
Si K	0.20	0.22
S K	0.21	0.20
Ca K	0.84	0.65
Cr K	-0.01	-0.01
Fe K	0.46	0.26
Zn L	64.95	31.01
Totals	100.00	



Inca

Comment: 2C, R/3

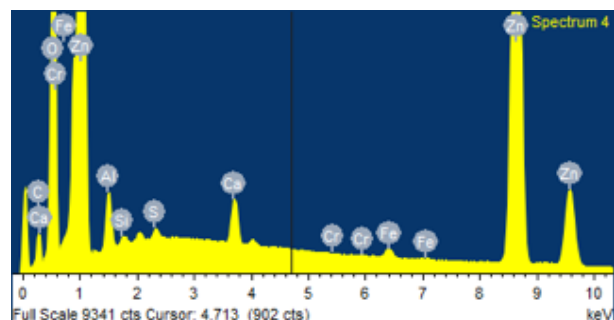
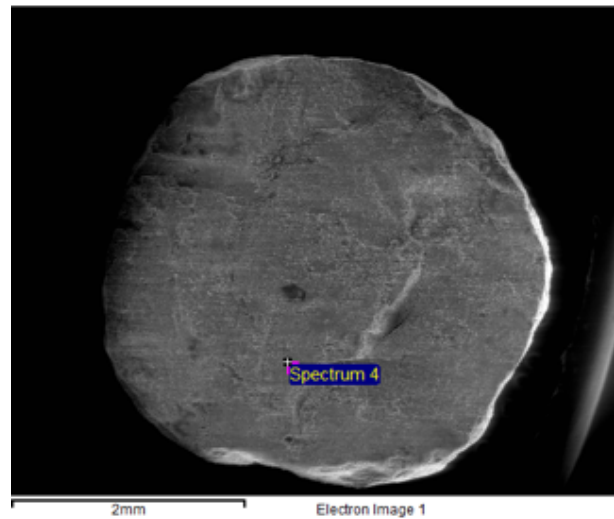
Spectrum processing :

Peaks possibly omitted : 17.267, 18.210 keV

Processing option : All elements analyzed (Normalised)

Number of iterations = 5

Element	Weight%	Atomic%
C K	5.59	14.97
O K	24.46	49.14
Al K	1.35	1.61
Si K	0.18	0.21
S K	0.18	0.18
Ca K	0.95	0.76
Cr K	-0.01	-0.01
Fe K	0.45	0.26
Zn L	66.85	32.88
Totals	100.00	



Inca

Comment: 2C, R/3

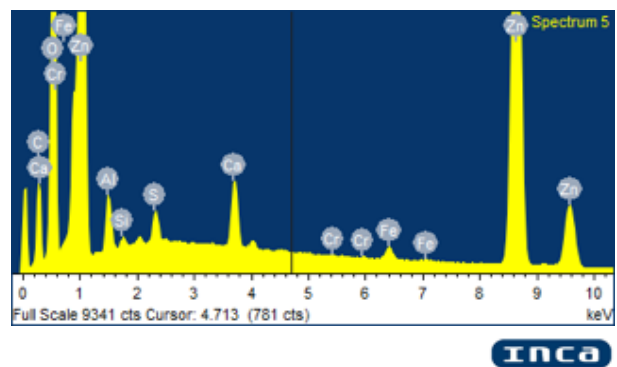
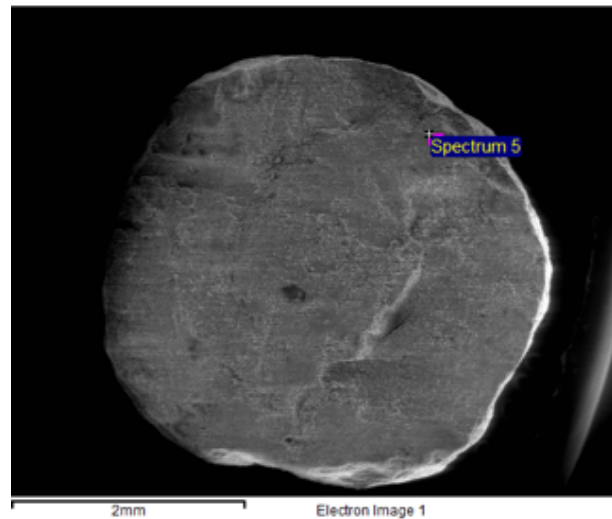
Spectrum processing :

Peaks possibly omitted : 4.545, 17.270, 18.180 keV

Processing option : All elements analyzed (Normalised)

Number of iterations = 6

Element	Weight%	Atomic%
C K	12.38	28.62
O K	24.92	43.25
Al K	1.22	1.26
Si K	0.19	0.19
S K	0.55	0.48
Ca K	1.33	0.92
Cr K	0.01	0.00
Fe K	0.65	0.32
Zn L	58.76	24.96
Totals	100.00	



Comment: 2C, 2R/3

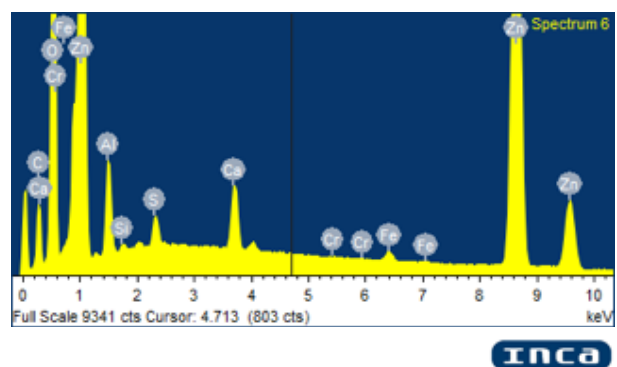
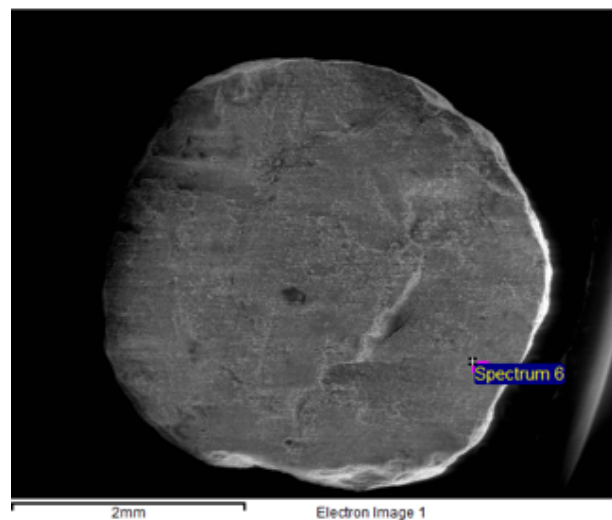
Spectrum processing :

Peaks possibly omitted : 10.600, 17.266 keV

Processing option : All elements analyzed (Normalised)

Number of iterations = 6

Element	Weight%	Atomic%
C K	10.73	25.63
O K	24.30	43.60
Al K	2.31	2.46
Si K	0.15	0.16
S K	0.58	0.52
Ca K	1.45	1.04
Cr K	0.03	0.02
Fe K	0.54	0.28
Zn L	59.91	26.30
Totals	100.00	



Comment: 2C, 2R/3

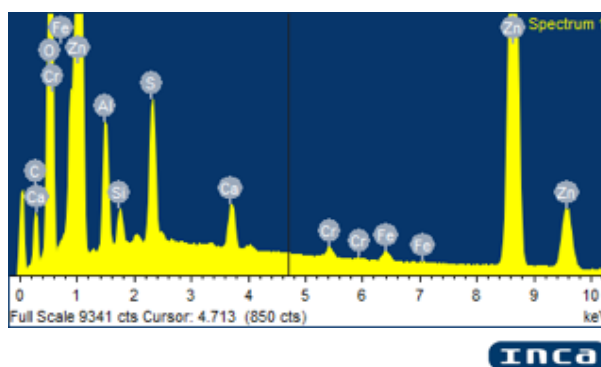
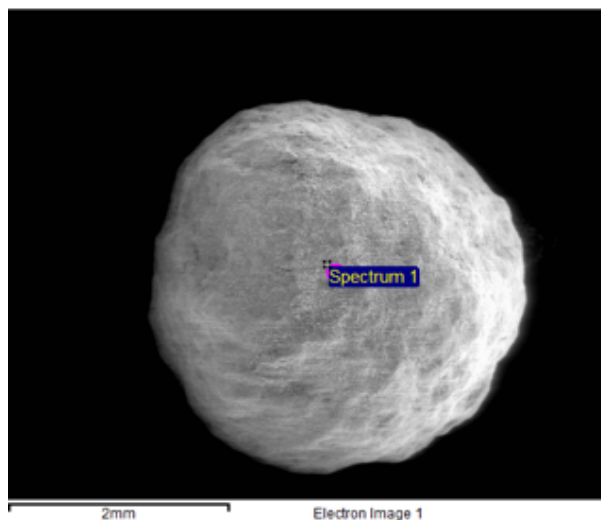
Spectrum processing :

Peaks possibly omitted : 17.252, 18.188 keV

Processing option : All elements analyzed (Normalised)

Number of iterations = 6

Element	Weight%	Atomic%
C K	7.63	17.89
O K	29.43	51.80
Al K	2.50	2.60
Si K	0.62	0.62
S K	2.29	2.01
Ca K	0.81	0.57
Cr K	0.32	0.18
Fe K	0.47	0.24
Zn L	55.93	24.09
Totals	100.00	



Comment: 3C, pellet surface

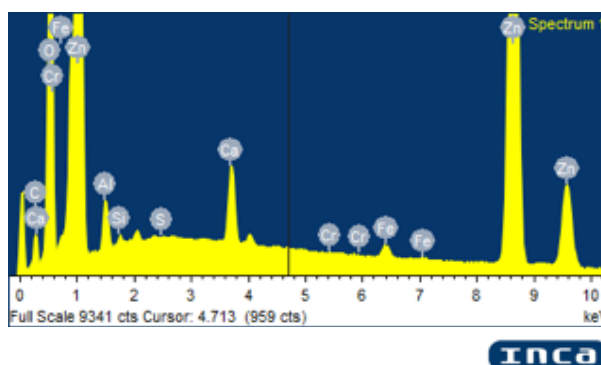
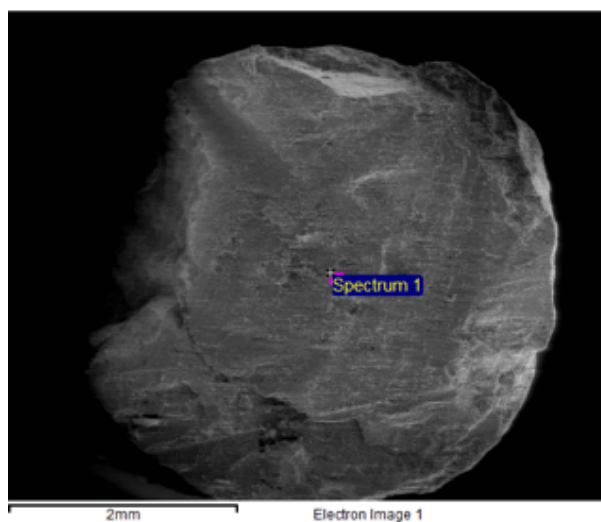
Spectrum processing :

Peaks possibly omitted : 17.251, 18.270 keV

Processing option : All elements analyzed (Normalised)

Number of iterations = 5

Element	Weight%	Atomic%
C K	5.04	13.60
O K	24.72	50.09
Al K	1.13	1.36
Si K	0.19	0.22
S K	0.05	0.05
Ca K	1.50	1.22
Cr K	-0.01	0.00
Fe K	0.61	0.36
Zn L	66.76	33.11
Totals	100.00	



Comment: 3C, pellet center

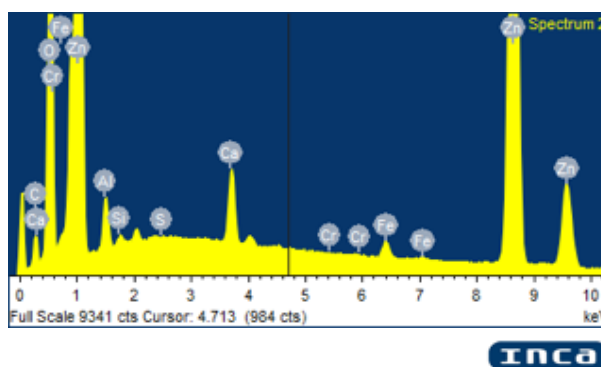
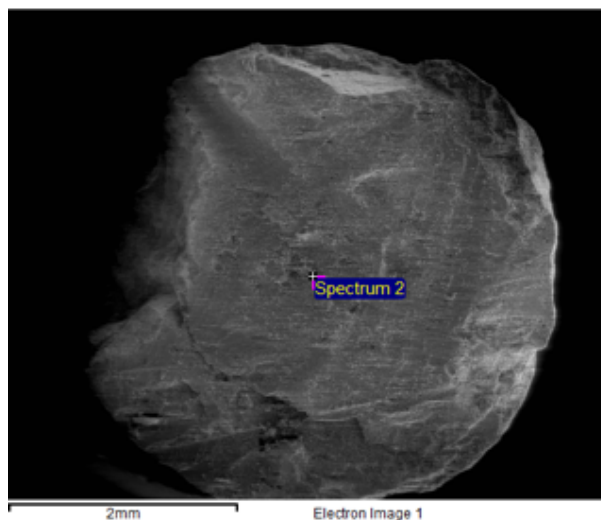
Spectrum processing :

Peaks possibly omitted : 4.515, 17.251, 18.197 keV

Processing option : All elements analyzed (Normalised)

Number of iterations = 5

Element	Weight%	Atomic%
C K	4.89	13.23
O K	24.82	50.38
Al K	1.15	1.38
Si K	0.18	0.21
S K	0.03	0.03
Ca K	1.42	1.15
Cr K	0.00	0.00
Fe K	0.80	0.46
Zn L	66.72	33.15
Totals	100.00	



Comment: 3C, pellet center

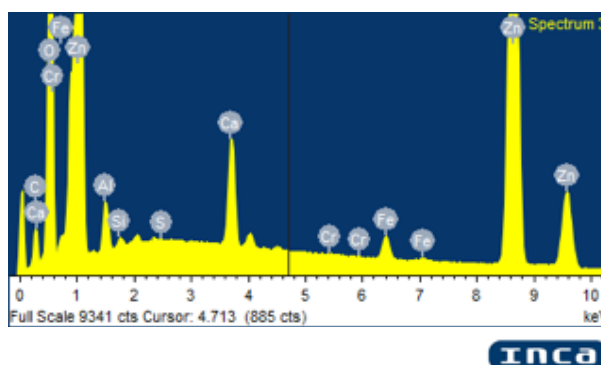
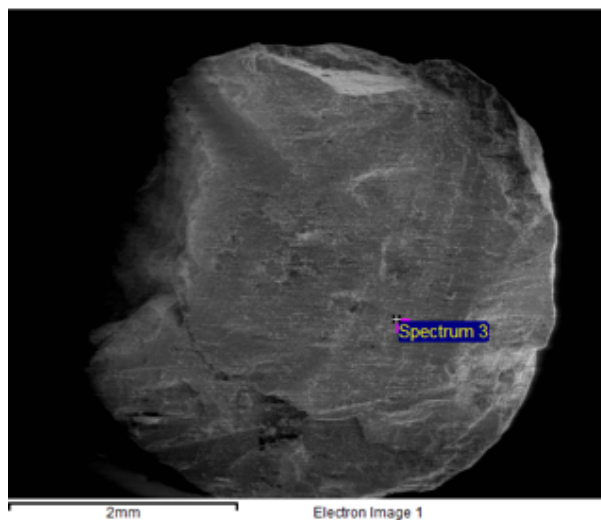
Spectrum processing :

Peaks possibly omitted : 4.515, 10.586, 17.262, 18.150 keV

Processing option : All elements analyzed (Normalised)

Number of iterations = 5

Element	Weight%	Atomic%
C K	6.04	15.81
O K	25.13	49.40
Al K	1.13	1.31
Si K	0.19	0.21
S K	0.04	0.04
Ca K	2.18	1.71
Cr K	0.02	0.01
Fe K	1.13	0.64
Zn L	64.15	30.87
Totals	100.00	



Comment: 3C, R/3

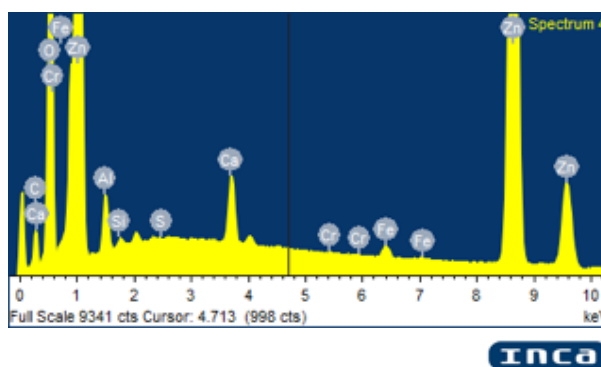
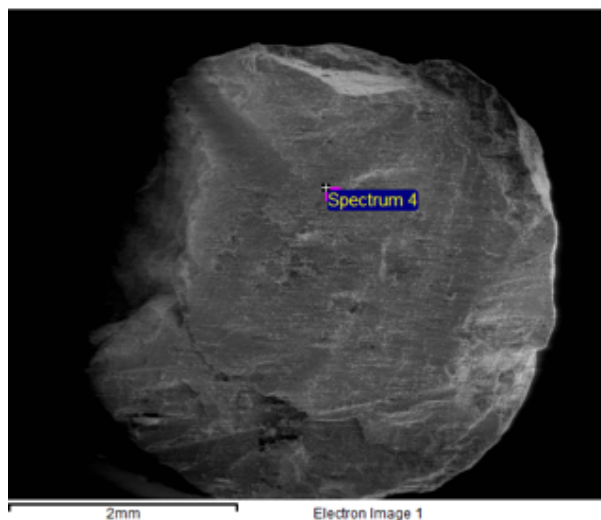
Spectrum processing :

Peaks possibly omitted : 17.259, 18.197 keV

Processing option : All elements analyzed (Normalised)

Number of iterations = 5

Element	Weight%	Atomic%
C K	6.06	16.10
O K	24.21	48.32
Al K	1.32	1.56
Si K	0.18	0.20
S K	0.05	0.05
Ca K	1.35	1.07
Cr K	0.01	0.01
Fe K	0.59	0.34
Zn L	66.23	32.35
Totals	100.00	



Comment: 3C, R/3

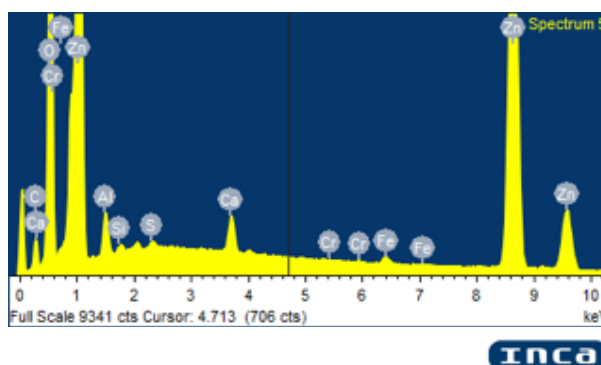
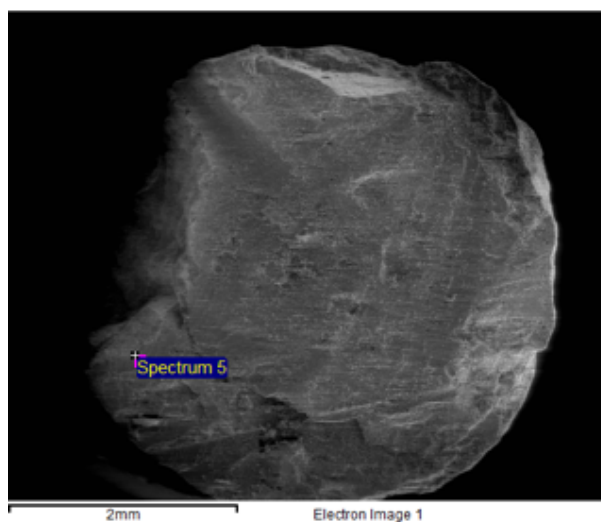
Spectrum processing :

Peaks possibly omitted : 12.850, 17.268 keV

Processing option : All elements analyzed (Normalised)

Number of iterations = 5

Element	Weight%	Atomic%
C K	5.82	15.42
O K	24.90	49.54
Al K	1.19	1.40
Si K	0.17	0.19
S K	0.14	0.14
Ca K	0.85	0.67
Cr K	0.00	0.00
Fe K	0.39	0.22
Zn L	66.55	32.41
Totals	100.00	



Comment: 3C, 2R/3

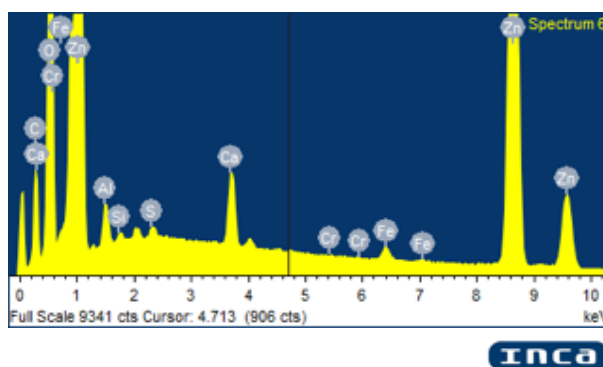
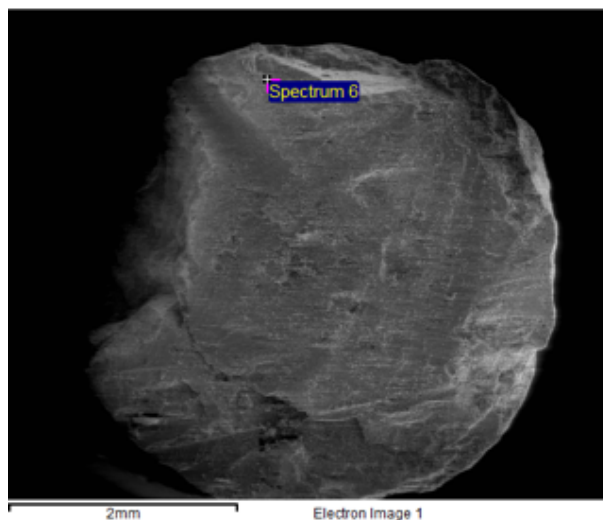
Spectrum processing :

Peaks possibly omitted : 4.512, 10.535, 10.585, 17.269, 18.200 keV

Processing option : All elements analyzed (Normalised)

Number of iterations = 6

Element	Weight%	Atomic%
C K	11.21	26.60
O K	25.06	44.64
Al K	0.71	0.75
Si K	0.15	0.16
S K	0.18	0.16
Ca K	1.21	0.86
Cr K	0.02	0.01
Fe K	0.51	0.26
Zn L	60.95	26.57
Totals	100.00	



Comment: 3C, 2R/3

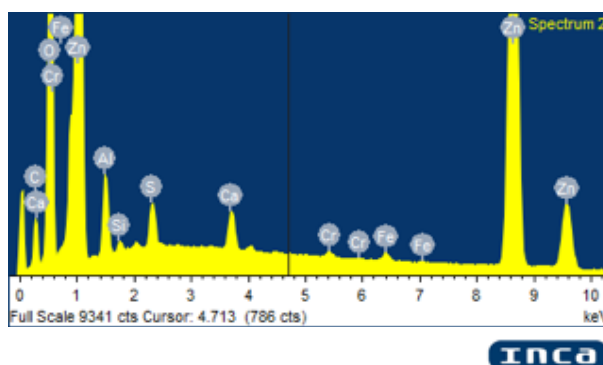
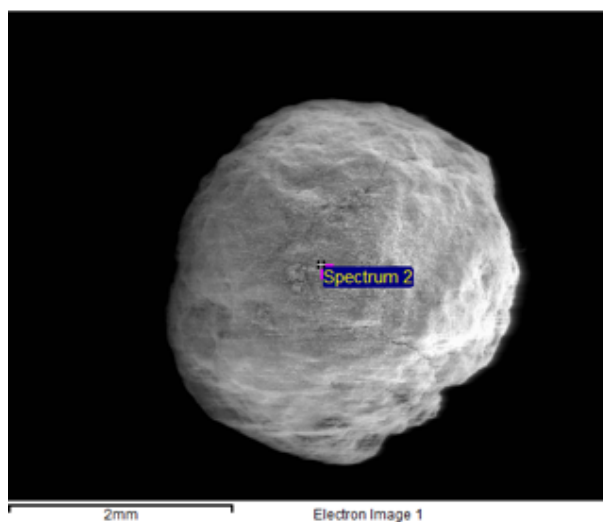
Spectrum processing :

Peaks possibly omitted : 4.480, 17.266, 18.215 keV

Processing option : All elements analyzed (Normalised)

Number of iterations = 6

Element	Weight%	Atomic%
C K	8.70	20.89
O K	26.98	48.62
Al K	2.01	2.15
Si K	0.23	0.23
S K	0.91	0.82
Ca K	0.86	0.62
Cr K	0.24	0.13
Fe K	0.44	0.23
Zn L	59.63	26.30
Totals	100.00	



Comment: 4C, pellet surface

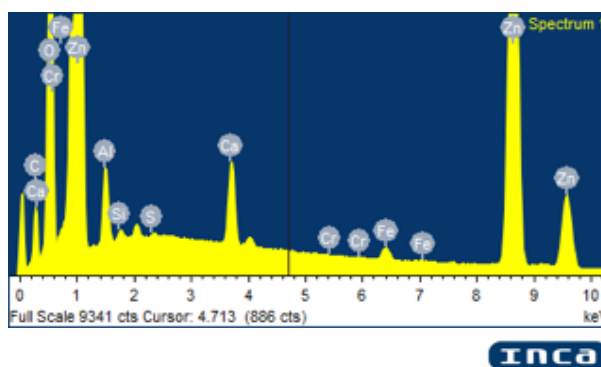
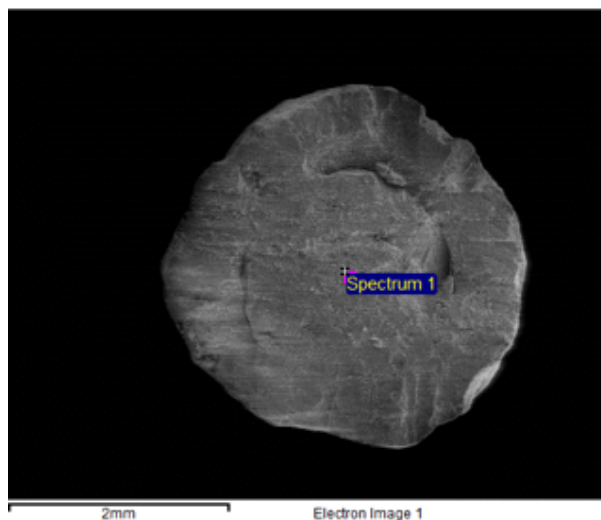
Spectrum processing :

Peaks possibly omitted : 10.480, 17.248, 18.207 keV

Processing option : All elements analyzed (Normalised)

Number of iterations = 5

Element	Weight%	Atomic%
C K	7.15	17.97
O K	26.40	49.82
Al K	1.42	1.59
Si K	0.17	0.19
S K	0.06	0.05
Ca K	1.38	1.04
Cr K	0.01	0.00
Fe K	0.55	0.29
Zn L	62.87	29.04
Totals	100.00	



Comment: 4C, pellet center

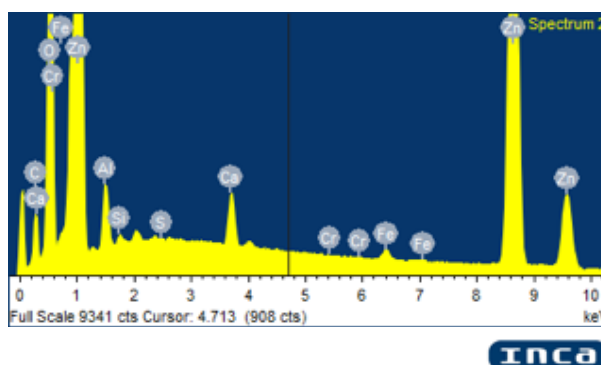
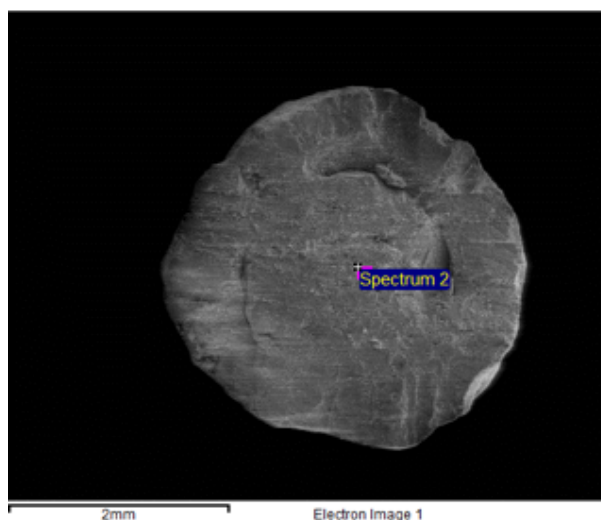
Spectrum processing :

Peaks possibly omitted : 17.261, 18.256 keV

Processing option : All elements analyzed (Normalised)

Number of iterations = 5

Element	Weight%	Atomic%
C K	7.40	18.77
O K	25.56	48.67
Al K	1.34	1.52
Si K	0.17	0.18
S K	0.03	0.03
Ca K	0.93	0.70
Cr K	-0.01	-0.01
Fe K	0.42	0.23
Zn L	64.15	29.90
Totals	100.00	



Comment: 4C, pellet center

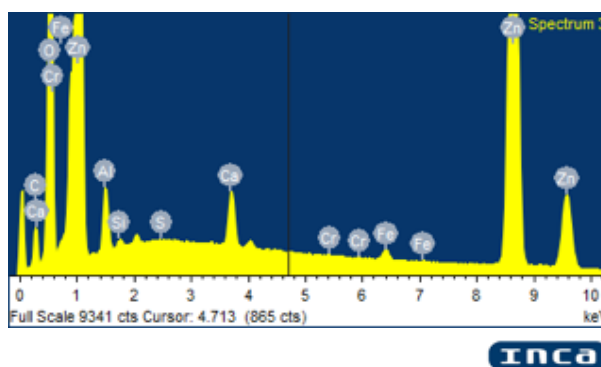
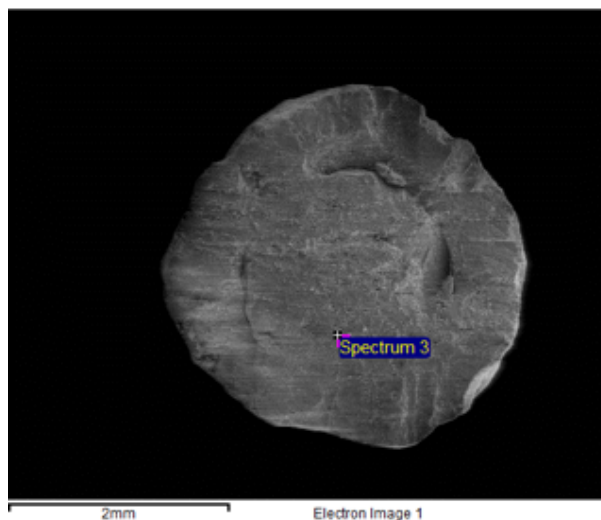
Spectrum processing :

Peaks possibly omitted : 10.560, 17.250, 18.195 keV

Processing option : All elements analyzed (Normalised)

Number of iterations = 5

Element	Weight%	Atomic%
C K	6.67	17.33
O K	24.85	48.47
Al K	1.48	1.72
Si K	0.18	0.21
S K	0.02	0.02
Ca K	1.11	0.86
Cr K	0.02	0.01
Fe K	0.49	0.28
Zn L	65.17	31.11
Totals	100.00	



Comment: 4C, R/3

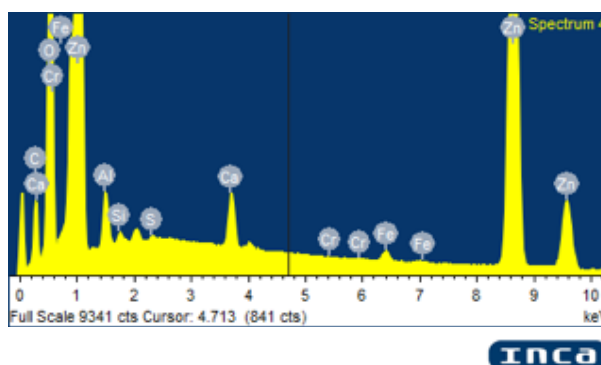
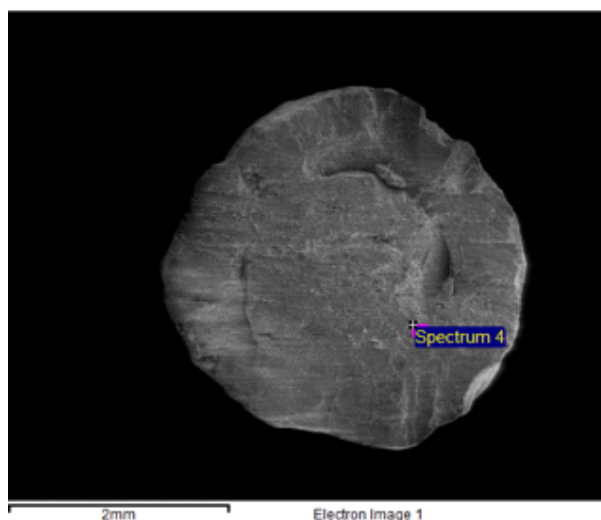
Spectrum processing :

Peaks possibly omitted : 10.555, 17.260 keV

Processing option : All elements analyzed (Normalised)

Number of iterations = 6

Element	Weight%	Atomic%
C K	8.71	21.55
O K	25.52	47.43
Al K	1.05	1.16
Si K	0.18	0.19
S K	0.07	0.06
Ca K	0.93	0.69
Cr K	0.00	0.00
Fe K	0.47	0.25
Zn L	63.08	28.69
Totals	100.00	



Comment: 4C, R/3

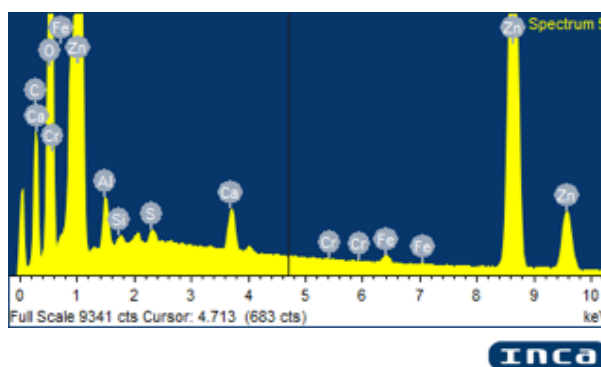
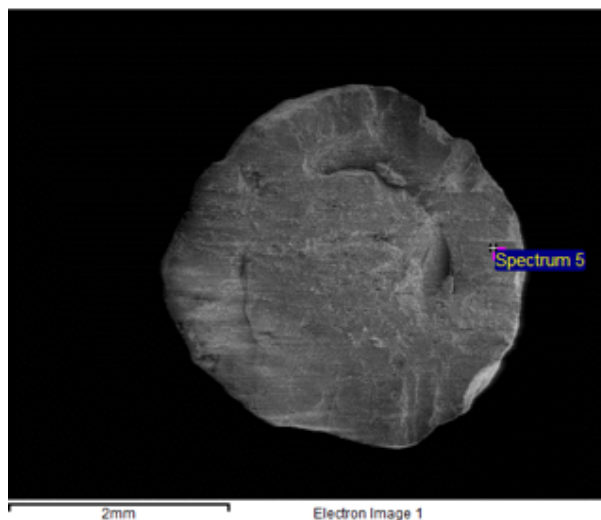
Spectrum processing :

Peaks possibly omitted : 10.565, 17.260, 18.217 keV

Processing option : All elements analyzed (Normalised)

Number of iterations = 6

Element	Weight%	Atomic%
C K	15.51	33.77
O K	25.58	41.81
Al K	0.86	0.84
Si K	0.14	0.13
S K	0.20	0.17
Ca K	0.69	0.45
Cr K	0.02	0.01
Fe K	0.34	0.16
Zn L	56.65	22.66
Totals	100.00	



Comment: 4C, 2R/3

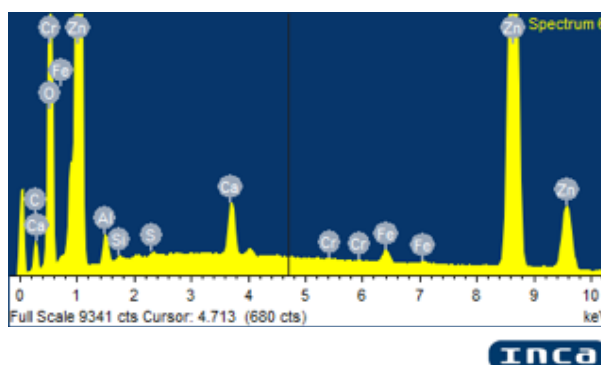
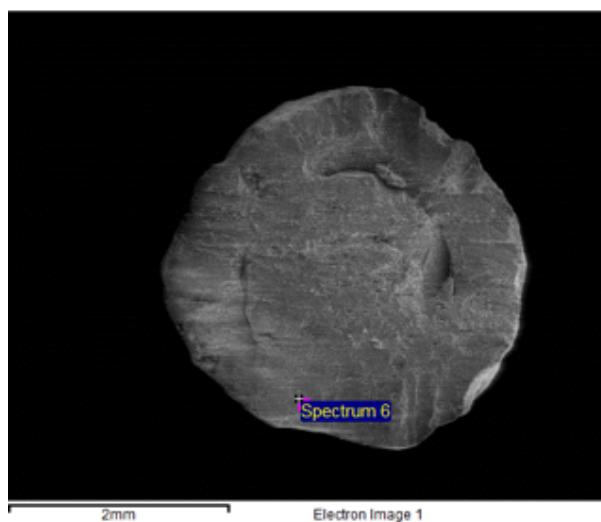
Spectrum processing :

Peaks possibly omitted : 4.490, 17.263, 18.170 keV

Processing option : All elements analyzed (Normalised)

Number of iterations = 5

Element	Weight%	Atomic%
C K	7.70	19.91
O K	23.61	45.86
Al K	1.16	1.34
Si K	0.15	0.16
S K	0.11	0.11
Ca K	1.84	1.43
Cr K	0.08	0.05
Fe K	1.10	0.61
Zn L	64.25	30.54
Totals	100.00	



Comment: 4C, 2R/3

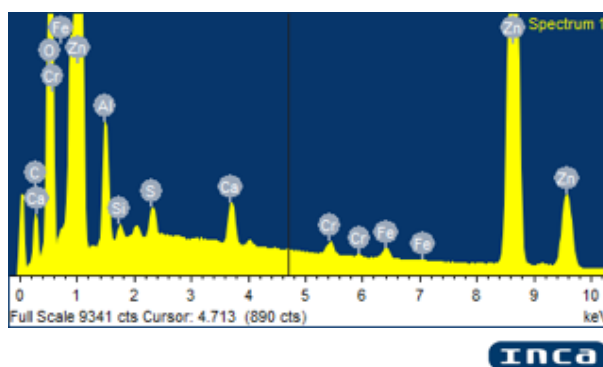
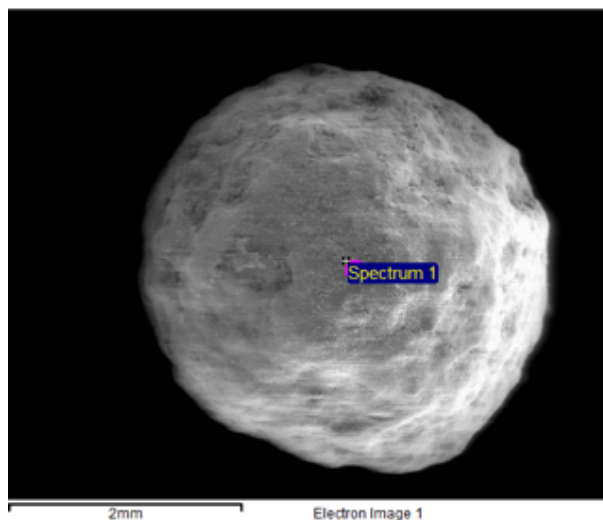
Spectrum processing :

Peaks possibly omitted : 10.620, 17.263, 18.275 keV

Processing option : All elements analyzed (Normalised)

Number of iterations = 5

Element	Weight%	Atomic%
C K	6.33	15.81
O K	27.57	51.72
Al K	2.24	2.49
Si K	0.26	0.27
S K	0.45	0.43
Ca K	0.69	0.52
Cr K	0.38	0.22
Fe K	0.44	0.23
Zn L	61.66	28.32
Totals	100.00	



Comment: 5C, pellet surface

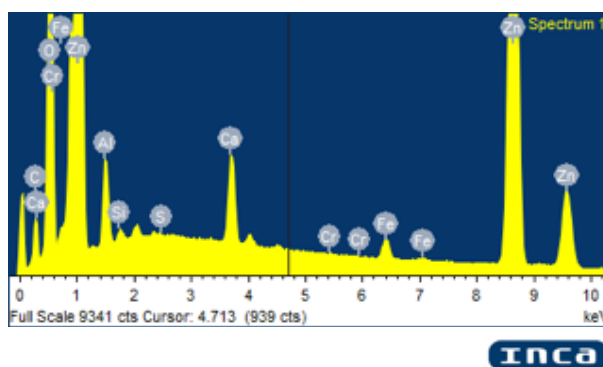
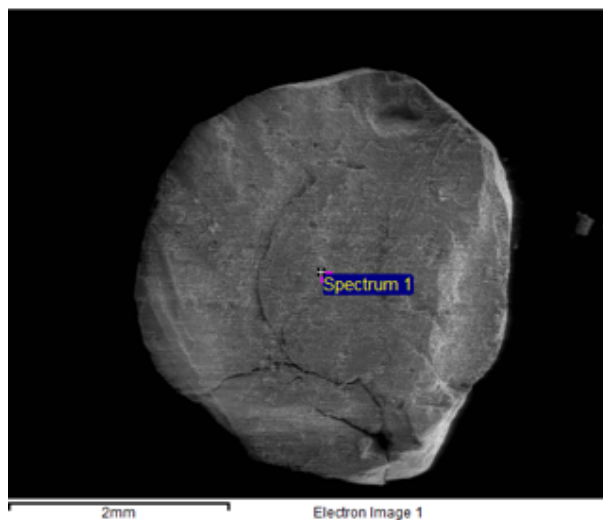
Spectrum processing :

Peaks possibly omitted : 4.511, 10.566, 17.261, 18.184 keV

Processing option : All elements analyzed (Normalised)

Number of iterations = 5

Element	Weight%	Atomic%
C K	6.09	15.72
O K	25.90	50.21
Al K	1.66	1.91
Si K	0.21	0.23
S K	0.05	0.05
Ca K	1.49	1.16
Cr K	0.01	0.01
Fe K	0.82	0.46
Zn L	63.77	30.26
Totals	100.00	



Comment: 5C, pellet center

Spectrum processing :

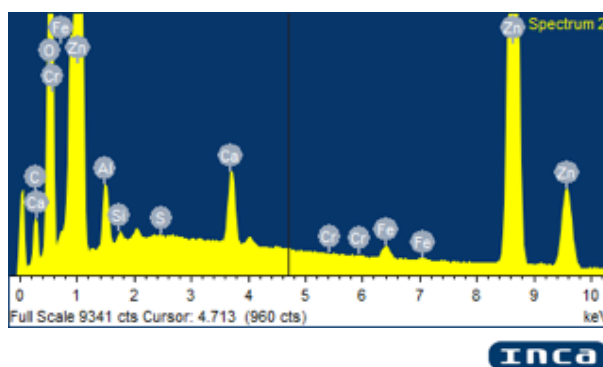
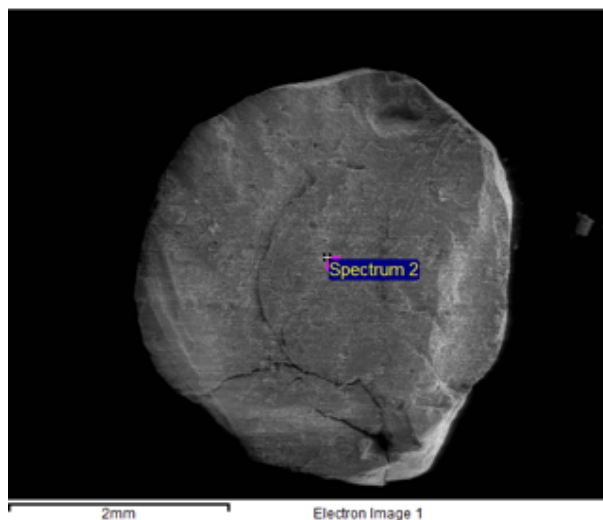
Peaks possibly omitted : 4.519, 10.610, 17.266, 18.204 keV

Processing option : All elements analyzed (Normalised)

Number of iterations = 5

Element	Weight%	Atomic%
C K	6.71	17.42
O K	24.88	48.51
Al K	1.29	1.49
Si K	0.18	0.20
S K	0.03	0.03
Ca K	1.28	0.99
Cr K	0.00	0.00
Fe K	0.57	0.32
Zn L	65.09	31.06
Totals	100.00	

Comment: 5C, pellet center



Spectrum processing :

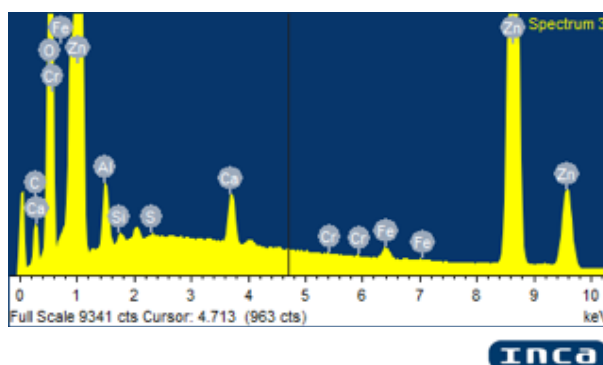
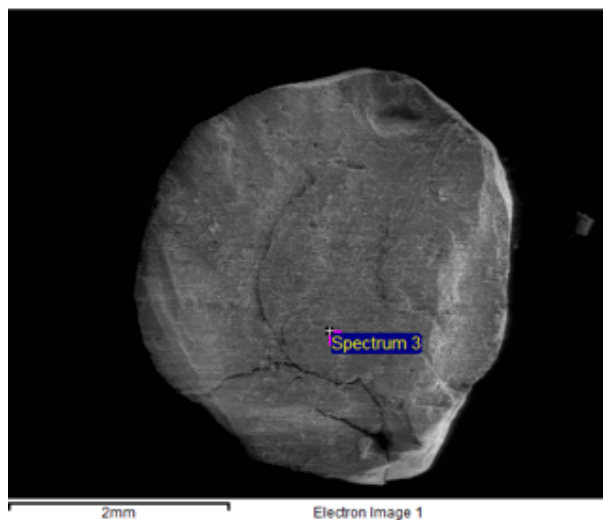
Peaks possibly omitted : 10.553, 17.253, 18.166 keV

Processing option : All elements analyzed (Normalised)

Number of iterations = 5

Element	Weight%	Atomic%
C K	6.19	16.30
O K	24.75	48.93
Al K	1.31	1.53
Si K	0.18	0.21
S K	0.05	0.05
Ca K	0.89	0.70
Cr K	0.00	0.00
Fe K	0.51	0.29
Zn L	66.11	31.99
Totals	100.00	

Comment: 5C, R/3



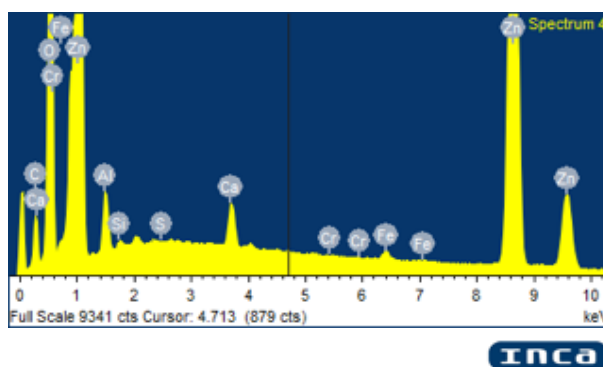
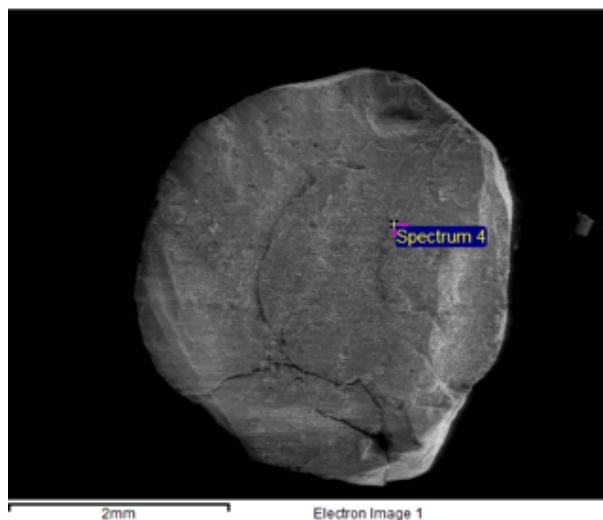
Spectrum processing :

Peaks possibly omitted : 17.253, 18.210 keV

Processing option : All elements analyzed (Normalised)

Number of iterations = 5

Element	Weight%	Atomic%
C K	7.95	20.30
O K	24.33	46.61
Al K	1.39	1.58
Si K	0.17	0.19
S K	0.03	0.03
Ca K	0.88	0.68
Cr K	0.01	0.01
Fe K	0.44	0.24
Zn L	64.79	30.38
Totals	100.00	



Comment: 5C, R/3

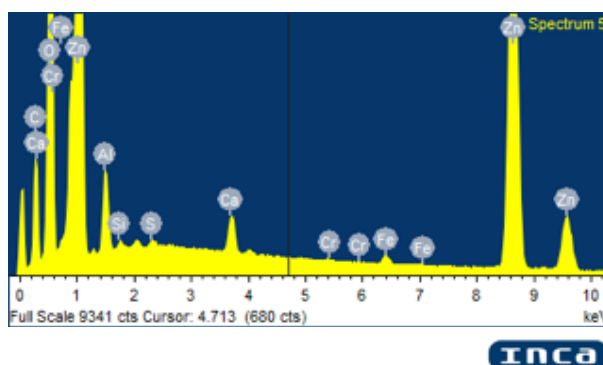
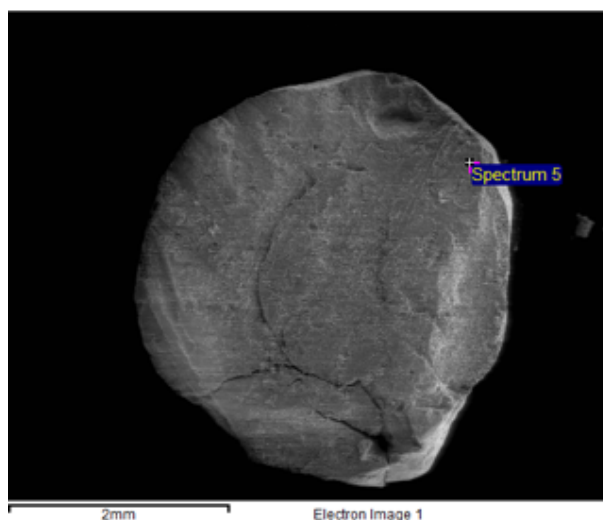
Spectrum processing :

Peaks possibly omitted : 10.581, 17.270, 18.195 keV

Processing option : All elements analyzed (Normalised)

Number of iterations = 6

Element	Weight%	Atomic%
C K	14.91	32.77
O K	25.37	41.86
Al K	1.62	1.58
Si K	0.13	0.12
S K	0.12	0.10
Ca K	0.70	0.46
Cr K	0.04	0.02
Fe K	0.42	0.20
Zn L	56.69	22.89
Totals	100.00	



Comment: 5C, 2R/3

Spectrum processing :

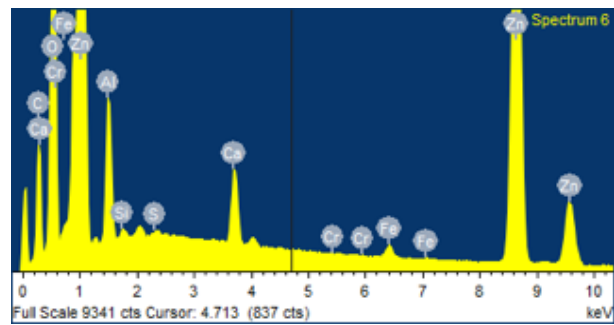
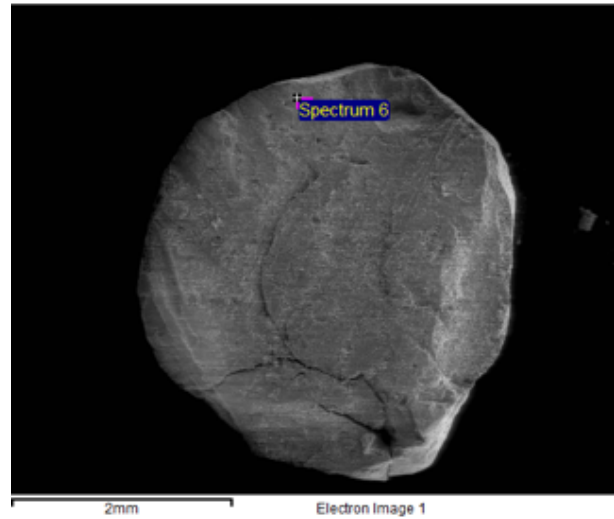
Peaks possibly omitted : 4.510, 10.626, 14.985, 17.256, 18.215 keV

Processing option : All elements analyzed (Normalised)

Number of iterations = 6

Element	Weight%	Atomic%
C K	13.21	29.54
O K	25.98	43.63
Al K	2.39	2.38
Si K	0.14	0.14
S K	0.08	0.06
Ca K	1.14	0.77
Cr K	-0.01	0.00
Fe K	0.45	0.21
Zn L	56.62	23.27
Totals	100.00	

Comment: 5C, 2R/3



**INCA**